**Naval Research Laboratory**

**Washington, DC 20375-5320**

**NRL/FR/8150--08-10,163**

# Characterization of Periodic Variations in the GPS Satellite Clocks

KEN L. SENIOR
RONALD L. BEARD

*Space Applications Branch*
*Space Systems Development Department*

JIM R. RAY

*National Geodetic Survey*
*National Oceanic and Atmospheric Administration*
*Silver Spring, Maryland*

August 8, 2008

# REPORT DOCUMENTATION PAGE

*Form Approved*
*OMB No. 0704-0188*



| **1. REPORT DATE** *(DD-MM-YYYY)* | **2. REPORT TYPE** | **3. DATES COVERED** *(From - To)* |
|---|---|---|
| 08-08-2008 | Formal Report | June 2007 - February 2008 |

**4. TITLE AND SUBTITLE**

Characterization of Periodic Variations in the GPS Satellite Clocks

**5a. CONTRACT NUMBER**

**5b. GRANT NUMBER**

**5c. PROGRAM ELEMENT NUMBER**
61153N

**6. AUTHOR(S)**

Ken L. Senior, Jim R. Ray,* and Ronald L. Beard

**5d. PROJECT NUMBER**

**5e. TASK NUMBER**

**5f. WORK UNIT NUMBER**
T065-08

**7. PERFORMING ORGANIZATION NAME(S) AND ADDRESS(ES)**

Naval Research Laboratory
4555 Overlook Avenue, SW
Washington, DC 20375-5320

**8. PERFORMING ORGANIZATION REPORT NUMBER**

NRL/FR/8150--08-10,163

**9. SPONSORING / MONITORING AGENCY NAME(S) AND ADDRESS(ES)**

Office of Naval Research
875 Randolph Street, Suite 1425
Arlington, VA 22203

**10. SPONSOR / MONITOR'S ACRONYM(S)**

ONR

**11. SPONSOR / MONITOR'S REPORT NUMBER(S)**

**12. DISTRIBUTION / AVAILABILITY STATEMENT**

Approved for public release; distribution is unlimited.

**13. SUPPLEMENTARY NOTES**

*National Geodetic Survey, National Oceanic and Atmospheric Administration, Silver Spring, MD, 20910

**14. ABSTRACT**

The clock products of the International Global Navigation Satellite Systems (GNSS) Service (IGS) are used to characterize the timing performance of the GPS satellites. Using 5-minute and 30-second observational samples and focusing only on the sub-daily regime, approximate power-law stochastic processes are found. The Block IIA Rb and Cs clocks obey predominantly random walk phase (or white frequency) noise processes. The Rb clocks are up to nearly an order of magnitude more stable and show a flicker phase noise component over intervals shorter than about 100 s. Due to the onboard Time Keeping System in the newer Block IIR and IIR-M satellites, their Rb clocks behave in a more complex way: as an apparent random walk phase process up to about 100 s then changing to flicker phase up to a few thousand seconds. Superposed on this random background, periodic signals have been detected in all clock types at four harmonic frequencies, $n \times (2.0029 \pm 0.0005)$ cycles per day (24 hr UTC), for n =1, 2, 3, and 4. The equivalent fundamental period is $11.9826 \pm 0.0030$ hours, which surprisingly differs from the reported mean GPS orbital period of $11.9659 \pm 0.0007$ hours by $60 \pm 11$ s. We cannot account for this apparent discrepancy but note that a clear relationship between the periodic signals and the orbital dynamics is evidenced for some satellites by modulations of the spectral amplitudes with eclipse season. All four harmonics are much smaller for the IIR and IIR-M satellites than for the older blocks. Awareness of the periodic variations can be used to improve the clock modeling, including for interpolation of tabulated IGS products for higher-rate GPS positioning and for predictions in real-time applications. This is especially true for high-accuracy uses, but could also benefit the standard GPS operational products. The observed stochastic properties of each satellite clock type are used to estimate the growth of interpolation and prediction errors with time interval.

**15. SUBJECT TERMS**

GPS clocks  Relativity  Harmonics

| **16. SECURITY CLASSIFICATION OF:** | | | **17. LIMITATION OF ABSTRACT** | **18. NUMBER OF PAGES** | **19a. NAME OF RESPONSIBLE PERSON** |
|---|---|---|---|---|---|
| **a. REPORT** | **b. ABSTRACT** | **c. THIS PAGE** | | | Ken L. Senior |
| Unclassified | Unclassified | Unclassified | UL | 63 | **19b. TELEPHONE NUMBER** *(include area code)* (202) 767-2043 |

**Standard Form 298 (Rev. 8-98)**
**Prescribed by ANSI Std. Z39.18**

## CONTENTS

INTRODUCTION ..... 1
IGS CLOCK PRODUCT ACCURACY ..... 2
RELATIVISTIC EFFECTS ..... 4
GPS SUB-DAILY CLOCK STABILITIES ..... 5
ESTIMATION OF GPS CLOCK SPECTRA ..... 8
Aggregate Constellation Spectrum ..... 8
Temporal Variation of GPS Spectral Peaks ..... 9
IMPROVED GPS CLOCK MODELING ..... 15
CONSEQUENCES FOR CLOCK INTERPOLATION AND PREDICTION ..... 15
CONCLUSIONS ..... 17
REFERENCES ..... 18
APPENDIX – Time-Varying Spectra for the GPS Constellation ..... 21

## FIGURES


Fig. 1 Overall GPS constellation frequency instability ..... 7
Fig. 2 Averaged amplitude spectrum of GPS constellation ..... 8
Fig. 3 SVN27 time-varying amplitudes of 12-, 6-, 4-, and 3-hour periodics ..... 10
Fig. 4 Correlations between 12-hour and 6-, 4-, and 3-hour periodics ..... 14
Fig. 5 RMS time prediction and interpolation errors ..... 16
Fig. A1 SVN13 time-varying amplitudes ..... 22
Fig. A2 SVN15 time-varying amplitudes ..... 23
Fig. A3 SVN17 time-varying amplitudes ..... 24
Fig. A4 SVN19 time-varying amplitudes ..... 25
Fig. A5 SVN21 time-varying amplitudes ..... 26
Fig. A6 SVN22 time-varying amplitudes ..... 27
Fig. A7 SVN23 time-varying amplitudes ..... 28
Fig. A8 SVN24 time-varying amplitudes ..... 29
Fig. A9 SVN25 time-varying amplitudes ..... 30
Fig. A10 SVN26 time-varying amplitudes ..... 31
Fig. A11 SVN27 time-varying amplitudes ..... 32
Fig. A12 SVN29 time-varying amplitudes ..... 33
Fig. A13 SVN30 time-varying amplitudes ..... 34
Fig. A14 SVN31 time-varying amplitudes ..... 35
Fig. A15 SVN32 time-varying amplitudes ..... 36
Fig. A16 SVN33 time-varying amplitudes ..... 37
Fig. A17 SVN34 time-varying amplitudes ..... 38
Fig. A18 SVN35 time-varying amplitudes ..... 39
Fig. A19 SVN36 time-varying amplitudes ..... 40
Fig. A20 SVN37 time-varying amplitudes ..... 41
Fig. A21 SVN38 time-varying amplitudes ..... 42
Fig. A22 SVN39 time-varying amplitudes ..... 43
Fig. A23 SVN40 time-varying amplitudes ..... 44
Fig. A24 SVN41 time-varying amplitudes ..... 45
Fig. A25 SVN43 time-varying amplitudes ..... 46
Fig. A26 SVN44 time-varying amplitudes ..... 47
Fig. A27 SVN45 time-varying amplitudes ..... 48
Fig. A28 SVN46 time-varying amplitudes ..... 49
Fig. A29 SVN47 time-varying amplitudes ..... 50
Fig. A30 SVN51 time-varying amplitudes ..... 51
Fig. A31 SVN52 time-varying amplitudes ..... 52
Fig. A32 SVN53 time-varying amplitudes ..... 53
Fig. A33 SVN54 time-varying amplitudes ..... 54
Fig. A34 SVN56 time-varying amplitudes ..... 55
Fig. A35 SVN58 time-varying amplitudes ..... 56
Fig. A36 SVN59 time-varying amplitudes ..... 57
Fig. A37 SVN60 time-varying amplitudes ..... 58
Fig. A38 SVN61 time-varying amplitudes ..... 59

# CHARACTERIZATION OF PERIODIC VARIATIONS IN THE GPS SATELLITE CLOCKS

## INTRODUCTION

The geodetic performance of the Global Positioning System (GPS) is intimately related to the characteristics of the satellite clocks. (The term "clock" is used here to encompass not only the onboard atomic frequency standards [AFSs], but also the integrated non-dispersive effects of all satellite components that affect the broadcast timing signals as observed from the ground. This usage is consistent with the definition of the International Telecommunication Union [ITU 1996; 2002].) A thorough understanding of the behavior of the GPS satellite clocks is useful in order to use the current system optimally and to plan future improvements.

Prior studies of the GPS clocks have been limited by the quality of the observational results available or by the scope of the analysis. The satellite clock values broadcast in the GPS navigation message are predictions for intervals up to about a day and are parameterized as a second-order polynomial (see the IS-GPS-200 interface specification document maintained by the Navstar GPS Joint Program Office [IS-GPS-200 2006]). In fact, the quadratic clock terms are never non-zero because of the quantization threshold for the broadcast model, so the effective representation is linear. In recent years, the root-mean-square (rms) precision of the broadcast GPS clocks is roughly 5 ns (about 1.5 m equivalent light travel distance), as monitored by the International Global Navigation Satellite Systems (GNSS) Service (IGS). By "precision" we mean only to gauge the internal consistency among the GPS clocks and not any offsets in timescale compared to some absolute standard. These values are not able to reveal clock properties at sub-daily intervals or to better than a few nanoseconds.

It became possible to examine the GPS clocks with higher accuracy and finer temporal resolution when the IGS was formed and started publishing regular satellite orbital ephemerides in late 1993 (see the IGS website at http://igscb.jpl.nasa.gov, updated 17 Jan 2008). These files give the geocentric coordinates and clock values for each satellite tabulated at 15-minute intervals and are based on a weighted combination of analyses by several independent groups using dual-frequency pseudorange and carrier phase data from a globally distributed tracking network. For background, Ray and Senior (2005) have reviewed geodetic methods for GPS time and frequency comparisons. The IGS combination procedures were improved and the clock products were densified to 5-minute samples beginning in November 2000 (Kouba and Springer 2001). Simultaneous estimates for the tracking receivers were added at that time. A further enhancement was achieved when the timescale of the IGS clocks was changed from a daily linear alignment to broadcast GPS time (GPST) to an internally realized timescale generated as a dynamically weighted ensemble of the IGS clocks themselves, including a number of tracking receivers, some of which use external hydrogen-maser (H-maser), cesium (Cs), or rubidium (Rb) frequency standards in addition to the satellite clocks (Senior et al. 2003; Ray and Senior 2003). The satellite AFSs are either Cs or Rb types. The sub-daily instability of the IGS timescale is consistent with a random walk (in phase) noise process with an Allan deviation of about $1 \times 10^{-15}$ at 1 day, about 20 times better than GPST. The instability at longer times increases because the scale remains loosely steered to GPST to maintain

Manuscript approved March 7, 2008

long-term consistency. Since January 2007 the sampling of the satellite (but not ground) clocks has increased from 5 minutes to 30 seconds.

This study uses the IGS clock products since late 2000 to examine the stability of the GPS satellite clocks, mostly in the sub-daily regime. We focus particular attention on periodic signals and their variations among different satellites and over time. Possible origins for these effects are considered. High-accuracy satellite clocks are also produced by the National Geospatial-Intelligence Agency (see the GEOINT Sciences Office GPS Division website at http://earth-info.nga.mil/GandG/sathtml/, updated 26 Dec 2007) as well as by individual IGS analysis centers, but those are not utilized for this investigation.

## IGS CLOCK PRODUCT ACCURACY

The central function of the IGS is to enable GPS to be useful for the most demanding scientific applications by generating and distributing satellite orbit and clock information with cm-level accuracy in lieu of the broadcast navigation ephemerides. All IGS products (see http://igscb.jpl.nasa.gov/components/prods.html, updated 10 June 2008) are formed as the weighted averages of solutions contributed by up to eight participating analysis centers (up to six for clocks). For more details of the IGS analysis combination strategy, see Beutler et al. (1995), Kouba and Springer (2001), and also annual reports of the IGS Analysis Coordinator. While the observational data used by the various groups overlap, the effects of differing analysis strategies, modeling approaches, and softwares are largely independent. In this way, the IGS combined products benefit in stability, reliability, completeness, and robustness compared with the results from any single center, and they are usually as precise and accurate as the best individual solutions.

To examine the stability of the GPS clocks, we rely on the IGS Final clock products, which are available about 13 days after the end of each GPS week and are tabulated at 5-min intervals (or every 30 s for satellite clocks since early 2007). The clock values are referenced to the internally realized IGS timescale, formed as a weighted ensemble of the included station and satellite clocks. The ensemble algorithm is a Kalman filter with a simple two-state polynomial model driven by white noise processes for each clock (Senior et al. 2003). Weights for individual clocks in the ensemble are determined iteratively and dynamically based on their observed instabilities over sub-daily intervals. The IGS timescale is then loosely steered to GPST over intervals longer than about a day. For this reason we limit our attention here primarily to sub-daily intervals.

The internal consistency of the IGS satellite orbits and clocks, which is critical for geodetic applications, is at the sub-cm level (Kouba and Springer 2001). This is routinely demonstrated by the use of these products for precise point positioning (PPP) (Zumberge et al. 1997) of isolated tracking stations. Daily PPP repeatabilities using the IGS Finals are around 3, 5, and 9 mm rms in the local north, east, and vertical components, respectively, as monitored by the IGS Analysis Center Coordinator (ACC) (during the period 2008–2011, the IGS ACC functions are performed by NOAA's National Geodetic Survey; see http://www.ngs.noaa.gov/igsacc/WWW/, updated 27 May 2008). The horizontal repeatabilities are asymmetric because carrier phase ambiguity resolution is impractical for undifferenced data from a single station. In the global solutions used as inputs for the IGS products, double-difference phase ambiguities are mostly fixed, which ensures symmetric horizontal errors.

Taken separately, the IGS combination statistics themselves set only lower limits for the product accuracies; see the combination reports at http://igscb.jpl.nasa.gov/mail/igsreport/igsreport.html (accessed 20 June 2008). For instance, the inter-center satellite clock agreement is usually about 50 ps (1.5 cm) rms if daily clock biases are ignored and are about 100 ps (3 cm) rms otherwise. The daily internal orbit agreements are similar, about 1 cm rms or better except for occasional anomalous satellites. However, if the orbits are compared to a dynamical fit over seven days (Beutler et al. 1995) then the residuals increase

to the 2 to 3 cm range. The latter metric is almost certainly a better gauge of the true orbit accuracy (Griffiths and Ray 2007).

These internal consistencies and mutual agreements suggest that the precision of the IGS products is probably around 1 cm (33 ps) and the accuracy about 3 cm (100 ps). However, those results do not address the nature of the IGS clock errors (whether dominantly stochastic or systematic) nor do they necessarily give a complete view of the product accuracy. In particular, it is well known that correlations between the clock and orbit parameter estimates can reduce the impact of ephemeris errors in geodetic positioning. This fact has been used intentionally to yield favorable user range errors (UREs) in the GPS broadcast ephemerides (Arthur Dorsey, Lockheed Martin Corporation, personal communication, 2007). However, the much denser and more globally distributed IGS tracking network greatly reduces the ability to shift satellite positions (mostly radially) to compensate clock errors compared to the GPS operational system.

The models and parameterizations used in the GPS data analyses to account for time-varying processes (e.g., tidal motions) can also affect the IGS clock estimates. Generally the IGS analysis groups follow recommendations in the IERS Conventions (McCarthy and Petit 2004) and its updates (IERS = International Earth Rotation and Reference Systems Service). The IERS models are typically accurate to about 1 mm. Parameter estimates, including both geodetic and nuisance quantities, are also typically good to the sub-cm level. Some parameter errors, such as for station heights, can reach to about 1 cm but these have mostly bias-like effects on the satellite clock estimates over daily intervals and therefore should not disturb the sub-daily clock stabilities appreciably.

Possibly more important for clock errors are models specific to the GPS technique that are not included in the IERS Conventions. These include, for instance, the offsets between the satellite antenna phase centers and their centers of mass, as well as the antenna phase patterns for both satellites and tracking stations. The issues and IGS approaches for dealing with them have been described by Gendt and Schmid (2005) and the generation of the current IGS calibration values is documented by Schmid et al. (2007). The absolute uncertainty in the radial location of the satellite antenna phase centers could be as large as 1 m, which would affect the clock estimates directly. However, the IGS products are far more sensitive to the internal consistency of the antenna calibration models, which is in the cm range. In any case, errors in the calibrations give rise to nearly constant clock biases with only minor effects on the observed sub-daily stabilities.

More important for clock estimates are factors related to the orientational control and modeling of the satellite's attitude, which must continuously vary to maintain full illumination of the vital solar panel arrays. This is most problematic during the eclipse periods experienced twice yearly by each satellite orbit plane. During shadowing, the orientational yaw control is dysfunctional in the Block II and IIA spacecraft and it can take up to 30 minutes afterwards to return to nominal behavior. The situation is much improved in the IIR and IIR-M satellites. Various approaches are taken by the IGS analysis centers to model the variations in signal phase caused by yaw motions, which otherwise can corrupt geodetic parameter estimates including clock values. Bar-Sever (1994) and colleagues have led in such efforts. Nevertheless, the success of modeling attempts for the older satellites especially is questionable given the relatively poor agreement of the clock solutions during these eclipse periods. Some groups omit much of the affected data, which together with frequently poor mutual agreement, can lead to gaps in the IGS clock products. It is difficult to estimate the size of associated clock errors, but they are likely to be much larger than during non-eclipse periods. Consequently, for much of our following analysis, we have tried to minimize use of data from these periods.

Another GPS-specific effect is the standard practice of using the dual-frequency observations to determine ionospheric delays including only the first-order correction term. The effect of neglecting the second-order contribution has been evaluated by Hernandez-Pajares et al. (2007) and found to affect the

satellite clock parameters most severely. The magnitude of the errors can reach or even exceed 1 cm, and varies with satellite position and time of day, being maximum during local daytime. Hernandez-Pajares et al. (2007) propose a convenient method to greatly mitigate the second-order ionosphere errors but it has not been routinely exploited yet.

Satellite laser ranging (SLR) observations of the two GPS satellites with retroreflector arrays, SVN35/PRN5 and SVN36/PRN6, provide a direct and independent validation of the IGS orbital quality, at least in the radial component that is most related to the satellite clocks. Urschl et al. (2007) report that the SLR ranges are shorter than the implied IGS orbital ranges by an average of −3 cm, with a mean standard deviation of 2.2 cm. These values correspond to light travel times of 75 to 100 ps and are consistent with the internal accuracy assessments above. At least some part of the SLR range bias could be caused by remaining errors in the measured positions of the retroreflectors relative to the GPS transmit antennas, which have been revised numerous times. More importantly, though, Urschl et al. (2007) also show that the SLR residuals have systematic patterns depending on the direction and orientation of the sun with respect to satellite orbital planes.

The latter results from Urschl et al. (2007) confirm the suspected significance of systematic once-per-revolution orbital errors and demonstrate that those are largest during eclipse seasons when the satellites in a given orbital plane pass through the Earth's shadow twice daily. (For reference, Agnew and Larson [2007] report an average GPS period of about 11.9659 hours.) Colombo (1989) already showed that unmodeled accelerations on an Earth-orbiting satellite tend to produce errors that are harmonics of the orbital period in each of the orthogonal components of a satellite-centered frame. Beutler et al. (1994) exploited this idea to develop an empirical representation for GPS orbital variations due to solar radiation pressure (SRP). This "extended CODE orbit model" consists of the usual six satellite state parameters together with offset and once-per-rev sine and cosine parameters in each direction towards the sun, along the solar panel axis, and orthogonal to the other two, for a total of up to nine SRP nuisance parameters. This model form and its variants have been widely influential and related developments are implemented operationally by most IGS groups.

Taken together, these observations and considerations suggest that the internal precision of IGS orbits and clocks is near 1 cm (33 ps) rms most of the time. However, the true accuracy (outside eclipse periods) is probably about three times poorer and very likely more systematic than random. Strong harmonics of the 12-hour orbital period are to be expected and errors may be correlated between orbits and clocks. At other time intervals, random observational noise, and stochastic oscillator and unmodeled ionospheric variations must also contribute. Note that if the orbit-related errors are predominantly sinusoidal, then a 3 cm (100 ps) rms error corresponds to an amplitude of 4.5 cm (150 ps).

## RELATIVISTIC EFFECTS

In order to ease comparisons and use with ground-based clocks, the GPS satellite clocks are treated in a way that aligns them in frequency (but not phase) approximately with terrestrial time (TT), which is authoritatively realized, apart from an offset, by the Coordinated Universal Time (UTC) scale formulated at the Bureau International des Poids et Mesures (BIPM) from an ensemble of many globally distributed AFSs at national timing laboratories. The GPST internal timescale is thus also a realization of TT, aligned in long-term frequency to UTC. Apart from the accumulated number of leap seconds, which GPST does not include, the two timescales have differed by less than 40 ns since July 1998.

Due to the relative motions between the GPS satellites and ground observers (special relativistic time dilation) and differences in gravitational potential (general relativity), a frequency offset has been applied to the onboard clock oscillators to align them approximately to TT. This first-order correction assumes nominal orbital elements. GPS users are expected to account for the second-order effects of non-circular orbits in their processing of observational data by applying a correction of magnitude $2(\mathbf{r} \cdot \mathbf{v})/c^2$, where r

is the satellite position vector, v its velocity, and *c* is the speed of light. Details are provided in IS-GPS-200 (GPS ICD-200 2006).

In addition to these conventional GPS treatments, the IERS Conventions recommend dynamical relativistic corrections to the satellite accelerations; see Chapter 10, equation (1) (McCarthy and Petit 2004). The primary effect is the Schwarzschild term, which affects GPS orbits by about 4 mm radially (U. Hugentobler, Astronomical Institute, University of Berne, Switzerland, personal communication, 2007, for this and following quantitative estimates). The Lense-Thirring precession (frame dragging) is about two orders of magnitude smaller than the Schwarzschild term for GPS, mainly causing a rotation of the orbit nodes by about −4 microarcseconds per day. The DeSitter (geodesic) precession is about one order smaller than the Schwarzschild effect for GPS, also mainly causing a rotation of the orbit nodes by about 50 microarcseconds per day. Neglect of the Earth's oblateness in these corrections introduces an error only at the micrometer level for GPS. The coordinate time of propagation effect of general relativity, including the gravitational delay (or "gravitational bending"), should be accounted for according to IERS Conventions 2003, Chapter 11, equation (17).

These conventional treatments provide a self-consistent dynamical framework that is accurate to 1 mm or better. However, the second-order model to relate moving GPS and TT clocks neglects smaller effects that are marginally observable (Kouba 2004). The most important of these is due to deviations in the geopotential from perfectly spherical, especially its oblateness ($J_2$). Using both analytical and numerical integrations of the satellite equations of motion, Kouba (2004) estimated the oblateness effect to produce secular rate differences up to 0.2 ns/day and a 6-hour variation of about 0.07 ns, as viewed by a TT observer. A further 0.2 ns variation with 14-day period was also found. These differences represent approximation error in the conventional transformations for comparing GPS satellite and ground clocks, but they have no geodetic consequence as long as users conform to the same conventions. They are relevant to interpreting the satellite clock behaviors, in forming ensembles of satellite and ground clocks together, or whenever one interpolates or extrapolates the satellite clocks (with respect to a TT-like timescale).

## GPS SUB-DAILY CLOCK STABILITIES

The purpose of inter-comparing clocks is to characterize their performance so that they may be evaluated without systematic or environmental influences. A simple quadratic model is often employed to represent any offset in frequency between the two clocks being compared as well as any slowly varying drift in frequency. Random behavior of multiple power-law types (e.g., white phase noise, random walk phase noise, flicker noise, etc.) are observed in all clocks, many of which leave the usual classical variance statistic divergent. Therefore, a number of specialized statistics have been developed for the characterization of clocks which remain convergent for these common power-law noise processes, including the Allan deviation, the modified Allan deviation (MDEV), and the Hadamard deviation (IEEE 1999; Baugh 1971). In this way, the underlying random characteristics of the clock behavior can be visualized graphically without being obscured by the usual systematic trends. This has the particular advantage of emphasizing the power-law nature of the noise processes that usually dominate timing instabilities, and aids in their identification. For instance, a time series of pure white phase noise has an MDEV that varies as $\tau^{-3/2}$ where $\tau$ is the time interval, while flicker phase varies as $\tau^{-1}$ and random walk phase (or equivalently, white frequency noise) varies as $\tau^{-1/2}$. As a practical matter, most commonly available AFSs exhibit $\tau^{-1/2}$ noise over a large portion of the sub-daily range (Allan 1987).

Figure 1 shows the MDEV calculated from IGS Final 30-s satellite clocks active during the three weeks from 15 June to 5 July 2007. The constellation block (IIA, IIR, or IIR-M) and AFS (Cs or Rb) types are also indicated for each. In order to demonstrate the quality of the underlying IGS timescale, the corresponding deviations for five of the most heavily weighted tracking station clocks are included (based on 5-min samples). The local frequency standards used at these stations are: BRUS, Quartzlock CH1-75

active H-maser; HRAO, Oscilloquartz EFOS C passive H-maser; BREW, Sigma Tau passive H-maser; STJO, passive H-maser; and NRC1, Kvarz CH-175 active H-maser. In order to mitigate the effect of frequency drift, all data were first detrended by removing a second-order polynomial prior to calculating the MDEV. All the satellites have instabilities at least a factor of five greater than the H-maser ground stations over most of the sub-daily range. All clocks were referenced to the IGS Final timescale, IGST.

It is immediately evident that the satellite clock behaviors depend on AFS oscillator type as well as block type. The Block IIA Cs clocks have instabilities that vary as $\tau^{-1/2}$ (random walk phase) for $\tau$ up to a few thousand seconds. The IIA Rb clocks behave similarly but are up to nearly an order of magnitude more stable than the Cs clocks and display a flicker phase component for intervals shorter than about 100 s. (Note that one main advantage of Cs clocks is their better stability over times longer than shown here.) Even though the GPS-based geodetic time transfer method itself follows approximately the same $\tau^{-1/2}$ power-law trend (Ray and Senior 2003), this is unlikely to account for the $\tau^{-1/2}$ behavior of the IIA clocks since the IGS timescale is so much more stable. Rather, the GPS clocks and the IGS methods probably both possess noise processes having temporal correlations like a random walk.

The instabilities of the newer Block IIR and IIR-M Rb satellites are poorer than the older Rb models for intervals up to nearly 1000 s. At the shortest interval of 30 s, the MDEV varies approximately as $\tau^{-1/2}$, consistent with random walk phase noise. This quickly transitions to a power-law which varies as $\tau^{-1}$, consistent with flicker phase noise for intervals up to several thousand seconds. This high-frequency noise behavior of the IIR and IIR-M satellites has been attributed to phase meter noise (Wu 1997; Petzinger et al. 2003; Phelan et al. 2006) in the Time Keeping System (TKS). The TKS phase meter comparator operates at 600 MHz with samples every 1.5 s, each having an accuracy estimated to be 1.67 ns.

For averaging intervals around $10^4$ s most of the GPS satellites display more complex, non-power-law behavior. Based on numerical simulations, the large broad band of high deviations near 13,600 s is the response of the MDEV statistic to a 12-hour periodic signal. Conventional spectral analysis techniques are much better suited to investigate the periodic signals present in the GPS clocks, as done in the next section.

The performance of the satellite clocks during the development of GPS in Block I showed significant effects due to the thermal sensitivity of the Rb clocks. At that time significant performance variations were seen during the time the satellites were being eclipsed by the Earth's shadow. Rb clocks being very thermally sensitive exhibited significant performance variations that were not observed with the Cs clocks, which were expected to have little thermal sensitivity. Consequently, the Rb clocks were installed in the satellites atop a thermal controller which regulated the temperature of the Rb clock very precisely (J. White, Naval Research Laboratory, personal communication, 2007). The II and IIA Rb clocks used a similar mounting arrangement since they were of the same design as the Block I units. The II and IIA Cs clocks are not thermally controlled and the internal temperature varies along with the other internal electronics as determined by the thermal design of the satellite. The II/IIA satellites' internal temperatures vary approximately ±5 °C with the orbit period, while the IIR/IIR-M temperatures vary approximately ±2.5 °C (Wu 1996). The IIR/IIR-M Rb clocks are of the same design and operating parameters. Those units were designed specifically for use in GPS and are thermally controlled by multiple internal ovens. The dual crystal oscillators that determine the output of the TKS and therefore the satellite are also ovenized oscillators which should have little thermal sensitivity.

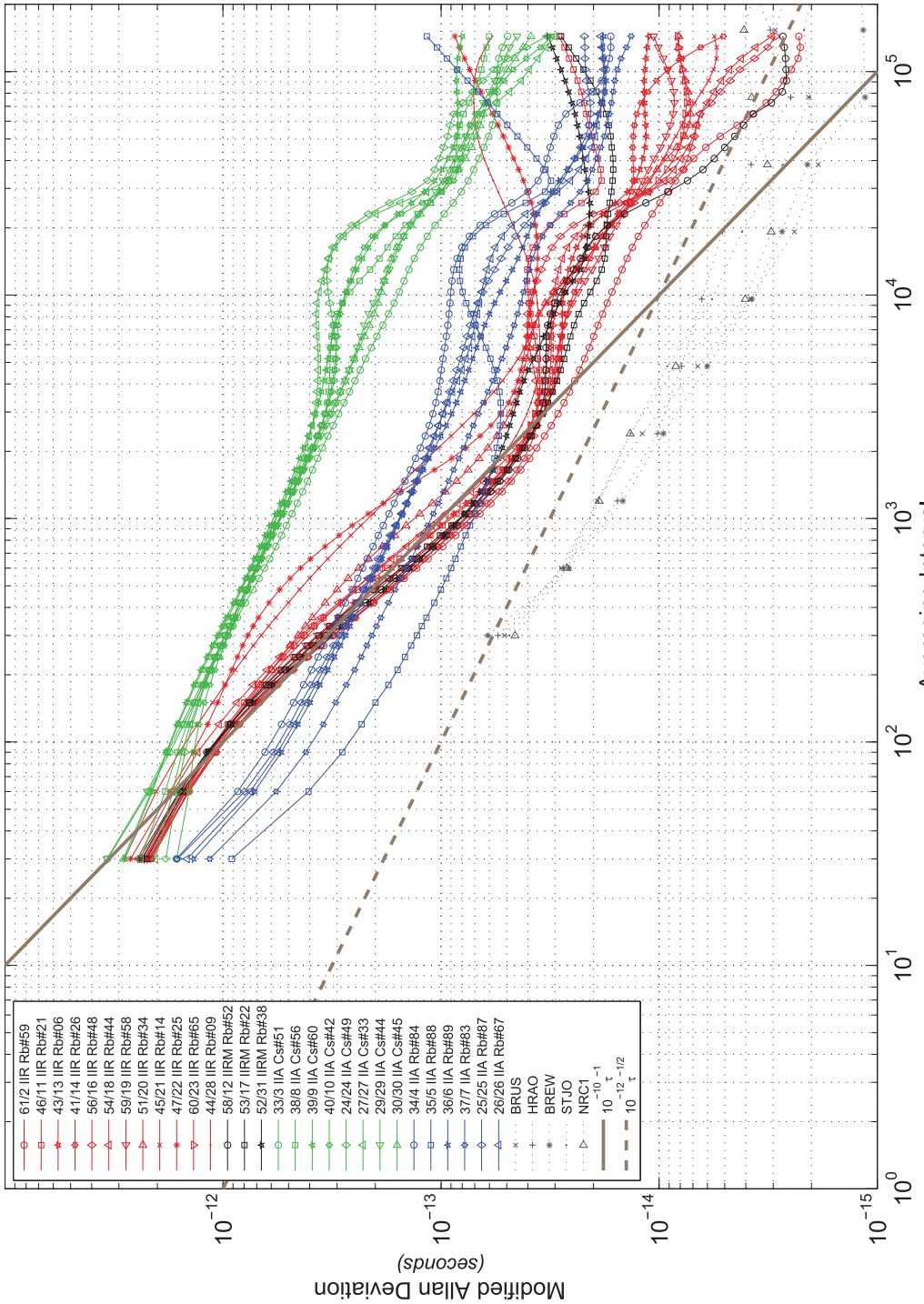


Fig. 1 — Frequency instability (modified Allan deviation) of each GPS satellite and five ground stations for the period 15 June 2007 (MJD 54266) to 5 July 2007 (MJD 54286) using IGS Final clocks. The five ground clocks are among the highest-weighted clocks making up IGST during this period. All data were detrended by removing a second-order polynomial prior to calculating the MDEV. For satellites, the legend indicates the Navstar vehicle number/PRN code, satellite block, and the frequency standard type and serial number for the standard active during this period. For reference, lines varying as $\tau^{-1}$, flicker phase, and $\tau^{-1/2}$, random walk phase, are drawn.

## ESTIMATION OF GPS CLOCK SPECTRA

Standard Fourier transform methods are used here to characterize and quantify the periodic variations in the IGS Final GPS clocks using two contrasting approaches. First, an aggregate assessment is made viewing the entire constellation overall to identify specific spectral peaks. Then, the temporal changes in those peaks for individual satellites are considered.

### Aggregate Constellation Spectrum

Data were first selected for each satellite in batches containing 150 contiguous days of 5-min data (43,200 points) during which no anomalous behavior (e.g., clock frequency resets or vehicle maneuvers) was observed. For satellites operating more than one AFS since 2000, multiple batches were selected giving a total of 50 batches: Block II, 9 batches for 5 SVNs; Block IIA, 26 batches for 18 SVNs; Block IIR, 12 batches for 12 SVNs; Block IIR-M, 3 batches for 3 SVNs. Sparse missing data points were interpolated (cubic spline), but only six batches required more than 20 points to be interpolated. Of these, the largest two had 53 and 71 interpolated values. After selection, each batch was detrended by fitting and removing a second-order polynomial. Using these detrended batches as input, an amplitude spectrum was calculated for each GPS clock and the ensemble averaged for the full GPS constellation, as shown in Fig. 2. Each satellite spectrum was calculated using a standard periodogram method with Blackman-Harris windowing (Harris 1978) to mitigate spectral leakage. The constellation-averaged spectrum was formed to emphasize common-mode spectral peaks by attenuating background random noise uncorrelated among the satellites.

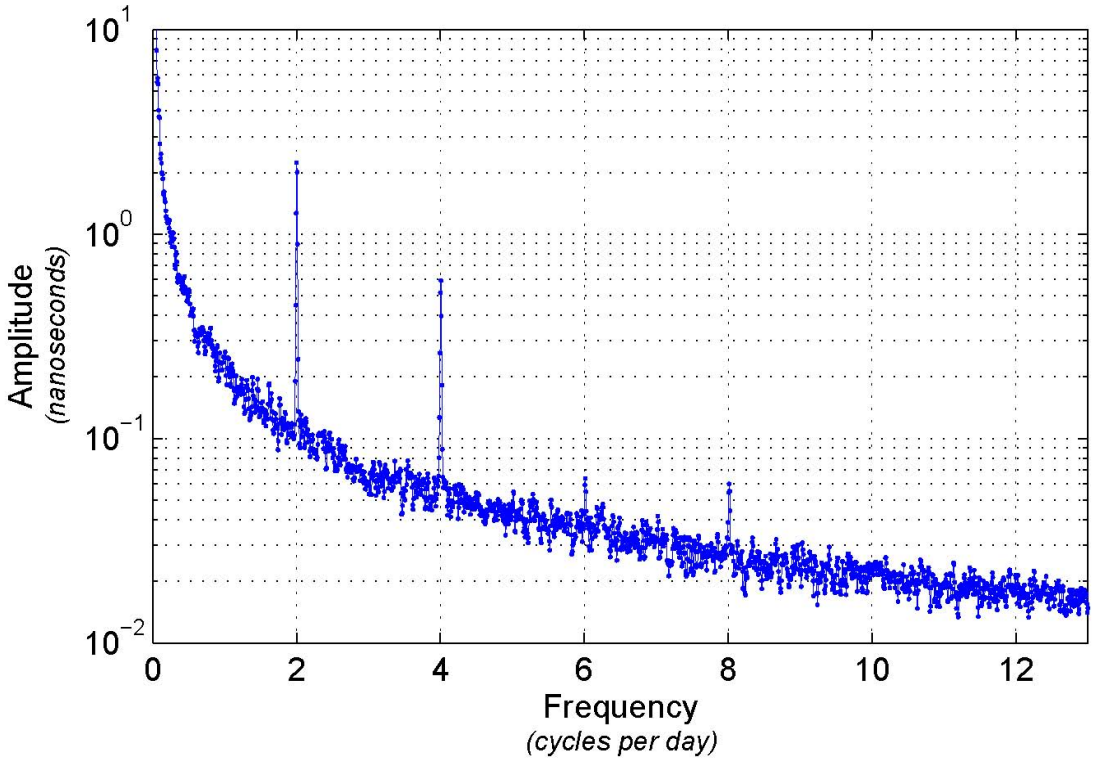


Fig. 2 — Averaged amplitude spectrum of the GPS constellation clocks. Individual satellite spectra were calculated by applying a standard periodogram with Blackman-Harris windowing to approximately 150 days of IGS Final clock data (detrended) for each satellite, referenced to IGST. The clock data for each satellite were detrended by fitting and removing a second-order polynomial prior to calculating its periodogram. The averaged spectrum was then obtained by averaging the individual satellite spectra at each Fourier frequency.

Pronounced 12-hour (2 cycles per day or cpd) and 6-hour (4 cpd) peaks stand out in the figure, along with lesser 4-hour (6 cpd) and 3-hour (8 cdp) variations. For a more precise determination of the peak frequencies, SVN15/PRN15 provided 1085 days of clean, continuous data (from 14 August 2003 to 2 August 2006). Using rectangular windowing (smallest frequency resolution) with a spectral resolution of 0.001 cpd, a periodogram (not shown) for SVN15/PRN15 (a Block II satellite) yields peaks at 2.003, 4.006, and 8.0115 cpd, or periods of 11.982 ± 0.006, 5.9910 ± 0.0015, and 2.9957 ± 0.0004 hours, respectively. No significant 4-hour (6 cpd) component was detected for this particular satellite. All the peaks can be understood as harmonics of a fundamental 11.982-hour signal. While this frequency is close to the average orbital period of the GPS satellites (namely, 11.9659 ± 0.0007 hours according to Agnew and Larson [2007]), the two differ in period by 0.016 ± 0.006 hours or 58 ± 22 s. (For comparison, a half-sidereal day is 11.9672 hours, which is about 9.7 s longer than the mean orbital periods; see Agnew and Larson [2007].) Since the most natural explanation for the twice-daily clock variations is insolation, thermal, or other environmental changes driven by the orbital motion, a close correspondence in the periods is expected.

In the event that SVN15 is not fully representative of the entire constellation, a more comprehensive verification has been sought. The longest possible spans of uninterrupted data were assembled for all satellite-clock pairs and a Fourier spectrum computed for each. The individual spectral resolutions were mostly 0.00203 cpd but ranged up to 0.00626 cpd in the worst case. For the 86 usable data sets available, the mean frequency of the 12-hour peak is 2.0029 ± 0.0005 cpd. Differential weighting has been applied here based on the frequency resolution of each individual spectrum. We thus conclude that the fundamental GPS clock harmonic has a period of 11.9826 ± 0.0030 hours. This differs from the mean orbital period by 60 ± 11 s. We cannot account for the apparent discrepancy, but it seems to be robust.

The analyses done here cannot be considered definitive for the smaller spectral peaks near 4, 6, and 8 cpd because of the risk of possible artificial peaks in the periodograms generated from the high low-frequency power. This concern is addressed in the next section.

**Temporal Variation of GPS Spectral Peaks**

In order to gauge how the amplitudes of spectral peaks for individual GPS clocks vary over time, spectra were next calculated over moving 20-day batches using all available data for each satellite since 2000. For each 20-day batch of 5-min samples a standard periodogram with Blackman-Harris windowing was determined. Successive batches overlapped by 10 days. Four separate periodograms were computed for each batch to determine sequentially the amplitudes of the 12-hour, 6-hour, 4-hour, and 3-hour peaks using the following procedure. First, the batches were detrended by fitting and removing a second-order polynomial. Next, a periodogram was calculated for the detrended batch and the amplitude corresponding to the 12-hour frequency recorded. Then a 12-hour sinusoid was fitted and removed from the detrended batch to produce a newly detrended batch to serve as input into a second periodogram calculation. The amplitude for a 6-hour frequency was then determined from the output of the second periodogram. A 6-hour sinusoid was next fitted and removed, and a third periodogram calculated to estimate a 4-hour amplitude, and so forth until finally an amplitude at 3-hour period was produced. The successive removal of longer-period, higher-power peaks was done to minimize the potential of spurious harmonics being generated at the higher frequencies. The results of this analysis for SVN27/PRN27 (a Block IIA satellite) are shown in Fig. 3. The results for the entire constellation are summarized in Table 1, where values are calculated separately over periods during which different AFSs operated. The Appendix contains the result of the above analysis for each SVN where IGS data were available (since November 2000).

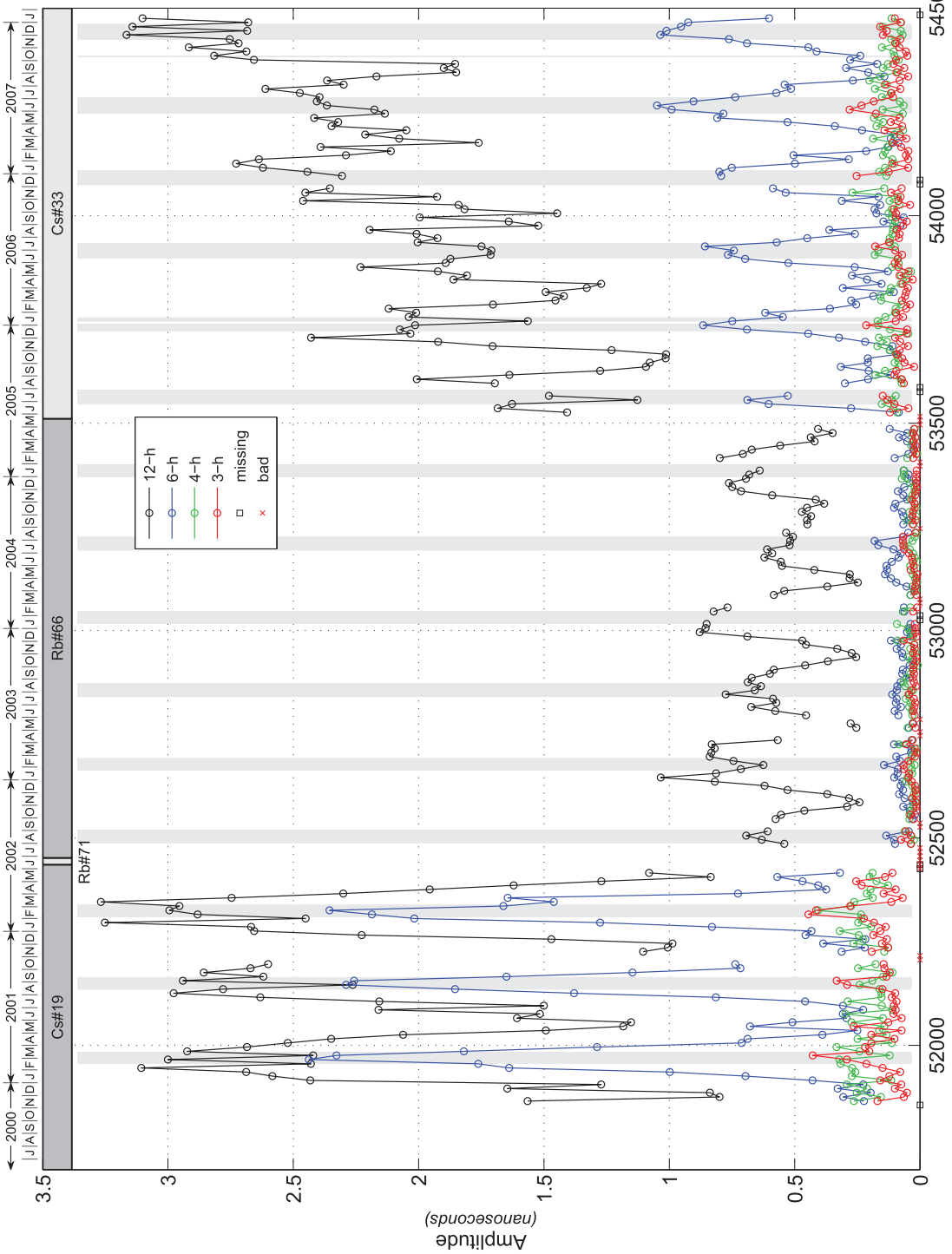


Fig. 3 — Time-varying amplitudes of the 12-hour (black), 6-hour (blue), 4-hour (green), and 3-hour (red) periodic variations in the IGS Final clock estimates for SVN27/PRN27 (Block IIA), referenced to the IGS Final timescale IGST. Shown across the top of the plot is the clock type and serial number of the frequency standard active during that period. Vertical shaded regions show periods during which the vehicle was eclipsed by the Earth.

Table 1 — Summary of the Average Amplitudes of the 12-, 6-, 4-, and 3-hour Periodics for Each GPS Satellite Clock

| **SVN/PRN** | **Block/Clock** | **# 20-day batches** | **12-h** *mean/rms* | **6-h** *mean/rms* | **4-h** *mean/rms* | **3-h** *mean/rms* |
|---|---|---|---|---|---|---|
| 13/2 | II/Cs #14 | 103 | 1.08/0.39 | 0.44/0.28 | 0.14/0.05 | 0.13/0.04 |
| 15/15 | II/Cs #17 | 128 | 1.75/0.30 | 0.40/0.18 | 0.15/0.05 | 0.12/0.05 |
| 17/17 | II/Cs #25 | 11 | 0.97/0.38 | 0.84/0.24 | 0.21/0.07 | 0.16/0.06 |
| | II/Rb #44 | 7 | 0.90/0.14 | 0.33/0.10 | 0.06/0.03 | 0.09/0.04 |
| | II/Rb #48 | 45 | 0.66/0.10 | 0.12/0.04 | 0.04/0.01 | 0.03/0.01 |
| 19/19 | II/Cs #27 | 14 | 0.67/0.26 | 0.55/0.44 | 0.29/0.11 | 0.20/0.11 |
| 21/21 | II/Cs #10 | 38 | 1.14/0.28 | 0.36/0.14 | 0.17/0.07 | 0.12/0.03 |
| 22/22 | IIA/Rb #54 | 13 | 0.42/0.17 | 0.06/0.03 | 0.03/0.01 | 0.01/0.00 |
| | IIA/Rb #78 | 28 | 0.67/0.24 | 0.13/0.05 | 0.04/0.01 | 0.03/0.01 |
| | IIA/Cs #28 | 8 | 5.42/1.36 | 1.33/0.70 | 0.25/0.10 | 0.27/0.11 |
| 23/23 | IIA/Cs #36 | 96 | 5.83/0.77 | 1.34/0.80 | 0.25/0.11 | 0.21/0.10 |
| 24/24 | IIA/Cs #49 | 204 | 1.68/0.38 | 0.28/0.15 | 0.12/0.04 | 0.09/0.03 |
| 25/25 | IIA/Cs #20 | 175 | 0.53/0.19 | 0.26/0.12 | 0.12/0.04 | 0.09/0.03 |
| | IIA/Rb #87 | 20 | 0.30/0.08 | 0.10/0.04 | 0.05/0.02 | 0.03/0.01 |
| 26/26 | IIA/Rb #67 | 222 | 0.40/0.09 | 0.10/0.04 | 0.04/0.02 | 0.03/0.02 |
| 27/27 | IIA/Cs #19 | 54 | 2.15/0.73 | 0.94/0.71 | 0.21/0.07 | 0.17/0.09 |
| | IIA/Rb #66 | 91 | 0.57/0.18 | 0.07/0.03 | 0.04/0.02 | 0.03/0.02 |
| | IIA/Cs #33 | 73 | 1.90/0.42 | 0.40/0.27 | 0.12/0.04 | 0.09/0.05 |
| 29/29 | IIA/Rb #73 | 170 | 0.49/0.12 | 0.10/0.04 | 0.04/0.02 | 0.03/0.02 |
| | IIA/Rb #74 | 11 | 0.95/0.06 | 0.13/0.03 | 0.02/0.01 | 0.03/0.01 |
| | IIA/Cs #44 | 10 | 0.62/0.13 | 0.48/0.14 | 0.13/0.05 | 0.08/0.03 |
| 30/30 | IIA/Cs #k3 | 27 | 0.84/0.32 | 0.22/0.15 | 0.08/0.03 | 0.06/0.02 |
| | IIA/Rb #72 | 140 | 0.36/0.13 | 0.10/0.04 | 0.03/0.02 | 0.02/0.01 |
| | IIA/Cs #45 | 37 | 0.58/0.17 | 0.24/0.12 | 0.13/0.06 | 0.10/0.05 |
| 31/31 | IIA/Cs #41 | 50 | 1.85/0.51 | 1.05/0.60 | 0.19/0.08 | 0.16/0.07 |
| | IIA/Rb #76 | 81 | 0.52/0.19 | 0.14/0.06 | 0.06/0.02 | 0.04/0.02 |
| | IIA/Cs #41 | 10 | 2.46/0.89 | 1.58/1.23 | 0.26/0.10 | 0.25/0.10 |
| 32/1 | IIA/Cs #43 | 224 | 3.10/0.57 | 1.57/0.71 | 0.18/0.07 | 0.16/0.08 |
| 33/3 | IIA/Cs #48 | 189 | 0.89/0.23 | 0.42/0.24 | 0.11/0.04 | 0.10/0.04 |
| | IIA/Rb #69 | 4 | 0.60/0.17 | 0.11/0.07 | 0.03/0.01 | 0.05/0.04 |
| | IIA/Cs #51 | 16 | 1.11/0.41 | 0.20/0.04 | 0.12/0.04 | 0.08/0.03 |
| 34/4 | IIA/Rb #84 | 220 | 0.51/0.09 | 0.11/0.05 | 0.04/0.01 | 0.03/0.02 |
| 35/5 | IIA/Cs #32 | 83 | 1.33/0.41 | 0.59/0.36 | 0.18/0.05 | 0.16/0.07 |
| | IIA/Rb #70 | 10 | 0.33/0.11 | 0.11/0.06 | 0.04/0.04 | 0.03/0.04 |
| | IIA/Cs #50 | 66 | 1.39/0.54 | 0.28/0.19 | 0.12/0.04 | 0.10/0.05 |
| | IIA/Rb #88 | 50 | 0.58/0.17 | 0.08/0.06 | 0.03/0.02 | 0.02/0.02 |

(table continues)

Table 1 (continued) — Summary of the Average Amplitudes of the 12-, 6-, 4-, and 3-hour Periodics for Each GPS Satellite Clock

| **SVN/PRN** | **Block/Clock** | **# 20-day batches** | **12-h** *mean/rms* | **6-h** *mean/rms* | **4-h** *mean/rms* | **3-h** *mean/rms* |
|---|---|---|---|---|---|---|
| 36/6 | IIA/Cs #46<br>IIA/Rb #89 | 107<br>103 | 7.80/1.61<br>0.39/0.20 | 1.71/1.16<br>0.11/0.06 | 0.21/0.09<br>0.04/0.03 | 0.21/0.13<br>0.04/0.02 |
| 37/7 | IIA/Rb #83 | 219 | 0.54/0.17 | 0.08/0.06 | 0.03/0.03 | 0.02/0.02 |
| 38/8 | IIA/Rb #30<br>IIA/Cs #56 | 113<br>111 | 2.84/0.81<br>0.93/0.25 | 0.69/0.26<br>0.35/0.23 | 0.30/0.13<br>0.11/0.04 | 0.18/0.07<br>0.09/0.03 |
| 39/9 | IIA/Cs #58<br>IIA/Cs #60 | 167<br>54 | 0.89/0.28<br>1.41/0.28 | 0.43/0.27<br>0.39/0.20 | 0.12/0.04<br>0.12/0.04 | 0.10/0.04<br>0.11/0.05 |
| 40/10 | IIA/Cs #42 | 228 | 1.50/0.20 | 0.38/0.15 | 0.11/0.04 | 0.09/0.04 |
| 41/14 | IIR/Rb #26 | 223 | 0.12/0.04 | 0.05/0.02 | 0.01/0.01 | 0.01/0.01 |
| 43/13 | IIR/Rb #06 | 232 | 0.09/0.03 | 0.06/0.03 | 0.02/0.01 | 0.03/0.02 |
| 44/28 | IIR/Rb #09 | 236 | 0.09/0.04 | 0.07/0.03 | 0.01/0.01 | 0.01/0.01 |
| 45/21 | IIR/Rb #14 | 144 | 0.08/0.03 | 0.08/0.03 | 0.03/0.01 | 0.03/0.02 |
| 46/11 | IIR/Rb #21 | 237 | 0.28/0.04 | 0.06/0.02 | 0.03/0.01 | 0.01/0.00 |
| 47/22 | IIR/Rb #25 | 102 | 0.13/0.05 | 0.09/0.04 | 0.02/0.01 | 0.02/0.01 |
| 51/20 | IIR/Rb #34 | 232 | 0.08/0.03 | 0.08/0.04 | 0.02/0.01 | 0.02/0.01 |
| 54/18 | IIR/Rb #44 | 221 | 0.26/0.06 | 0.08/0.04 | 0.02/0.01 | 0.02/0.01 |
| 56/16 | IIR/Rb #48 | 154 | 0.20/0.07 | 0.12/0.06 | 0.02/0.01 | 0.02/0.01 |
| 59/19 | IIR/Rb #58 | 115 | 0.09/0.04 | 0.10/0.05 | 0.01/0.01 | 0.02/0.01 |
| 60/23 | IIR/Rb #65 | 104 | 0.09/0.03 | 0.07/0.03 | 0.02/0.01 | 0.02/0.01 |
| 61/2 | IIR/Rb #59 | 87 | 0.07/0.03 | 0.04/0.02 | 0.02/0.01 | 0.01/0.00 |
| 52/31 | IIR-M/Rb #38 | 27 | 0.11/0.03 | 0.07/0.03 | 0.01/0.01 | 0.02/0.01 |
| 53/17 | IIR-M/Rb #22 | 59 | 0.10/0.04 | 0.08/0.02 | 0.01/0.00 | 0.02/0.01 |
| 58/12 | IIR-M/Rb #52 | 21 | 0.14/0.03 | 0.09/0.04 | 0.01/0.00 | 0.01/0.01 |

Blue values indicate > 0.7 correlation with Earth eclipse.
The values in this table were calculated using a standard periodogram approach with Blackman-Harris windowing over successive 20-day batches. The amplitudes for each 20-day batch were then averaged to obtain the mean and rms for a given clock.

Inspection of the temporal amplitude variations for each satellite reveals the following general patterns by block type:

- Block II – While only a few satellites with robust clock data are available, amplitudes of the 12-hour peak generally vary seasonally with the twice-yearly eclipsing cycle from about 0.5 to 1.0 ns midway between eclipses up to 1.5 to 2.5 ns in eclipse. The 6-hour peaks are correlated with the 12-hour eclipse variations but with amplitudes between 0.2 and 1.5 ns. The 4- and 3-hour peaks do not follow the eclipsing cycle but vary in a noise-like way with amplitudes between about 0.1 and 0.2 ns.

- Block IIA – These satellites have some of the largest 12-hour variations, up to about 8 ns, but amplitudes for others are only about 0.3 ns. There is a general tendency to track the eclipsing season with the highest 12-hour signals during eclipse. However, a few satellites have the opposite behavior (SVN23/PRN23, SVN32/PRN1, SVN38/PRN8) and others have no discernible correlation (SVN25/PRN25, SVN29/PRN29, SVN33/PRN3, SVN34/PRN4, SVN40/PRN10). The 12-hour amplitude grows with time for some satellites (SVN23/PRN23, SVN24/PRN24, SVN27/PRN27 for its latest Cs clock, SVN32/PRN1, SVN36/PRN6), all of which are equipped with Cs AFSs—however, not all Cs clocks show this tendency. The 12-hour levels usually differ by AFS type, with Cs clocks having larger signals than the Rb clocks on the same satellite, except for SVN38/PRN8 which is opposite. The 6-hour amplitudes in the IIA Cs satellites are maximum during eclipse season, but the Rb clocks show no regular behavior and the signals are markedly smaller. The 4- and 3-hour variations show only limited correlations with eclipse season and just for the Cs clocks; variations for the Rb clocks are invariably smaller.

- Block IIR – The 12-hour peaks of the IIR satellites are all below the levels of the older blocks, from about 0.1 to 0.3 ns. The only obvious correlation with eclipse season is for SVN56/PRN16, which has peak amplitudes during eclipses. The 6-hour amplitudes range from about 0.05 to 0.12 ns, in some cases being quite similar in magnitude to the 12-hour peaks. There may be a general correlation with eclipses but it is most clear for SVN51/PRN20, SVN54/PRN18, and SVN56/PRN16, whereas SVN46/PRN11 seems to be weakly anti-correlated. The 4- and 3-hour peaks are very small, below 0.04 ns in both cases, and featureless.

- Block IIR-M – Being the newest block of satellies with only three on orbit, the available data are sparse. The peaks have amplitudes of about 0.12, 0.08, 0.01, and 0.02 ns for the 12-, 6-, 4-, and 3-hour signals, respectively. Temporal variations generally follow no apparent patterns but the 3-hour peaks are correlated with eclipse seasons for a third of the satellites.

Figure 4 shows the dispersion in the average amplitudes of the 6-, 4-, and 3-hour peaks for the various satellite clocks versus the corresponding 12-hour amplitudes. The different block types are distinguished. There is a general correlation in the magnitudes of the spectral peaks with the IIA satellites attaining the largest values followed by the Block II clocks. The IIR and IIR-M peaks are smallest and are not correlated in magnitude in the same way as the II and IIA clocks (see figure insets).

Also indicated in Fig. 4 for comparison is our previous estimate of the upper limit for systematic orbital error contributions to the IGS clock values, a 12-hour sinusoid with 150 ps amplitude. For the 6-hour peak, the expected variation of about 70 ps due to neglect of the Earth's oblateness in the relativistic time transformation (Kouba 2004) is also marked. Contamination by orbit error can be confidently ruled out as an explanation of the 12-hour peaks for all the Block II and IIA clocks. The same cannot be said for the IIR and IIR-M clocks except that SVN46/PRN11, SVN54/PRN18, and SVN56/PRN16 must possess major non-orbit error sources for their 12-hour variations. The 6-hour variations have amplitudes in the expected range of the neglected relativistic effect for all the IIR and IIR-M clocks, as well as a number of the IIA clocks. But most of the satellites show excess 6-hour periodics, especially the Block II and many IIA clocks.

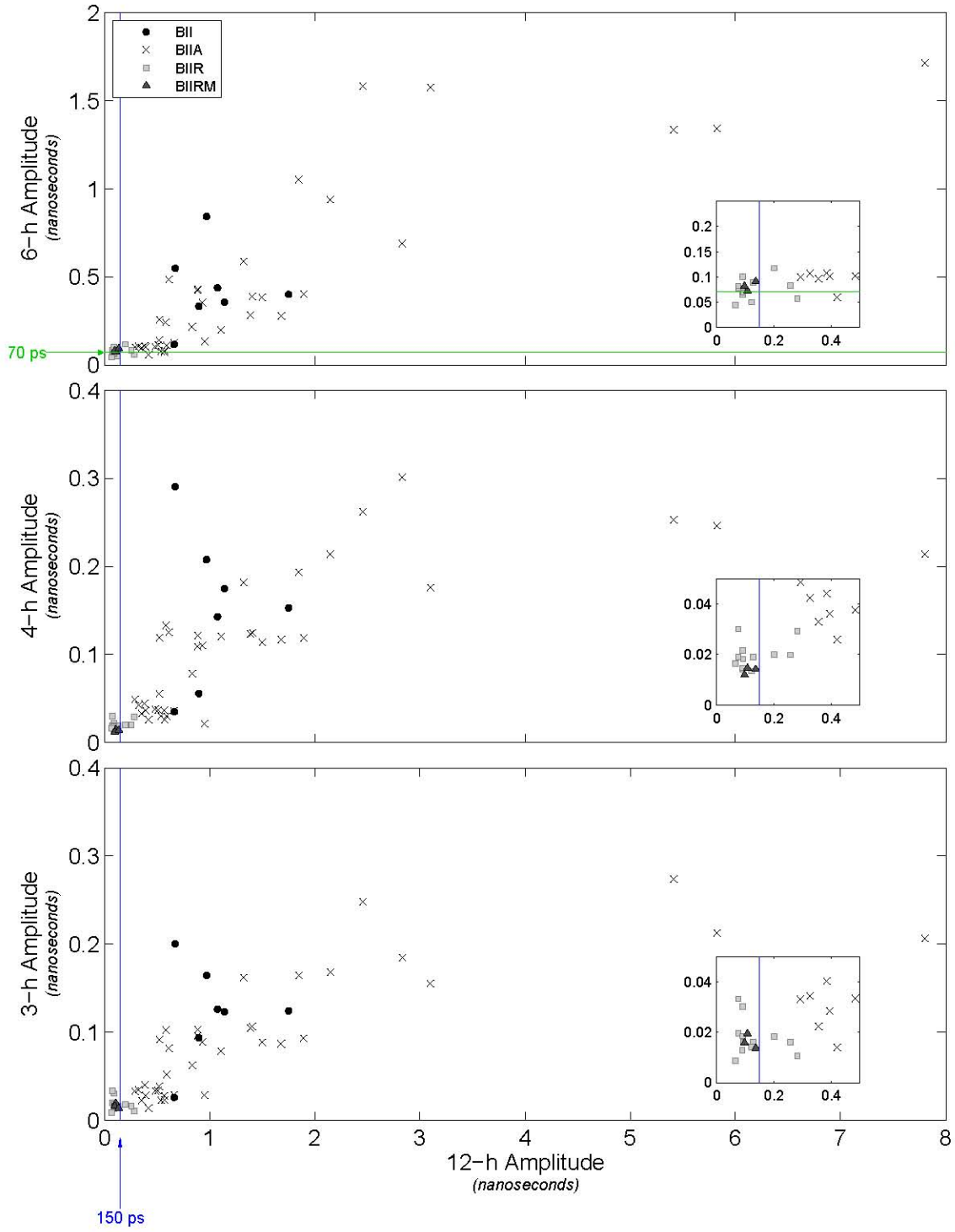


Fig. 4 — Correlations between the 12-hour amplitudes of the GPS constellation clocks and each of the 6-hour (top panel), 4-hour (middle panel), and 3-hour (bottom panel) amplitudes. For reference, the horizontal (green) line drawn at 70 ps in the 6-hour plot marks the expected variation due to neglect of $J_2$ in the relativistic time transformations, and the vertical line (blue) at 150 ps indicates our estimated upper limit for IGS clock errors if entirely of a 12-hour sinusoidal character and due to an equivalent 4.5 cm amplitude orbit error. The insets show expanded views of the distributions near the plot origins. The data for this plot are given in Table 1.

## IMPROVED GPS CLOCK MODELING

As discussed in the IGS Clock Product Accuracy section of this report, the IGS timescales consist of a weighted average among the ground and satellite clocks included in the IGS published products. However, the presence of periodic variations currently limits the weights of the GPS clocks in the ensemble to about 1–2% for the best GPS clocks. Recall that the weights are determined based on the instability of the clock for intervals less than a day. Also, because the current IGS Kalman filter is a two-state integrated (frequency + drift) frequency filter it does not contain any phase states. Therefore, the relatively large level of high-frequency noise present in the Block IIR clocks often results in complete filter resets for these clocks, removing them from the ensemble for a period. To improve this situation, modifications to the IGS timescale filter are currently under way which include new GPS satellite clock modeling. The new filter will contain at least four states for every clock, allowing for modeling of white noise in phase, random walk in phase, random walk in frequency, and random walk in drift. Four additional states are being added for the satellite clocks (a total of eight states) to compensate for the 6- and 12-hour periodics. With the addition of phase states and compensation of the periodics, we estimate that the weighting of the GPS satellite clocks in the IGS ensemble timescales should improve by about a factor of two.

## CONSEQUENCES FOR CLOCK INTERPOLATION AND PREDICTION

The results presented in the GPS Sub-Daily Clock Stabilities section of this report can be used to infer the performance of GPS clocks when predicted beyond the range of available observations or when interpolated for temporal spacings finer than provided in the IGS products. In doing this, we make several assumptions: that any underlying systematic variations are identified and modeled separately, that the observed stochastic variations are superpositions of standard power-law processes, and that we use the prediction formulas given in Allan (1987) and Allan and Hellwig (1978). Noise process superposition is clearly violated for the Block IIR Rb clocks. For these clocks, we determine the prediction errors by utilizing an average of the best and worst case prediction errors for the flicker and random walk phase power-laws. Finally, the prediction and interpolation errors for $\tau < 30$ s are extrapolated from the observed power-law behavior at 30 s.

Any underlying non-stochastic, systematic clock variations must be modeled deterministically and removed from the published clock values before prediction or interpolation, then restored afterwards. This should include the 12-hour and 6-hour harmonics discussed already. The errors in the tabulated IGS clock values or in the deterministic fitting process are not of interest here, only the added error due to extrapolation or interpolation of the stochastic time series. The usual procedure to find reasonable total uncertainties for the inferred values would be to combine the error of the nearest published clock value quadratically with the estimated interpolation or extrapolation error. It is furthermore assumed that the stochastic properties of the clocks during the interpolation or prediction region are the same as those during the characterization period. This is a very weak condition for interpolations since the clock conditions do not change significantly very often and can be easily detected. However, it can be a problem for predictions since an unexpected, uncharacteristic event is intrinsically not predictable. For this reason (and others), all real-time users should always make internal consistency checks regardless of the source of the satellite information or service.

With the above considerations, we determine the clock prediction errors for each satellite block as shown in Fig. 5. The solid lines show the results for the Block IIA Rb, IIA Cs, and IIR/IIR-M Rb clocks taking the mean instability for each group of satellites as representative. The range of variation among each set is illustrated by the associated “error bars.”

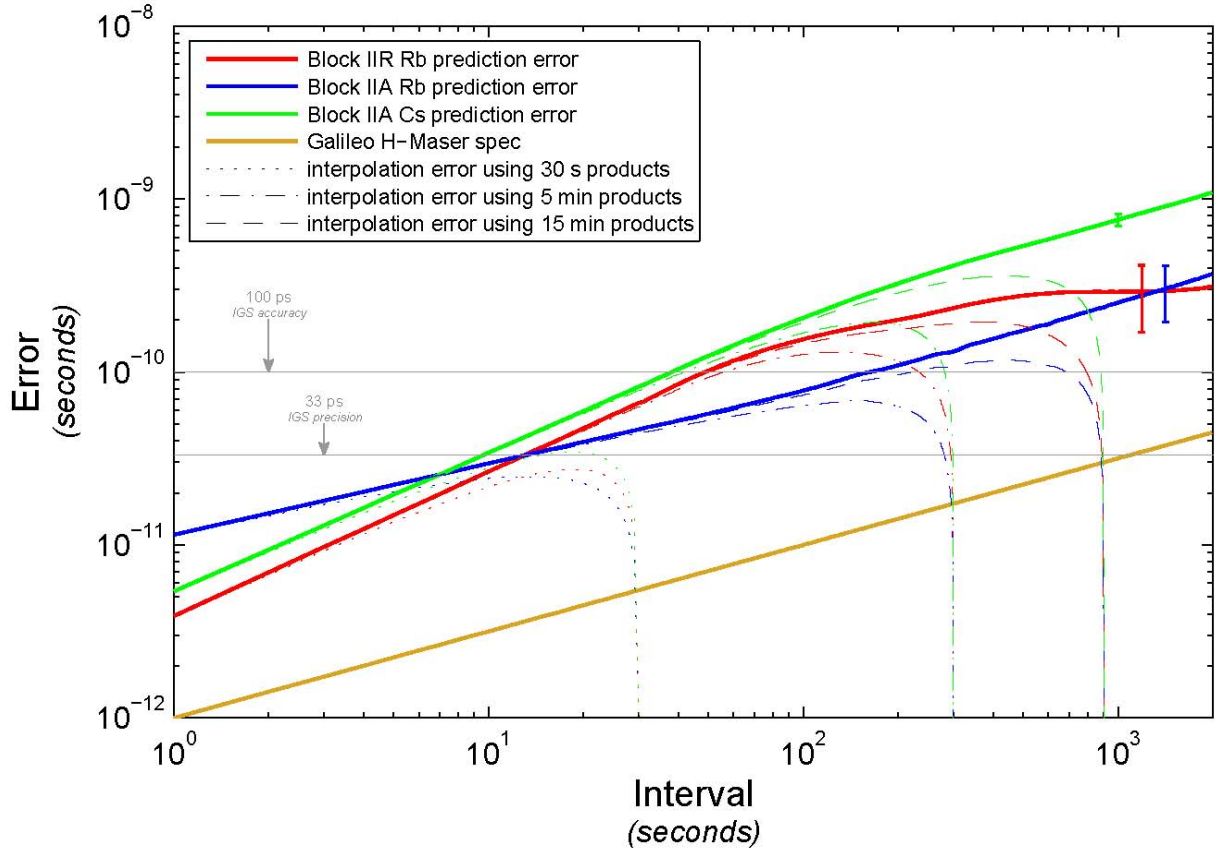


Fig. 5 — RMS time prediction and interpolation errors for the GPS Block IIA and Block IIR/IIR-M clocks, estimated using IGS Final 30-s products over the period 15 June 2007 (MJD 54266) to 5 July 2007 (MJD 54286). Bold solid lines indicate the mean prediction errors for each block/clock; a vertical "error bar" is shown on the far right of the plot to indicate the range of performances for the satellites in that block/clock type. Interpolation errors are also shown for tabulation spacings of 30 s (dotted), 5 min (dash-dotted), and 15 min (dashed). For comparison, the expected Galileo H-Maser prediction errors are shown, based on specifications given in Rochat et al. (2005).

Interpolation errors are smaller than the (one-sided) prediction errors for equal intervals because interpolation is essentially a two-sided prediction. At the midpoint between tabular clock values, the interpolation error is smaller than its corresponding prediction error by $1/\sqrt{2}$ . The general relationship is

$$\sigma_{\text{interp}}(t) = \sigma(t)\sqrt{\frac{T - t}{T}}$$

where $T$ is the interval between tabular points and $\sigma(t)$ is the growth in prediction error. This formula has been used in Fig. 5 to generate interpolation errors, shown as dotted, dash-dotted, and dashed lines. Three different interpolation intervals are considered for each clock type, corresponding to the density of current IGS clock products: 30 s for the IGS Final satellite clocks; 5 min for the IGS Rapid and Final clocks (both receivers and satellites); and 15 min for the satellite clocks in IGS SP3 orbit files. The interpolation errors approach zero at adjacent starting and ending values for each tabulation interval.

For comparison, the estimated precision (33 ps) and accuracy (100 ps) levels for IGS clocks are also indicated by constant lines in Fig. 5. (These should not be confused with the power-law inferences for the

satellite clocks and do not imply that the IGS clock errors are uncorrelated white noise. Indeed, the intrinsic IGS errors are correlated and would behave differently if averaged over various intervals.)

It can be seen that all satellite clock types can be interpolated between 30-s spacings with an added error that barely reaches the IGS precision level. For 5-min observational samples the interpolation error usually exceeds the IGS precision but only surpasses the level of the estimated accuracy for the IIR Rb (slightly) and IIA Cs (by up to a factor of two) clocks. For longer tabular spacings, the IIA Rb interpolations would add noise modestly exceeding the level of the IGS measurement errors, but IIR Rb and IIA Cs interpolations would be up to two to four times greater.

Alternatively, for users wishing to apply the existing IGS clock products with data rates higher than the available samplings, one could consider introducing differential satellite data weights based on the clock instabilities and their expected interpolation errors. This could be done by block and clock type or even based on the observed Allan deviations of individual satellites (which tend to remain unchanged for long periods). This procedure should give significantly better geodetic performance compared to equal weighting of all satellite clocks, although we have not yet tested the method.

The near-term clock predictions in Fig. 5 could be useful in the context of near-real-time operations where the latency of clock correction updates is an issue, for instance. To simulate prediction errors for intervals longer than about 2000 s would require a more careful consideration of changes in the noise processes of the satellite clocks. It is also likely that errors in extrapolating the deterministic systematic effects (such as variations in the amplitudes of the 12-hour and 6-hour periodics) will be important over spans of hours and longer. Between about 10 and 1000 s the IIA Rb satellites yield the smallest prediction errors. At shorter times, assuming no error in the extrapolation procedure described earlier, the IIR Rb and IIA Cs clocks can be predicted more accurately. Since all satellite prediction errors are below 100 ps for $\tau < 40$ s, it seems that a reasonable update lag interval for a near-real-time correction service should be around 50 s without suffering too much prediction error.

Included in Fig. 5 for comparison with the GPS prediction errors is the corresponding behavior of the planned Galileo passive H-maser based on published specifications (Rochat et al. 2005). We do not consider interpolation errors in this case since no published products are available yet. If the Galileo passive H-maser performs as expected, then it is clear that its satellite clocks could be predicted or interpolated up to about 1000 s with no discernible degradation compared to the current IGS product precision. Such clocks would in fact eliminate the need for the IGS to tabulate clock values at higher samplings and would allow users to adopt any data analysis rates they desire. However, before doing so, it will be necessary to evaluate the actual on-orbit Galileo performance carefully for any unexpected characteristics.

## CONCLUSIONS

The pervasiveness and prominence of the 12-hour and 6-hour periodics in most GPS clocks dictates that these variations should be explicitly modeled in all high-accuracy applications. This includes timescale formation and maintenance, interpolation of tabulated clock products for higher-rate GPS positioning, and predictions for real-time uses. Modeling will also suffice to overcome the effect at 6-hour periods due to the conventional neglect of the Earth's oblateness in time transformations and is more effective than directly modifying the relativistic modeling considering that other causes of 6-hour periodics are usually greater, often by large amounts. Even the GPS operational system would benefit by including these periodics in its own modeling and navigation products since the errors can exceed 2 m. Only in the most demanding applications should it be necessary to account for the variations with 4- and 3-hour periods, as their amplitudes rarely exceed 0.3 ns (9 cm).

We cannot conclusively identify the underlying cause of the GPS clock harmonics, although the observed link to orbital dynamics and the variability with clock type suggest an environmental coupling. The difference we find in the fundamental periods of the IGS clock harmonics and the mean GPS orbits of nearly 1 minute, and the tendency for the maximum amplitudes to occur during eclipse seasons suggest a loose coupling with orbit period such as would occur in the thermal balance of the satellite. That the Cs clocks are more strongly affected than the Rb clocks, whose thermal environment is tightly controlled, further supports this conclusion. The variations are invariably much smaller for the Block IIR and IIR-M satellites compared to earlier generations, but the periodics do not vanish.

After accounting for at least the 12- and 6-hour harmonics, together with the usual quadratic variations, it is possible to interpolate or extrapolate the residual stochastic clock time series with minimal degradation for all the satellites up to tens of seconds. Over longer intervals, prediction errors grow slowest for the IIA Rb satellites, up to about 1000 s, and grow fastest for the IIA Cs satellites.

In any future improved GPS clock systems, it would be highly beneficial to reduce the short-term noise of the Time Keeping System. For short-term performance comparable to the level expected for the Galileo H-masers, further reduction of the GPS clock instabilities would be necessary. If methods can be found to attenuate the GPS harmonics at the satellites, that would be useful, but modeling of these effects is probably similarly effective and does not require any understanding of the driving mechanisms.

## REFERENCES

Agnew, D.C., and K.M. Larson, 2007, "Finding the Repeat Times of the GPS Constellation," *GPS Solutions* **11**, 71-76. doi:10.1007/s10291-006-0038-4.

Allan, D.W., 1987, "Time and Frequency (Time-Domain) Characterization, Estimation, and Prediction of Precision Clocks and Oscillators," *IEEE Trans. Ultrason. Ferroelectr. Freq. Control* **34**(6), 647-654.

Allan, D.W., and H. Hellwig, 1978, "Time Deviation and Time Prediction Error for Clock Specification, Characterization, and Application," *Proceedings of the IEEE Position Location and Navigation Symposium (PLANS), San Diego, CA, 1978*, pp. 29-36.

Bar-Sever, Y.E., 1994, "New GPS attitude model," IGSMAIL #591, http://igscb.jpl.nasa.gov/mail/igsmail/1994/msg00166.html (accessed June 20, 2008).

Baugh, R.A., 1971, "Frequency Modulation Analysis with the Hadamard Variance," *Proceedings of the 25th Annual Symposium on Frequency Control, Atlantic City, NJ, 1971*, pp. 222-225.

Beutler, G., E. Brockmann, W. Gurtner, U. Hugentobler, L. Mervart, and M. Rothacher, 1994, "Extended Orbit Modeling Techniques at the CODE Processing Center of the International GPS Service for Geodynamics (IGS): Theory and Initial Results," *Manuscripta Geodaetica* **19**(B7), 367-387.

Beutler, G., J. Kouba, and T. Springer, 1995, "Combining the Orbits of the IGS Analysis Centers," *Bulletin Geodesique* **69**, 200-222.

Colombo, O.L., 1989, "The Dynamics of Global Positioning Orbits and the Determination of Precise Ephemerides," *J. Geophys. Res.* **94**, 9167-9182.

Gendt, G., and R. Schmid, 2005, "Planned Changes to IGS Antenna Calibrations," IGSMAIL #5189, http://igscb.jpl.nasa.gov/mail/igsmail/2005/msg00111.html (accessed 20 June 2008).

Griffiths, J., and J. Ray, 2007, "On the Accuracy of IGS Orbits," *Eos Trans. AGU* **88**(52), AGU Fall Meeting Suppl. 2007, Abstract G11A-03.

Harris, F.J., 1978, "On the Use of Windows for Harmonic Analysis with the Discrete Fourier Transform," *Proceedings of the IEEE* **66**, 51-83.

Hernandez-Pajares, M., J.M. Juan, J. Sanz, and R. Orus, 2007, "Second-Order Ionospheric Term in GPS: Implementation and Impact on Geodetic Estimates," *J. Geophys. Res.* **112**, B08417. doi:10.1029/2006JB004707.

IEEE, 1999, IEEE Standard Definitions of Physical Quantities for Fundamental Frequency and Time Metrology—Random Instabilities, IEEE Std 1139-1999, Institute of Electrical and Electronics Engineers, Inc., New York, NY.

IS-GPS-200, 2006, NAVSTAR GPS Space Segment/Navigation User Interfaces, Interface Specification IS-GPS-200, IRN-200D-001, U.S. Air Force GPS Wing, Headquarters, Space and Missile Systems Center, NAVSTAR GPS Joint Program Office, El Segundo, CA. Available at http://www.navcen.uscg.gov/gps/geninfo/IS-GPS-200D.pdf.

ITU, 1996, Definitions and Terminology for Synchronization Networks. ITU-T Recommendation G.810, International Telecommunication Union, Geneva.

ITU, 2002, Glossary and Definitions of Time and Frequency Terms. ITU-R Recommendation TF.686-2, International Telecommunication Union, Geneva.

Kouba, J., 2004, "Improved Relativistic Transformations in GPS," *GPS Solutions* **8**, 170-180.

Kouba, J., and T. Springer, 2001, "New IGS Station and Satellite Clock Combination," *GPS Solutions* **4**, 31-36.

McCarthy, D.D., and G. Petit, eds., 2004, *IERS Conventions (2003)*, IERS Technical Note 32, Verlag des Bundesamts für Kartographie und Geodäsie, Frankfurt am Main.

Petzinger, J., R. Reith, and T. Dass, 2003, "Enhancements to the GPS Block IIR Timekeeping System," in L. Breakiron, ed., *Proceedings of the 34th Annual Precise Time and Time Interval (PTTI) Systems and Applications Meeting, Reston, Virginia, 2002*, pp. 89-107 (U.S. Naval Observatory, Washington, DC).

Phelan, J., T. Dass, G. Freed, J. Rajan, J. D'Agostino, and M. Epstein, 2006, "GPS Block IIR Clocks in Space: Current Performance and Plans for the Future," in L. Breakiron, ed., *Proceedings of the 37th Annual Precise Time and Time Interval (PTTI) Systems and Applications Meeting, Vancouver, Canada, 2005*, pp. 19-25 (U.S. Naval Observatory, Washington, DC).

Ray, J.R., and K.L. Senior, 2003, "IGS/BIPM Pilot Project: GPS Carrier Phase for Time/Frequency Transfer and Time Scale Formation," *Metrologia* **40**, S270-S288.

Ray, J.R., and K.L. Senior, 2005, "Geodetic Techniques for Time and Frequency Comparisons Using GPS Phase and Code Measurements," *Metrologia* **42**, 215-232.

Rochat, P., F. Droz, P. Mosset, G. Barmaverain, Q. Wang, D. Boving, L. Mattioni, M. Belloni, M. Gioia, U. Schmidt, T. Pike, and F. Emma, 2005, "The Onboard Galileo Rubidium and Passive Maser, Status and Performance," *Proceedings of the 2005 IEEE International Frequency Control Symposium and Exposition, Vancouver, Canada*, pp. 26-32. doi:10.1109/FREQ.2005.1573898.

Schmid, R., P. Steigenberger, G. Gendt, M. Ge, and M. Rothacher, 2007, "Generation of a Consistent Absolute Phase-Center Correction Model for GPS Receiver and Satellite Antennas," *Journal of Geodesy* **81**(12), 781-798. doi:10.1007/s00190007-0148-y.

Senior, K., P. Koppang, and J. Ray, 2003, "Developing an IGS Time Scale," *IEEE Trans. Ultrason. Ferroelectr. Freq. Control* **50**, 585-593.

Urschl, C., G. Beutler, W. Gurtner, U. Hugentobler, and S. Schaer, 2007, "Contribution of SLR Tracking Data to GNSS Orbit Determination," *Advances in Space Research* **39**, 1515-1523.

Wu, A., 1997, "Performance Evaluation of the GPS Block IIR Time Keeping System," in L. Breakiron, ed., *Proceedings of the 28th Annual Precise Time and Time Interval (PTTI) Applications and Planning Meeting, Reston, Virginia, 1996*, pp. 441-453 (U.S. Naval Observatory, Washington, DC).

Zumberge, J.F., M.B. Heflin, D.C. Jefferson, and M.M. Watkins, 1997, "Precise Point Positioning for the Efficient and Robust Analysis of GPS Data from Large Networks," *J. Geophys. Res.* **102**, 5005-5017.

# Appendix

## TIME-VARYING SPECTRA FOR THE GPS CONSTELLATION

Figures A1 through A38 show the time-varying amplitudes of the 12-, 6-, 4-, and 3-hour periodic variations for each GPS SVN. Each point represents an amplitude obtained by calculating a simple periodogram with Blackman-Harris windowing on a 20-day batch of detrended clock data. The procedure used to calculate each amplitude was discussed in the Temporal Variation of GPS Spectral Peaks subsection of this report. Shown across the top of each plot is the clock type and serial number of the frequency standard active during the period depicted. Vertical shaded regions show periods during which the vehicle was eclipsed by the Earth.

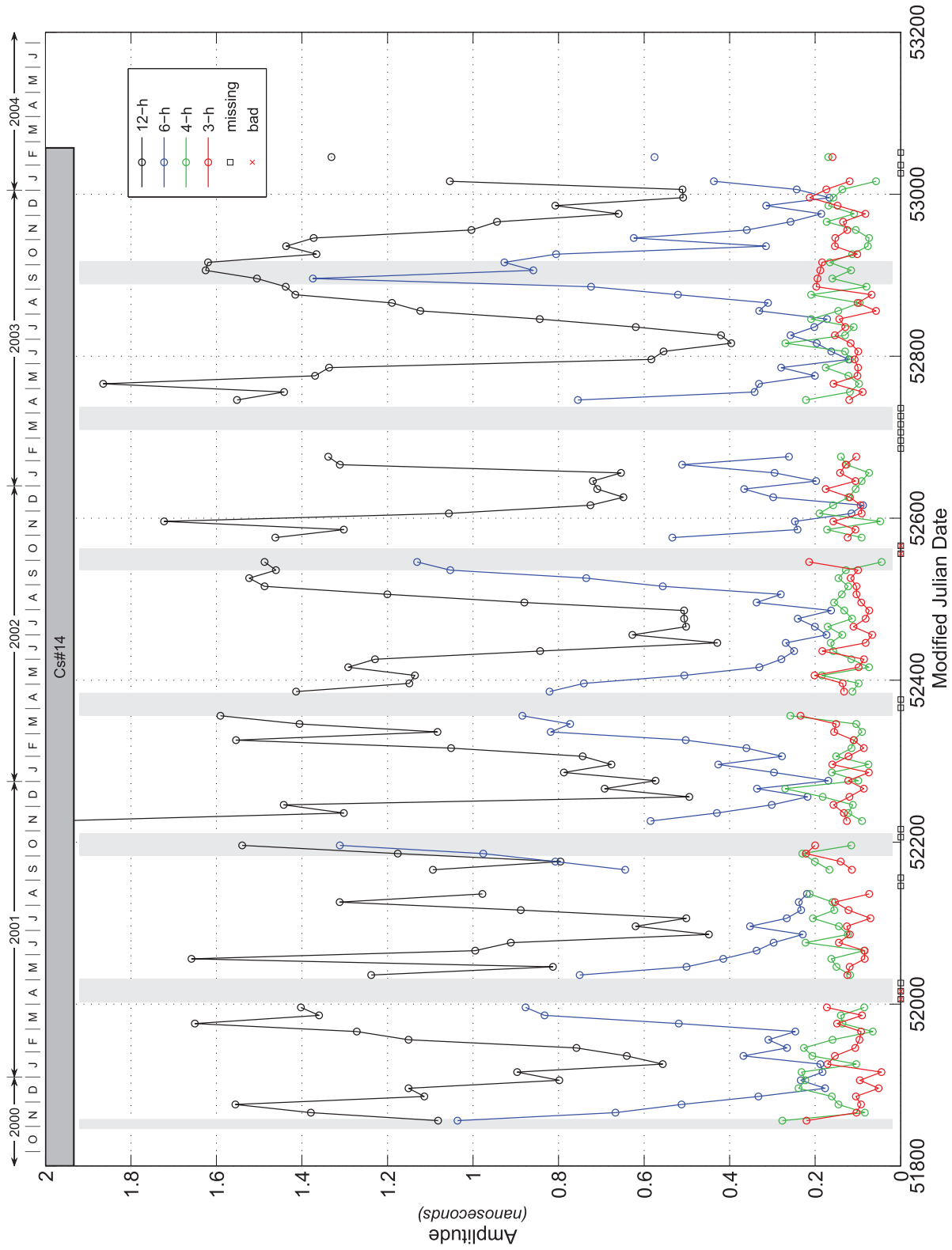


Fig. A1 — SVN13/PRN2 (Block II) time-varying amplitudes, 12-hour (black), 6-hour (blue), 4-hour (green), and 3-hour (red).

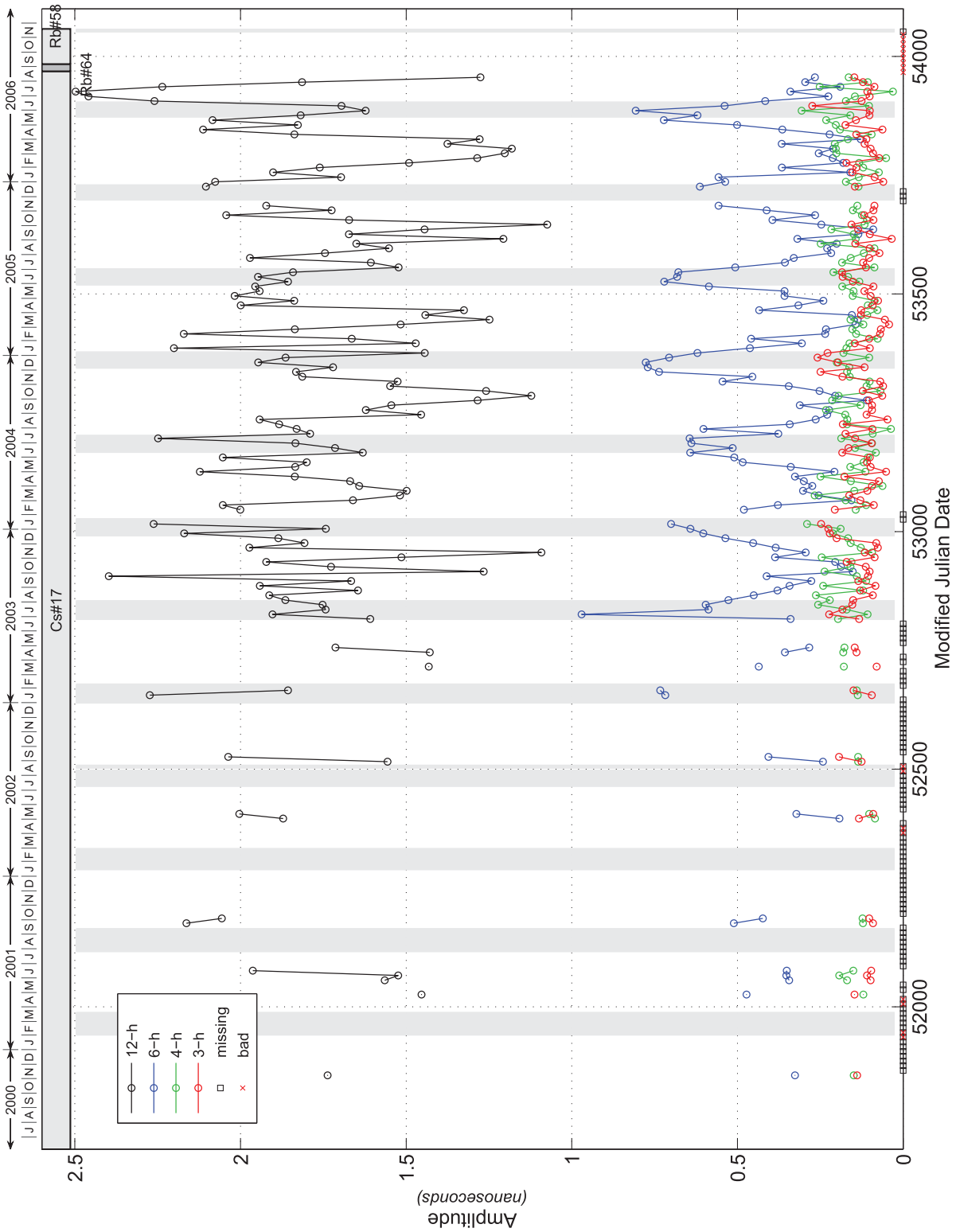


Fig. A2 — SVN15/PRN15 (Block II) time-varying amplitudes, 12-hour (black), 6-hour (blue), 4-hour (green), and 3-hour (red).

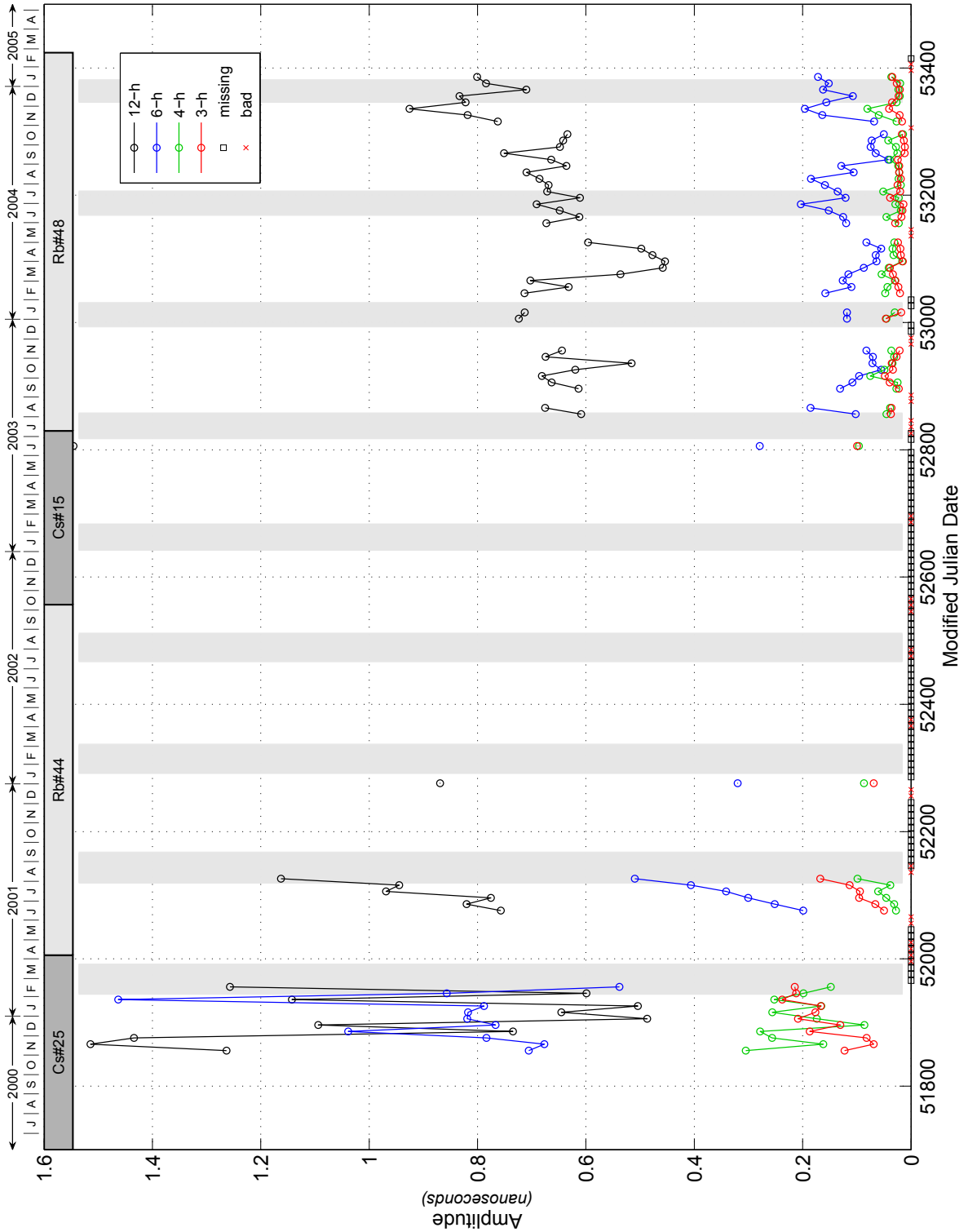


Fig. A3 — SVN17/PRN17 (Block II) time-varying amplitudes, 12-hour (black), 6-hour (blue), 4-hour (green), and 3-hour (red).

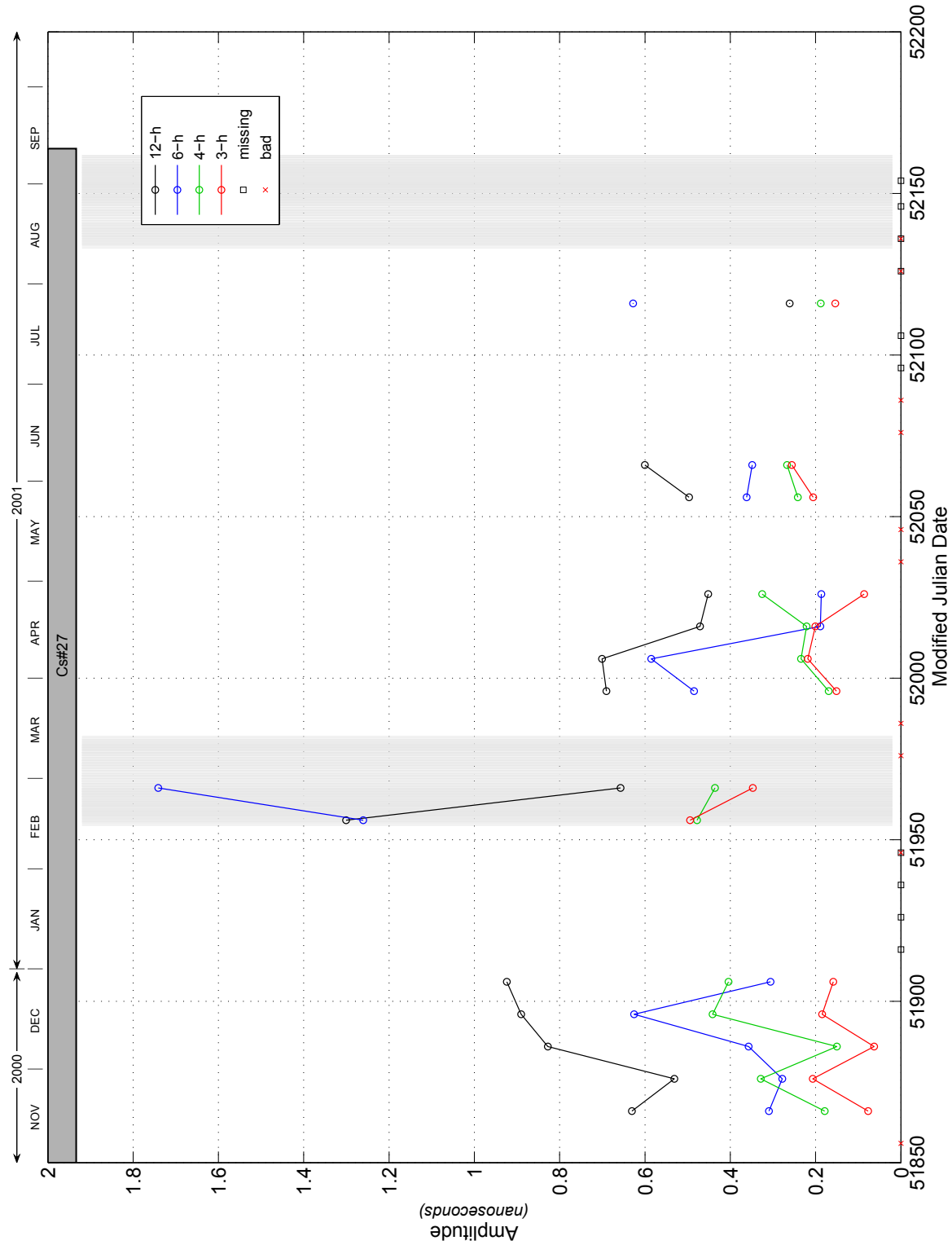


Fig. A4 — SVN19/PRN19 (Block II) time-varying amplitudes, 12-hour (black), 6-hour (blue), 4-hour (green), and 3-hour (red).

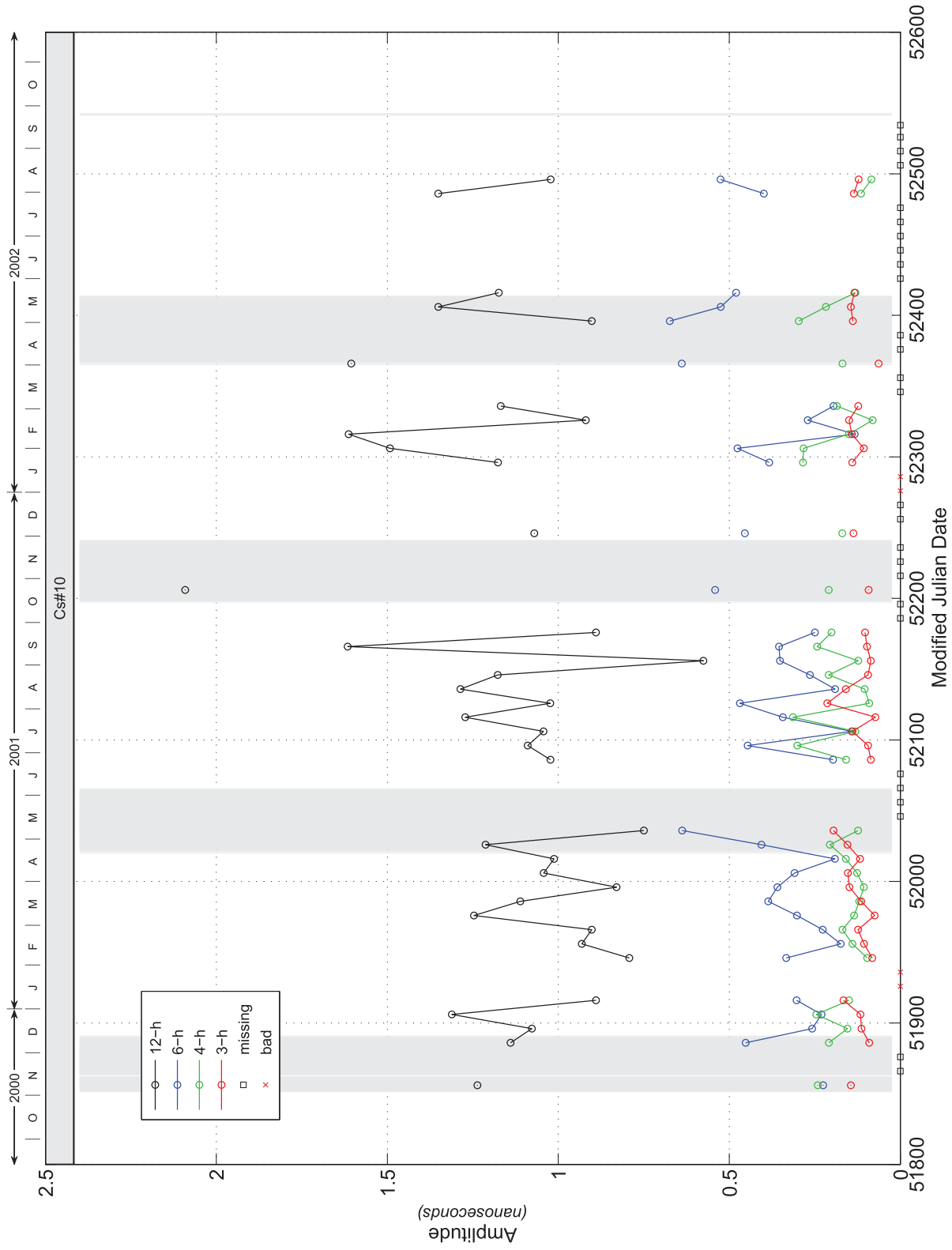


Fig. A5 — SVN21/PRN21 (Block II) time-varying amplitudes, 12-hour (black), 6-hour (blue), 4-hour (green), and 3-hour (red).

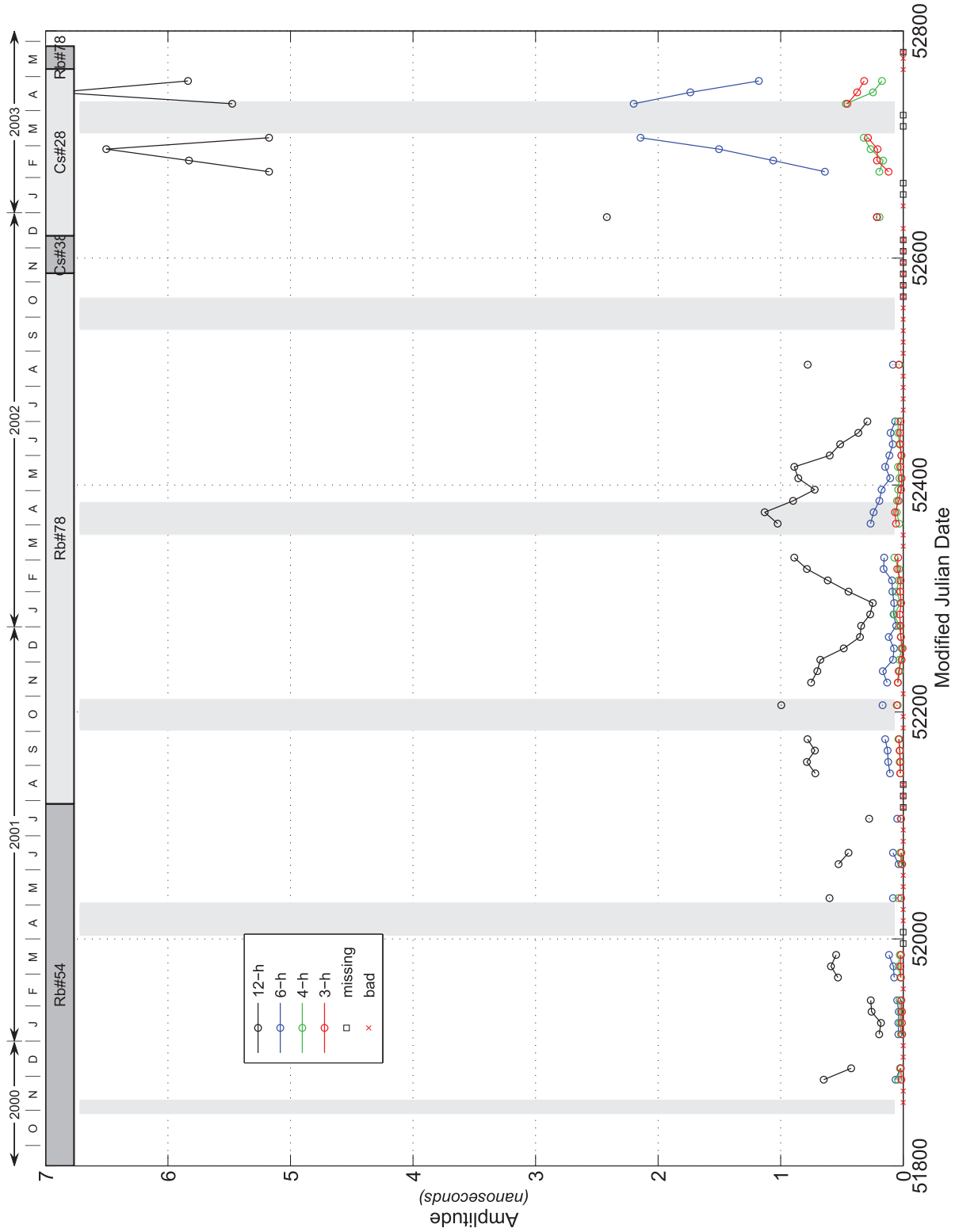


Fig. A6 — SVN22/PRN22 (Block IIA) time-varying amplitudes, 12-hour (black), 6-hour (blue), 4-hour (green), and 3-hour (red).

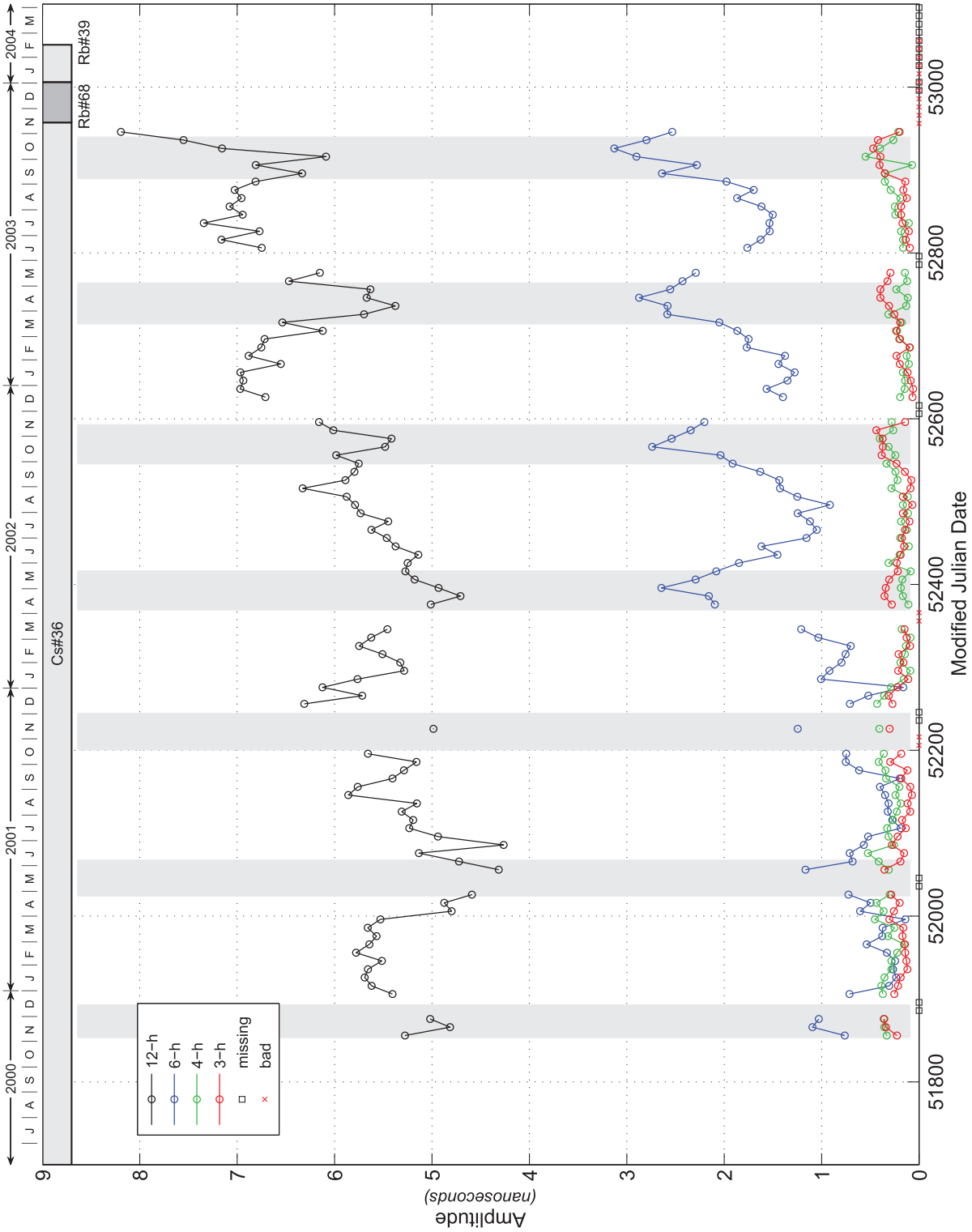


Fig. A7 — SVN23/PRN23 (Block IIA) time-varying amplitudes, 12-hour (black), 6-hour (blue), 4-hour (green), and 3-hour (red).

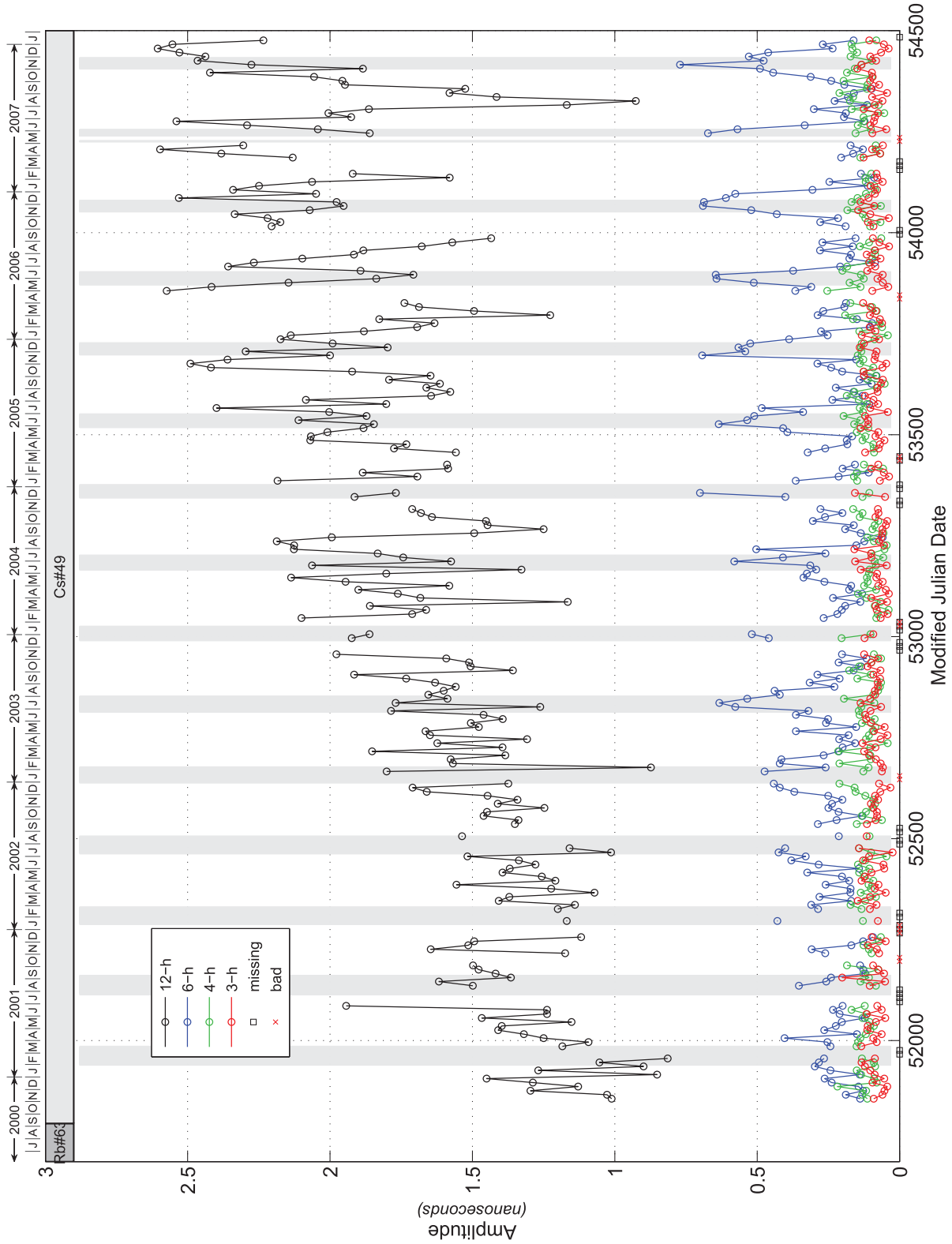


Fig. A8 — SVN24/PRN24 (Block IIA) time-varying amplitudes, 12-hour (black), 6-hour (blue), 4-hour (green), and 3-hour (red).

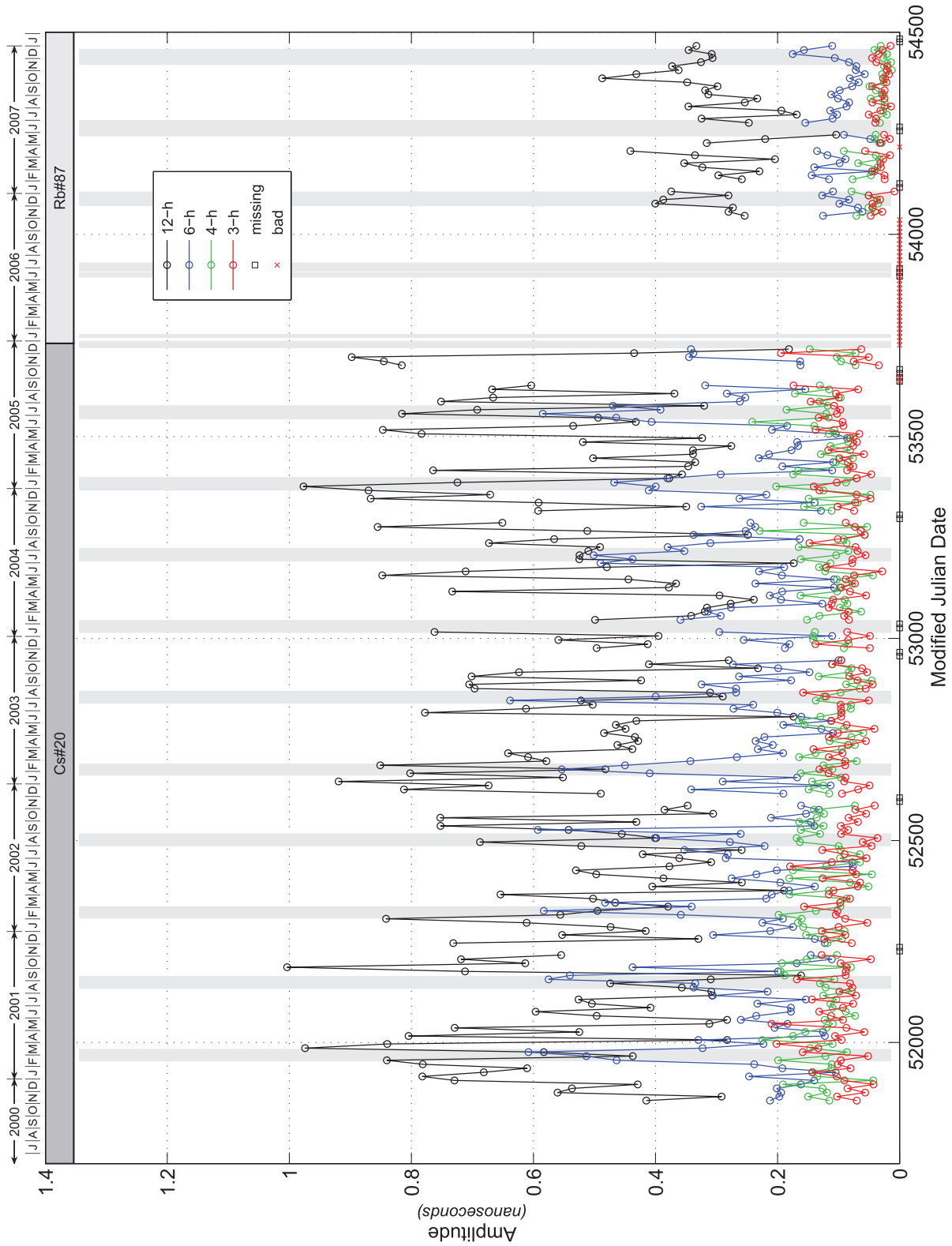


Fig. A9 — SVN25/PRN25 (Block IIA) time-varying amplitudes, 12-hour (black), 6-hour (blue), 4-hour (green), and 3-hour (red).

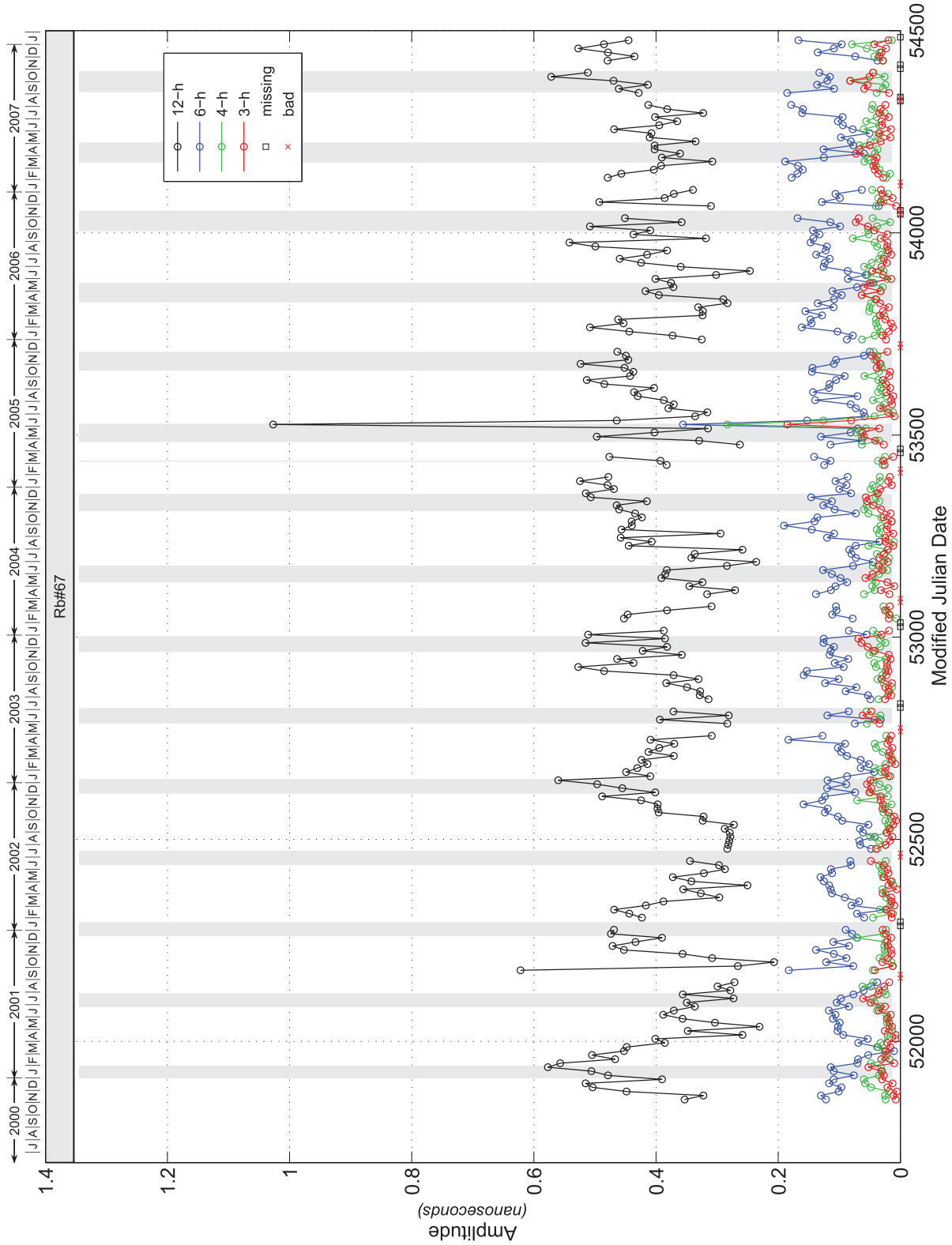


Fig. A10 — SVN26/PRN26 (Block IIA) time-varying amplitudes, 12-hour (black), 6-hour (blue), 4-hour (green), and 3-hour (red).

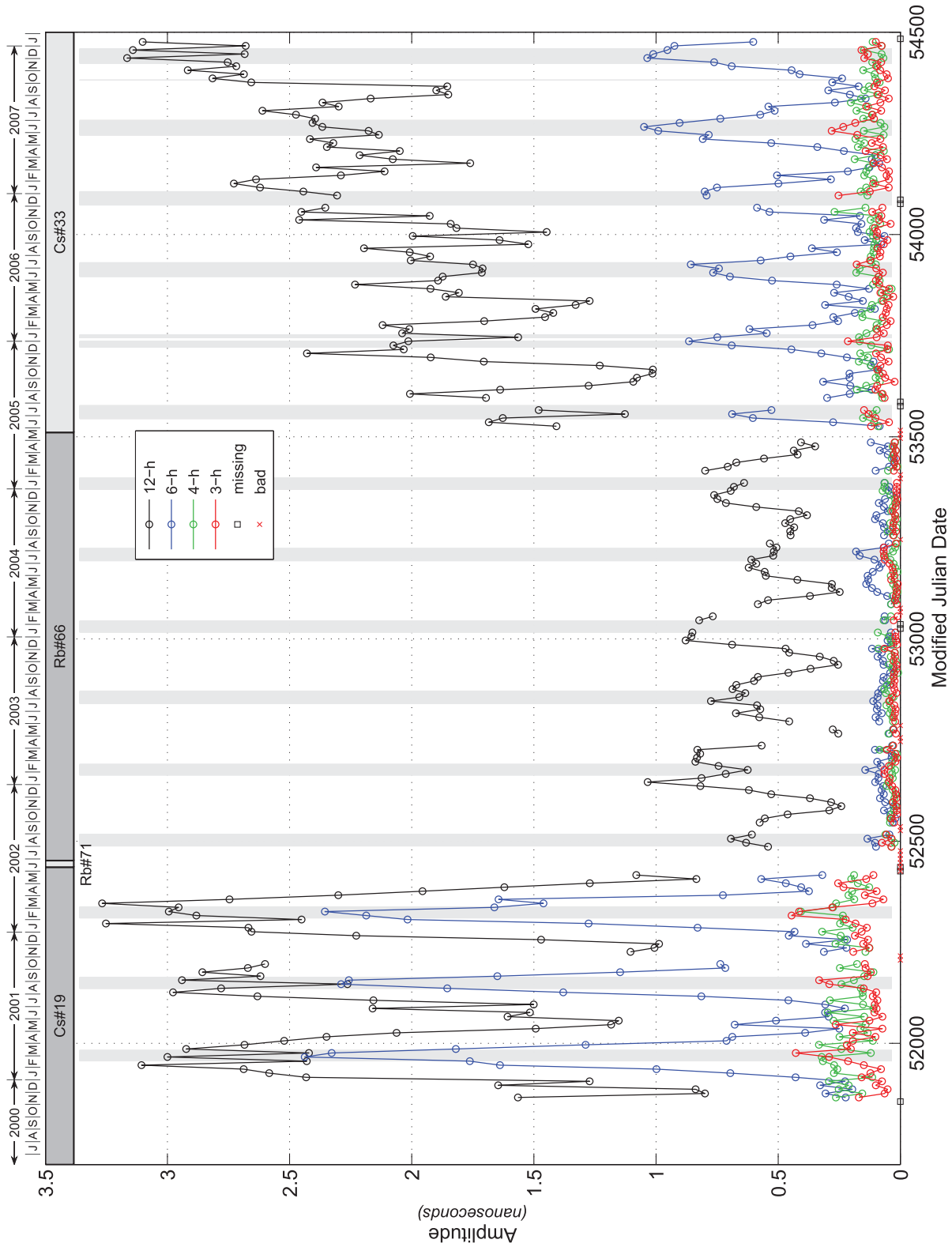


Fig. A11 — SVN27/PRN27 (Block IIA) time-varying amplitudes, 12-hour (black), 6-hour (blue), 4-hour (green), and 3-hour (red).

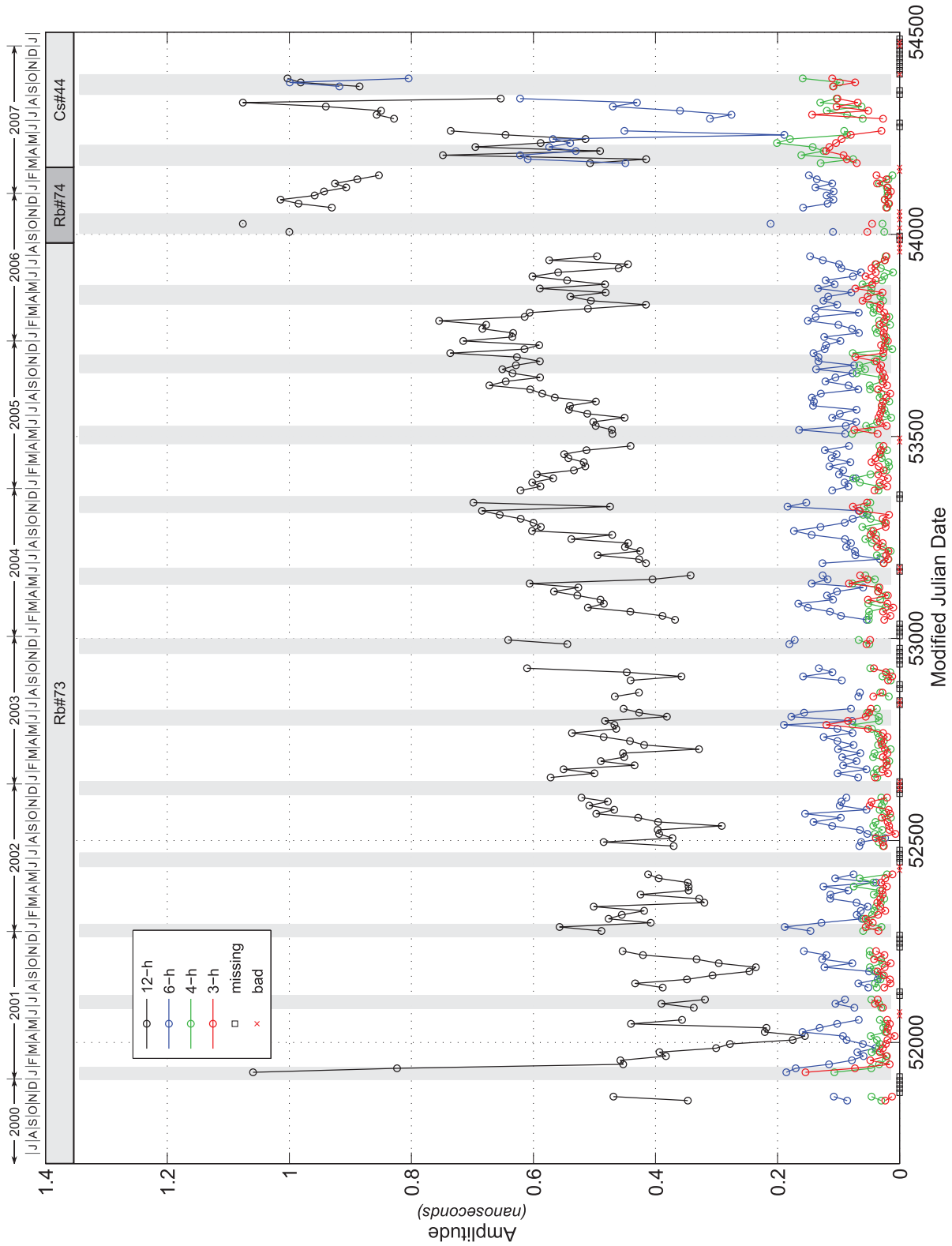


Fig. A12 — SVN29/PRN29 (Block IIA) time-varying amplitudes, 12-hour (black), 6-hour (blue), 4-hour (green), and 3-hour (red).

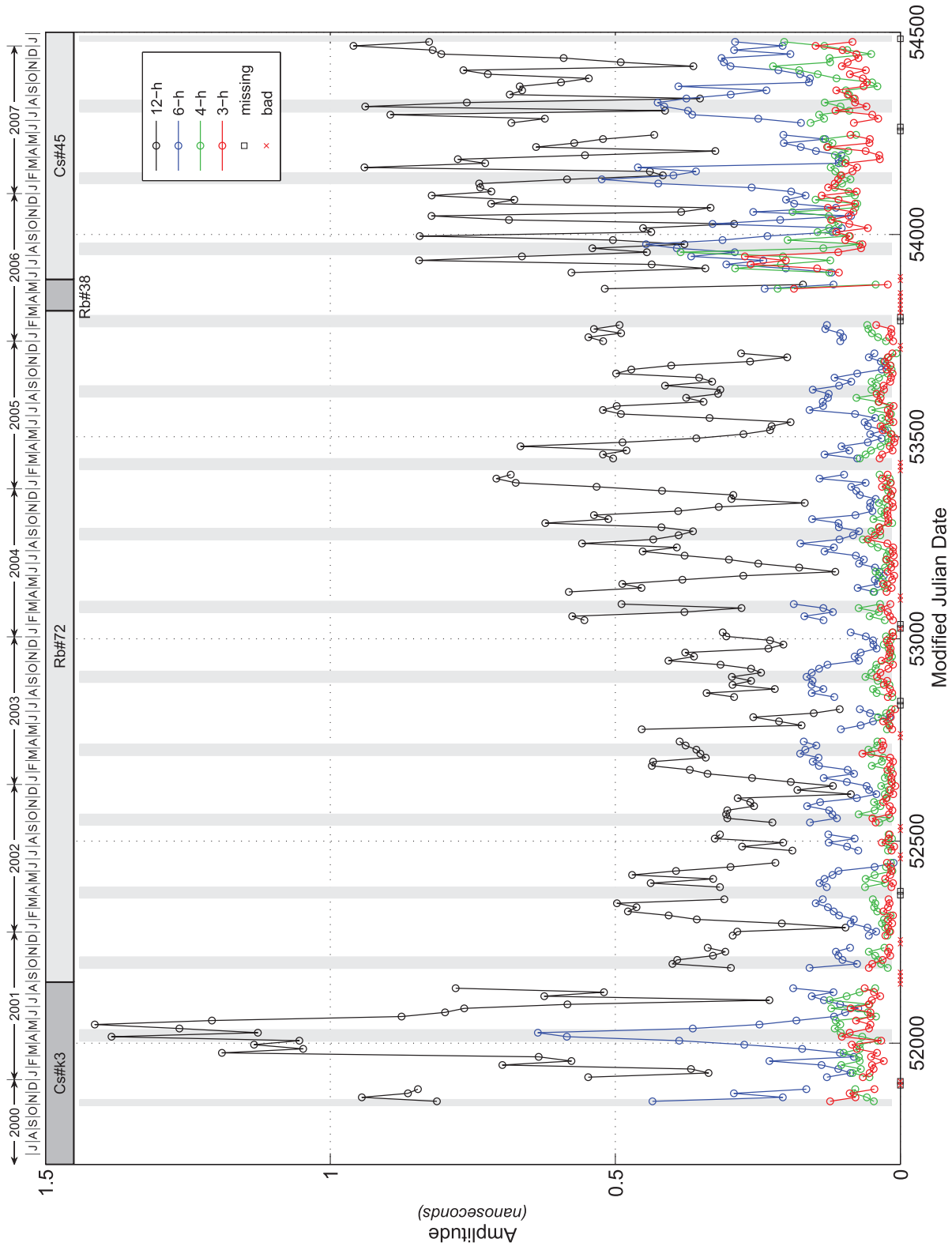


Fig. A13 — SVN30/PRN30 (Block IIA) time-varying amplitudes, 12-hour (black), 6-hour (blue), 4-hour (green), and 3-hour (red).

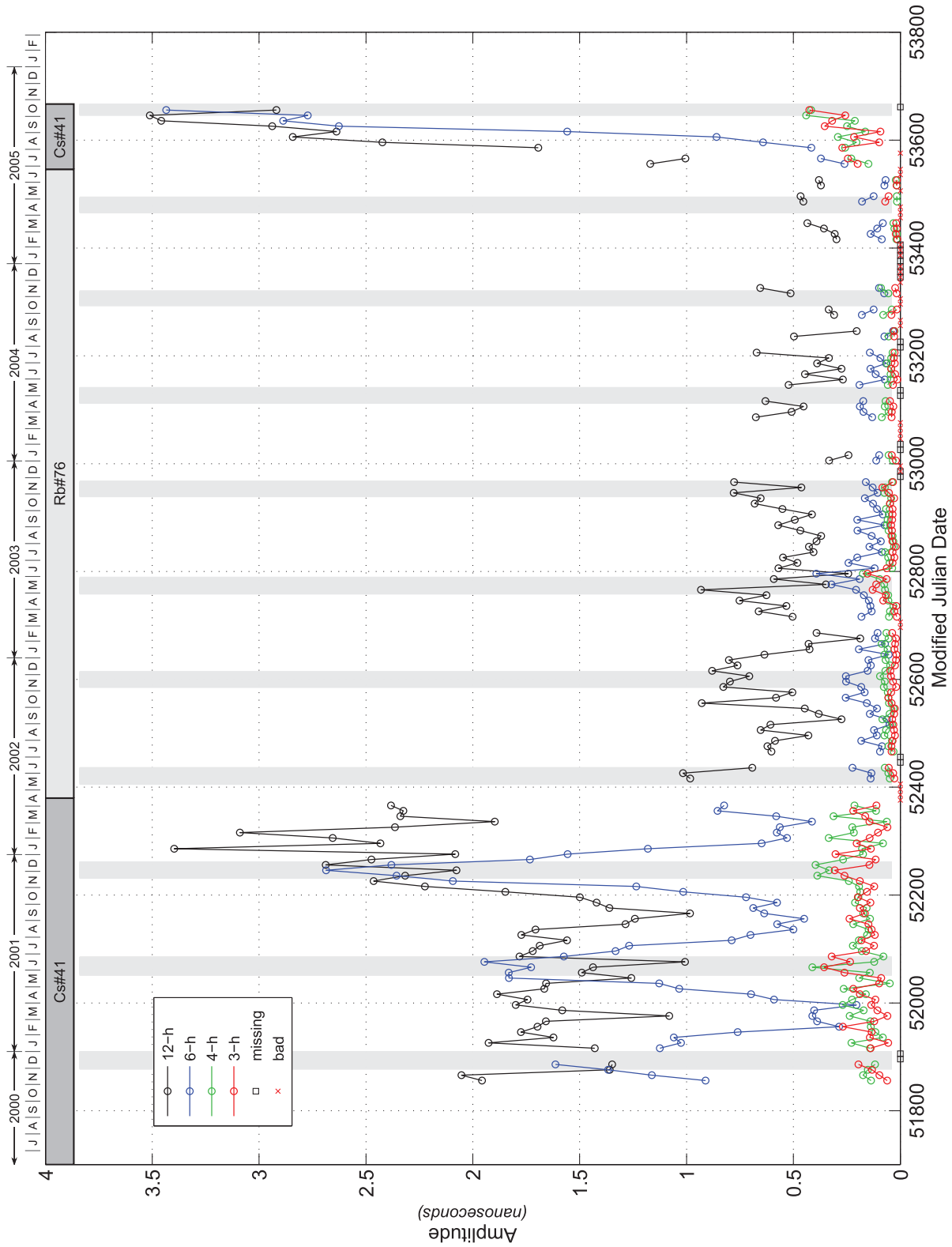


Fig. A14 — SVN31/PRN31 (Block IIA) time-varying amplitudes, 12-hour (black), 6-hour (blue), 4-hour (green), and 3-hour (red).

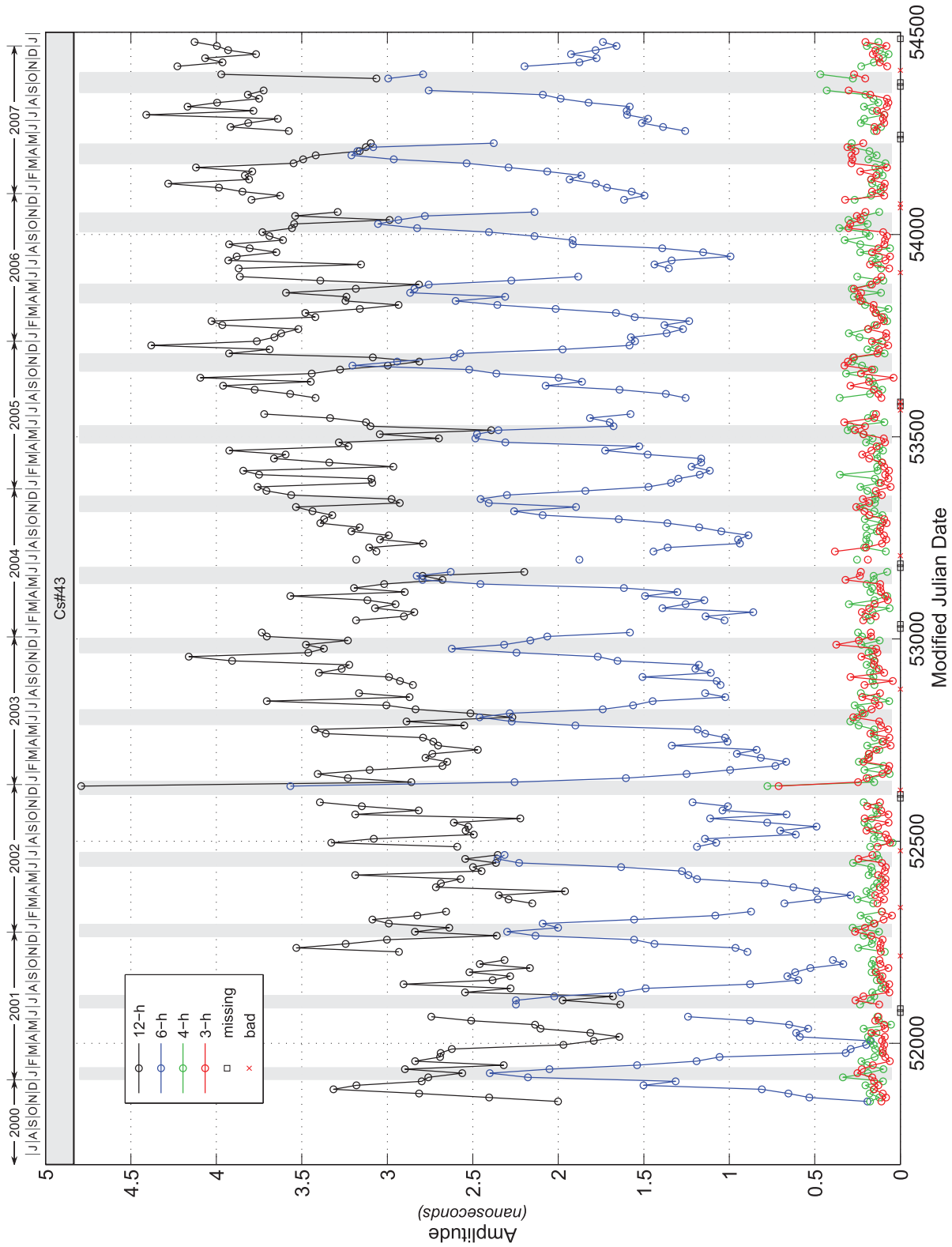


Fig. A15 — SVN32/PRN1 (Block IIA) time-varying amplitudes, 12-hour (black), 6-hour (blue), 4-hour (green), and 3-hour (red).

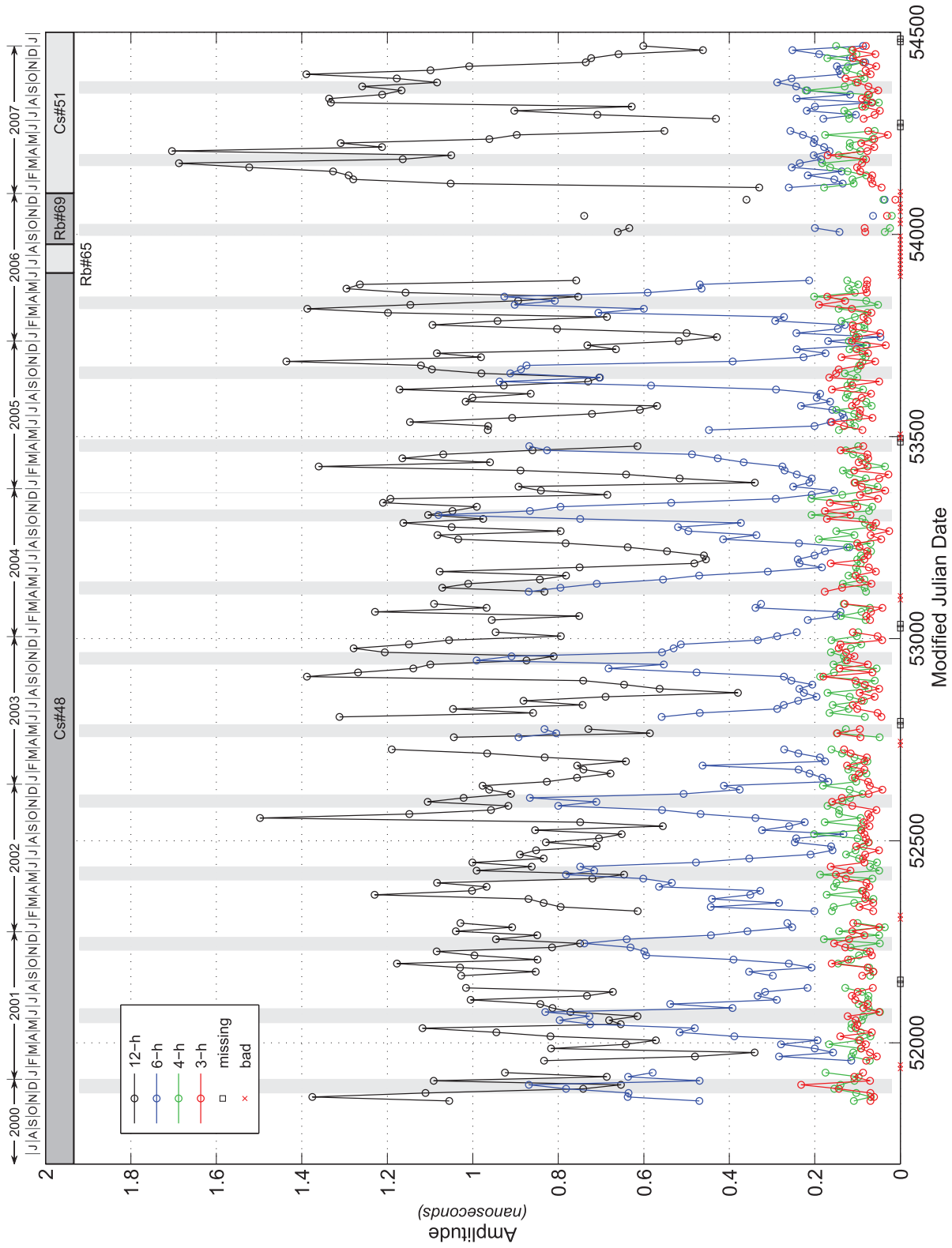


Fig. A16 — SVN33/PRN3 (Block IIA) time-varying amplitudes, 12-hour (black), 6-hour (blue), 4-hour (green), and 3-hour (red).

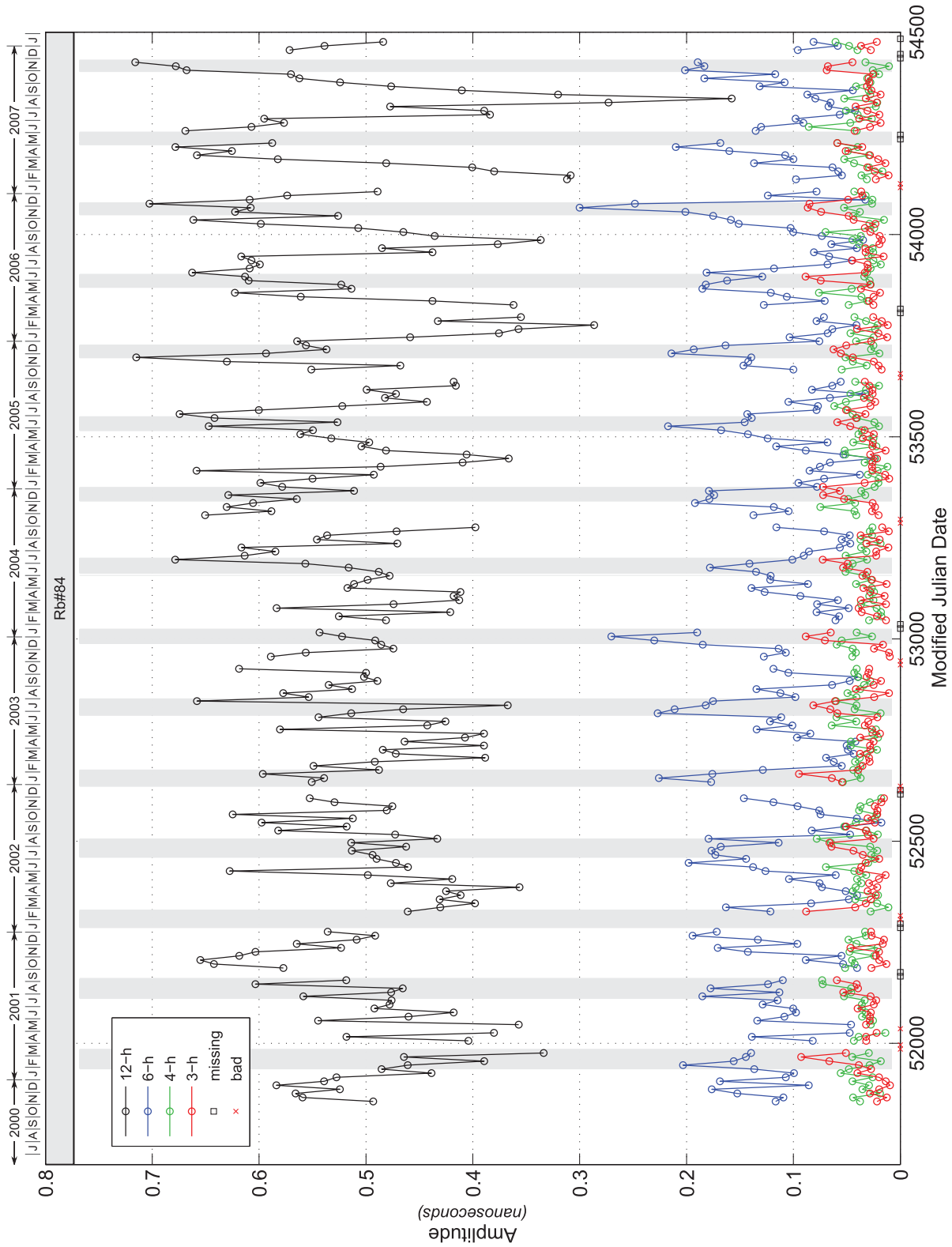


Fig. A17 — SVN34/PRN4 (Block IIA) time-varying amplitudes, 12-hour (black), 6-hour (blue), 4-hour (green), and 3-hour (red).

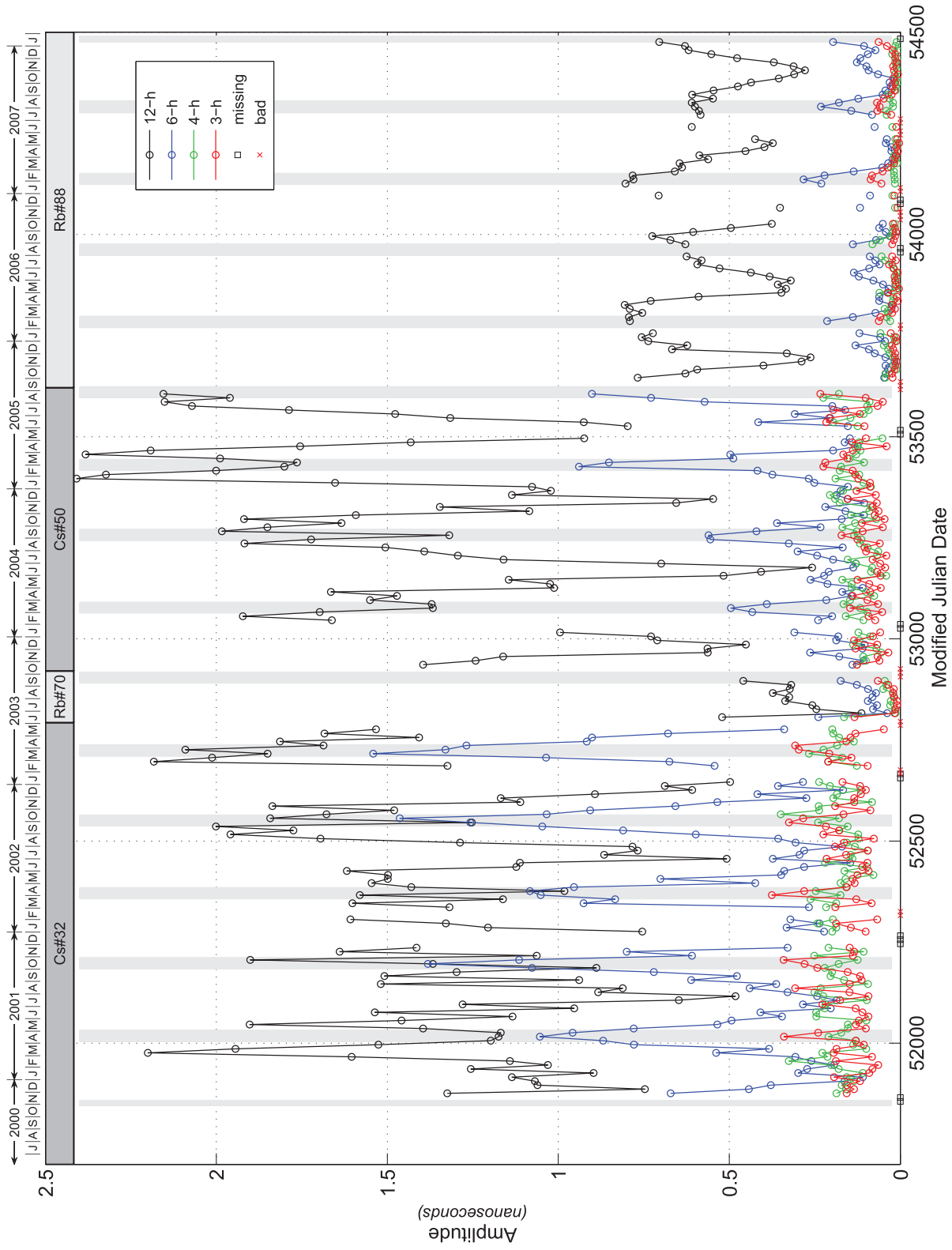


Fig. A18 — SVN35/PRN5 (Block IIA) time-varying amplitudes, 12-hour (black), 6-hour (blue), 4-hour (green), and 3-hour (red).

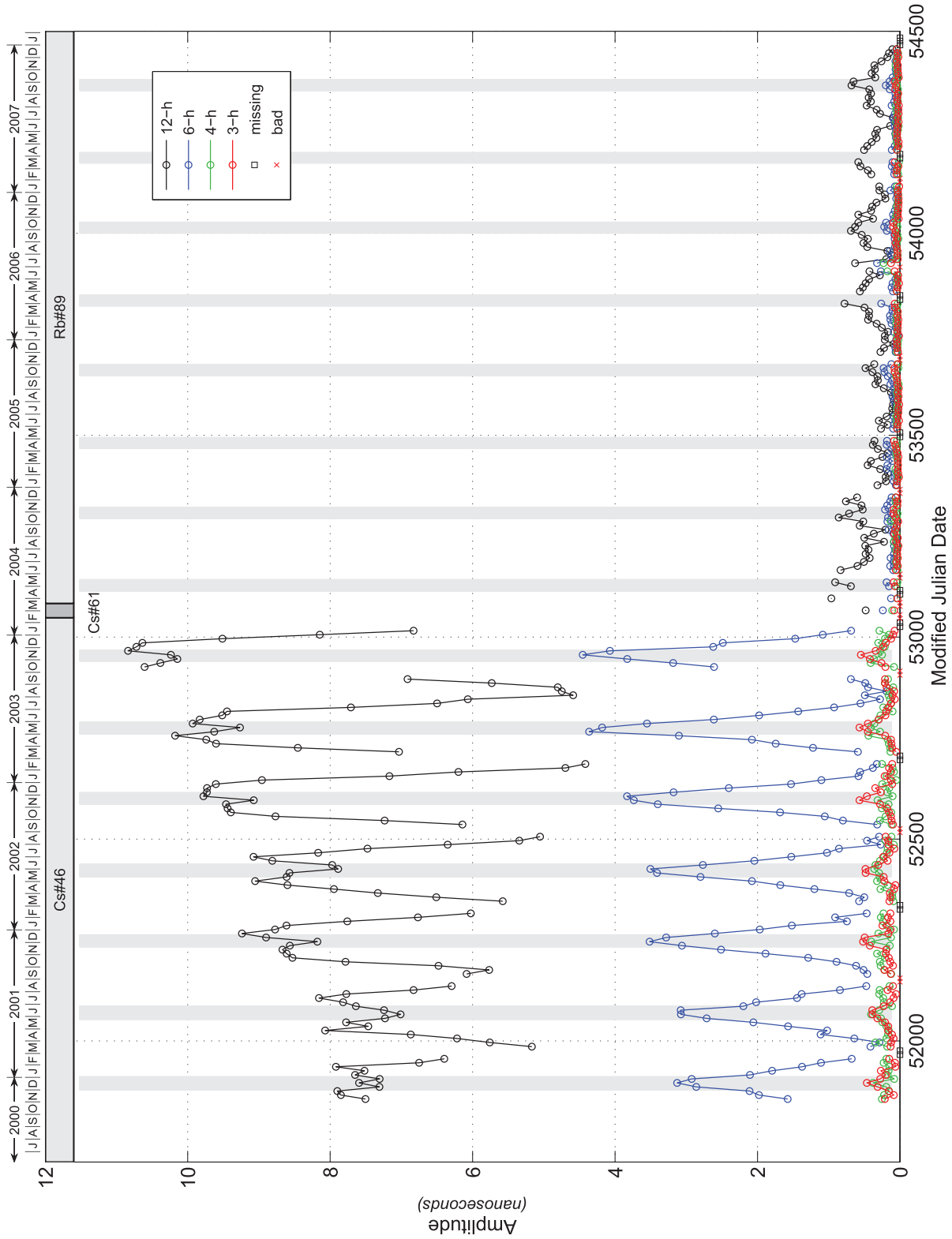


Fig. A19 — SVN36/PRN6 (Block IIA) time-varying amplitudes, 12-hour (black), 6-hour (blue), 4-hour (green), and 3-hour (red).

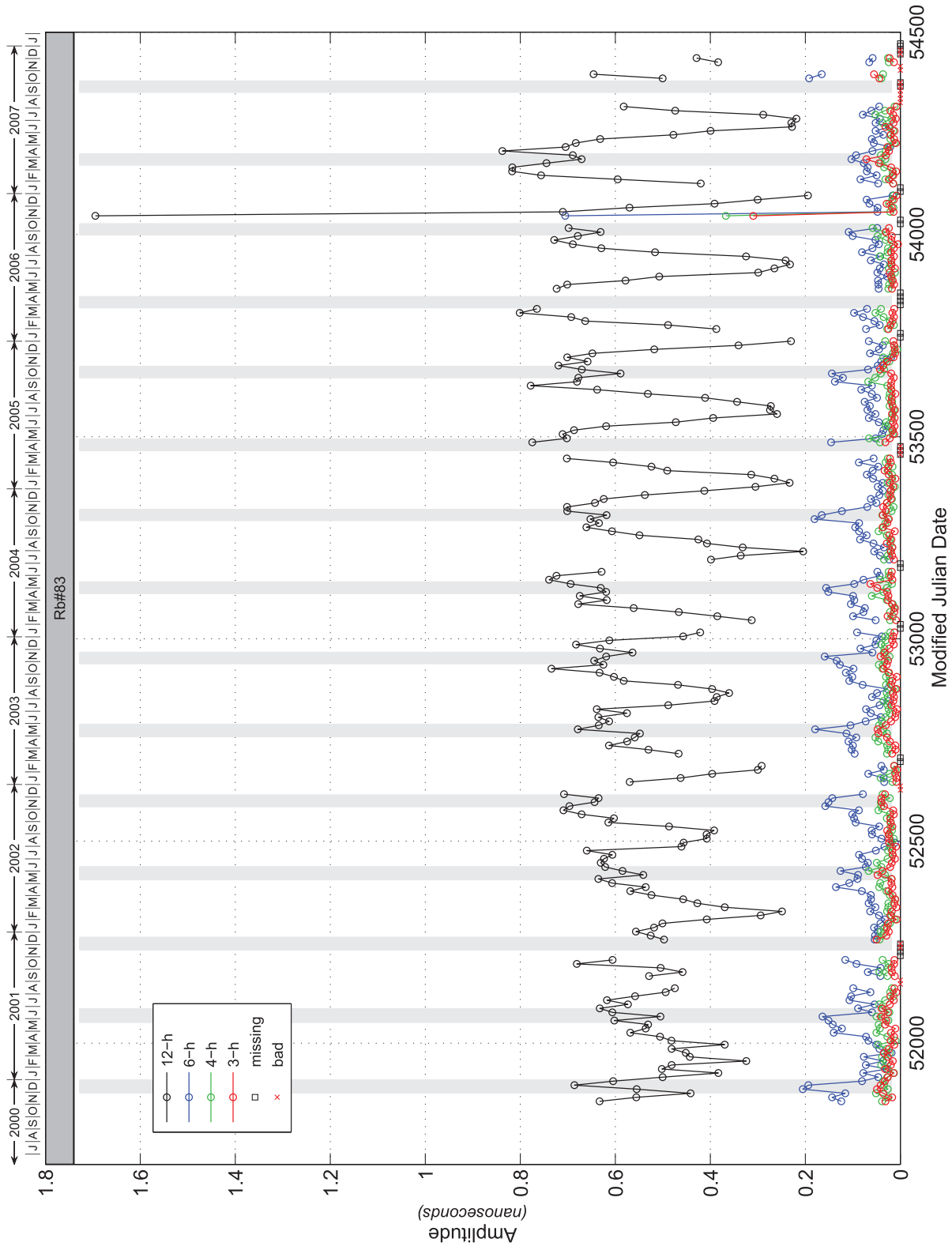


Fig. A20 — SVN37/PRN7 (Block IIA) time-varying amplitudes, 12-hour (black), 6-hour (blue), 4-hour (green), and 3-hour (red).

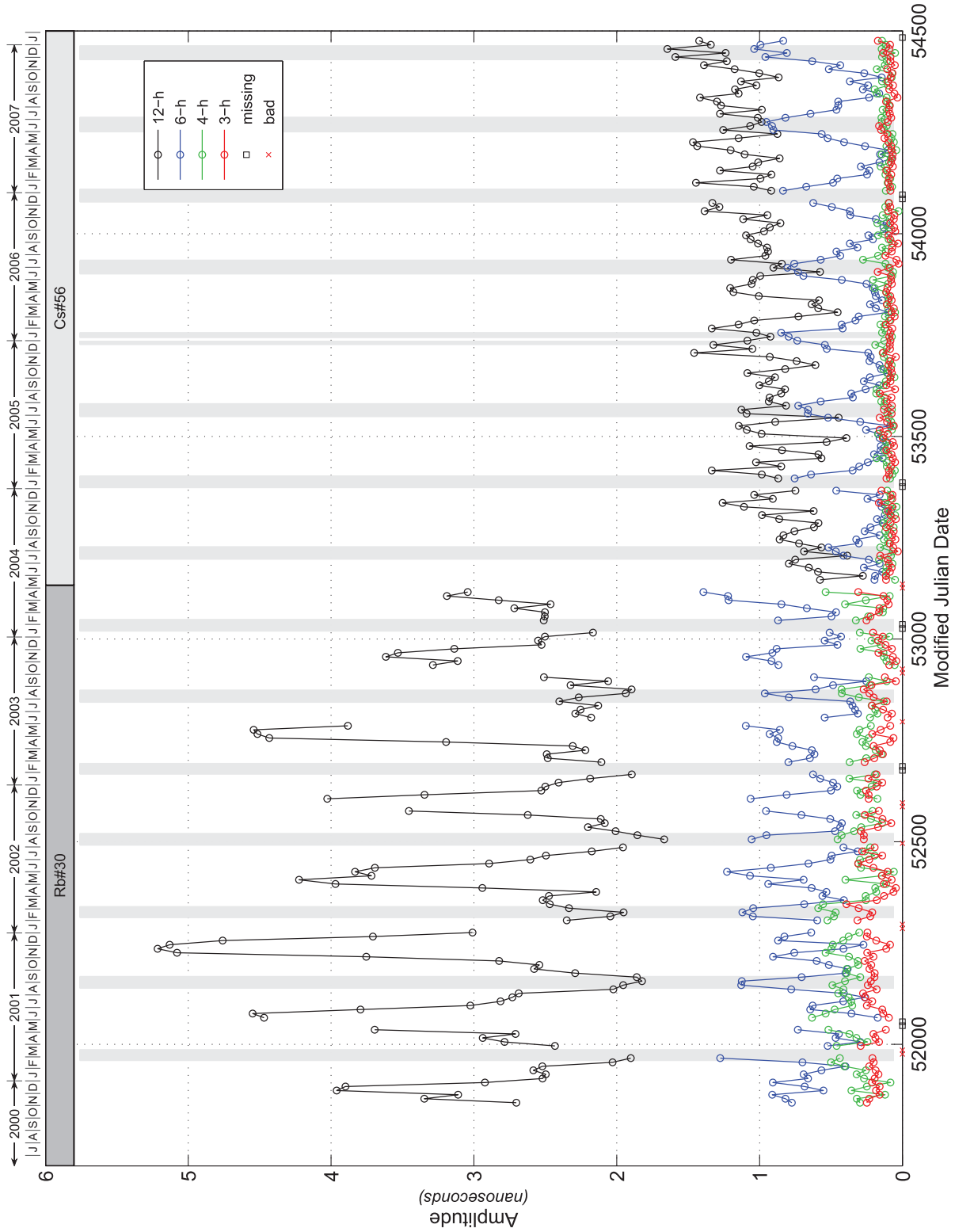


Fig. A21 — SVN38/PRN8 (Block IIA) time-varying amplitudes, 12-hour (black), 6-hour (blue), 4-hour (green), and 3-hour (red).

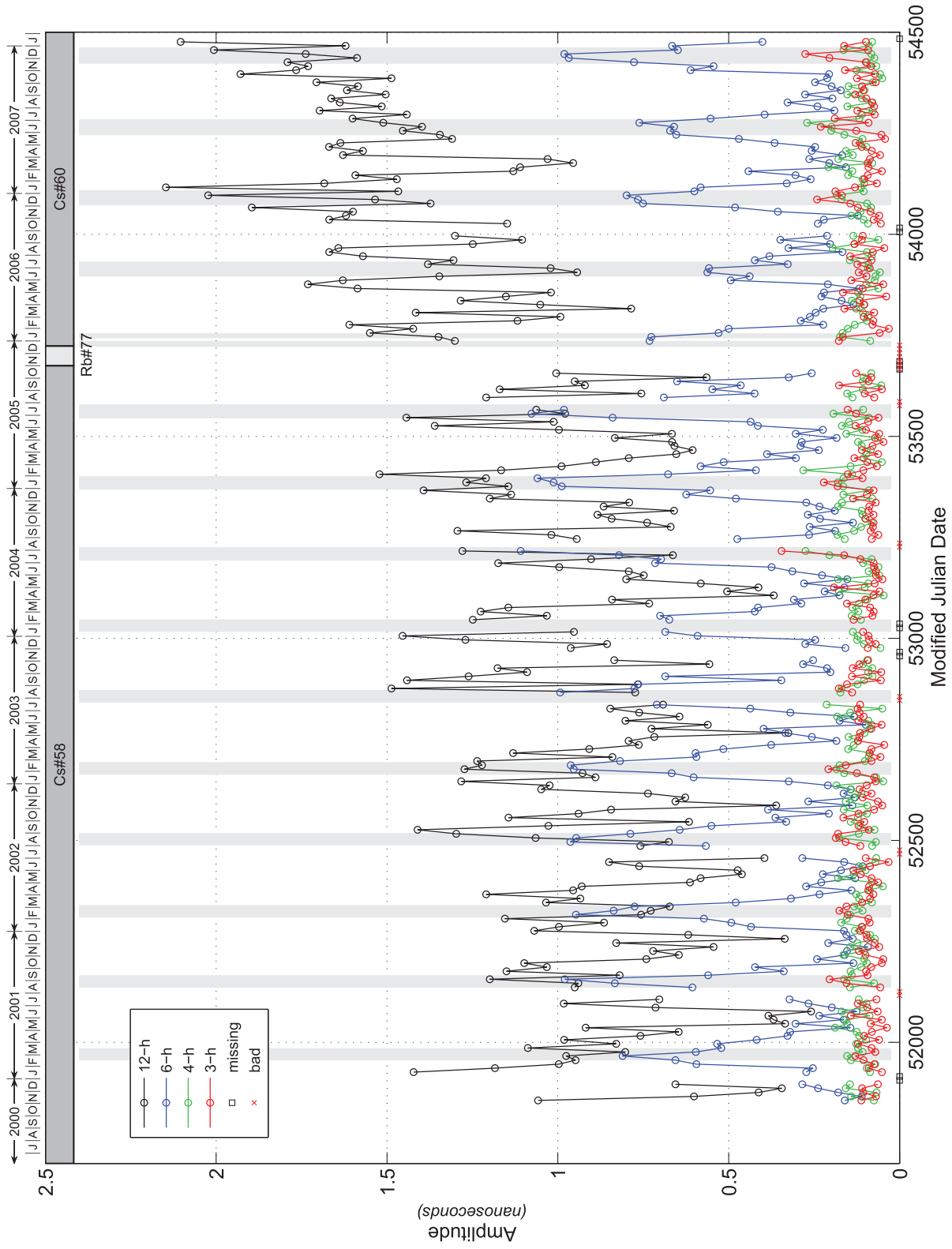


Fig. A22 — SVN39/PRN9 (Block IIA) time-varying amplitudes, 12-hour (black), 6-hour (blue), 4-hour (green), and 3-hour (red).

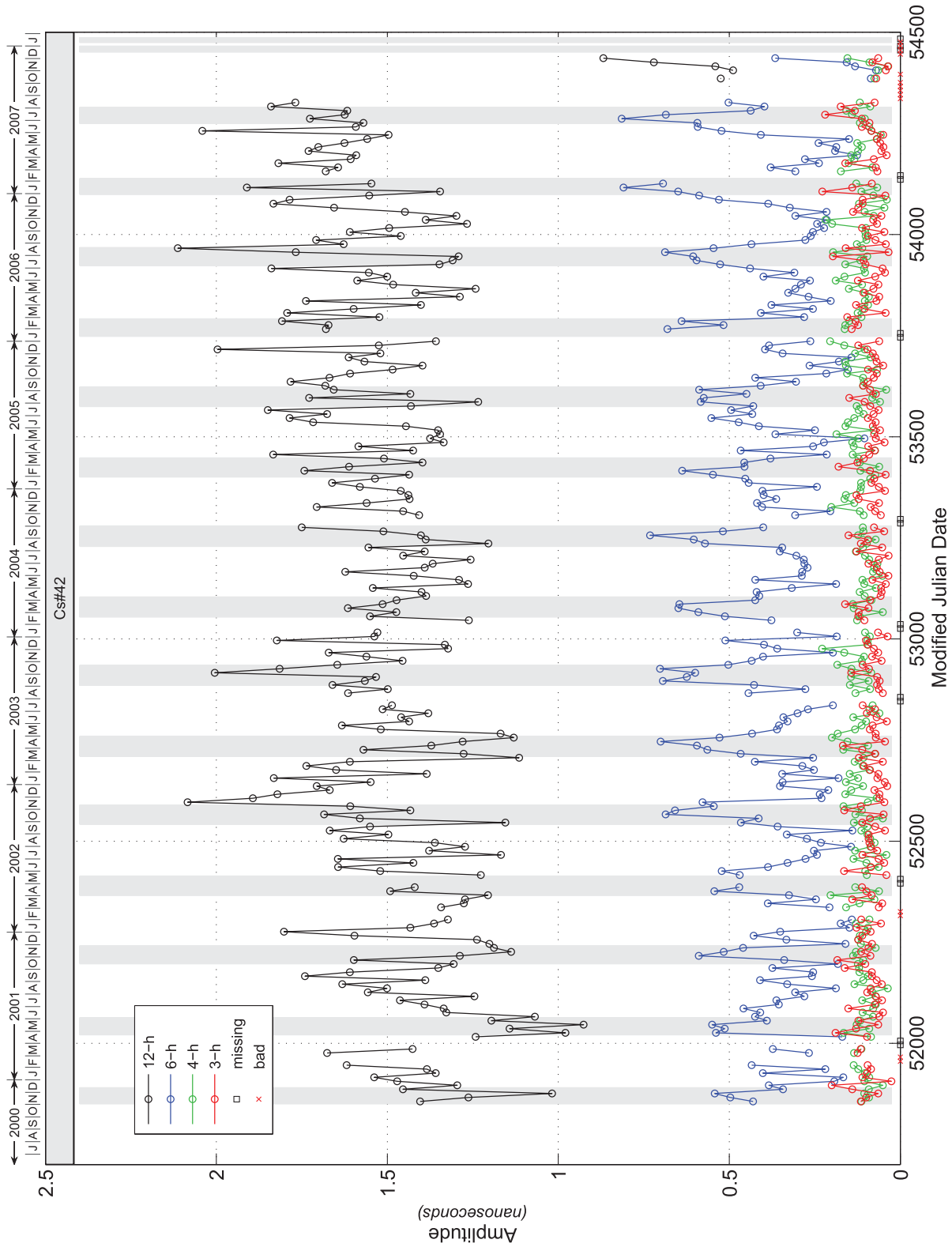


Fig. A23 — SVN40/PRN10 (Block IIA) time-varying amplitudes, 12-hour (black), 6-hour (blue), 4-hour (green), and 3-hour (red).

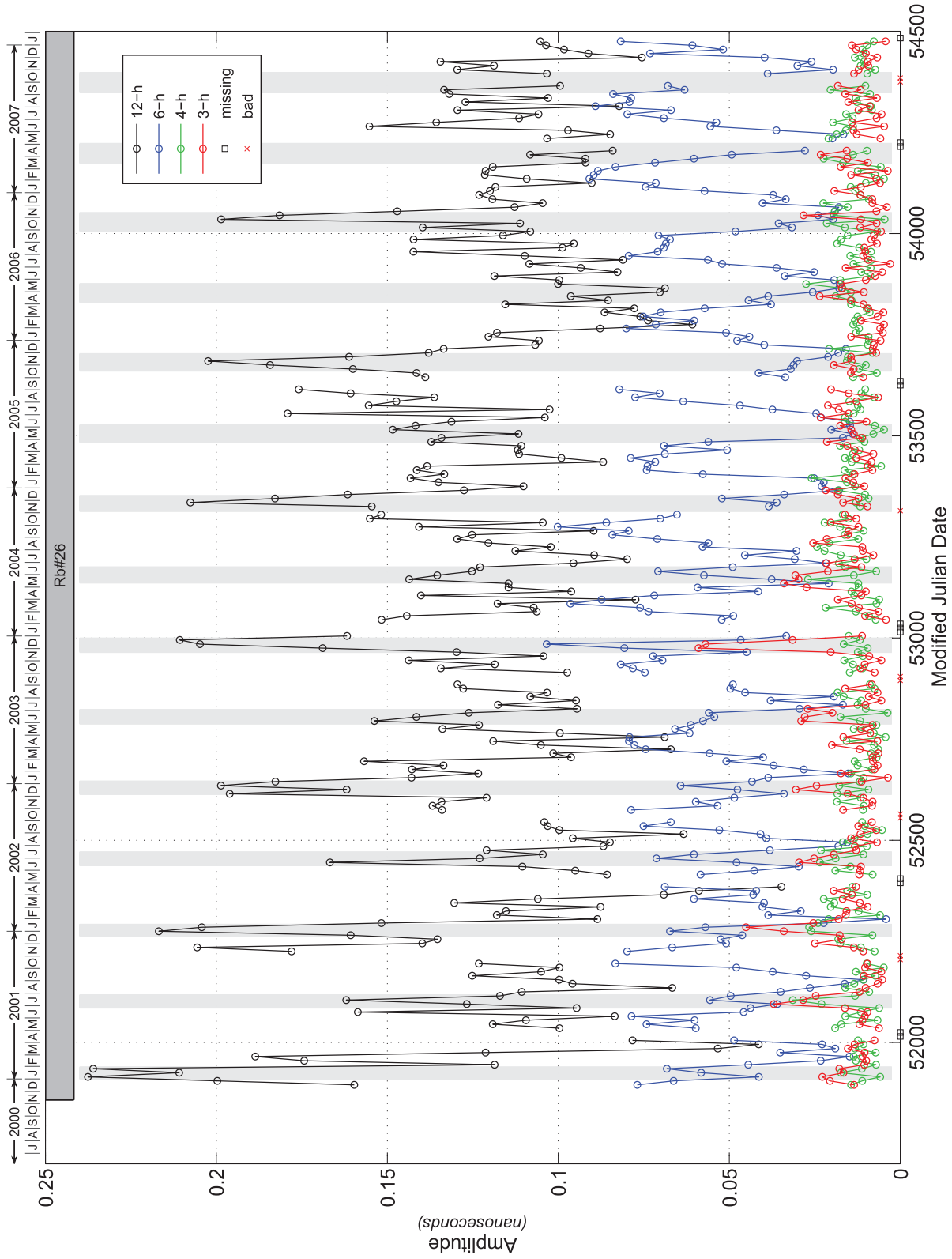


Fig. A24 — SVN41/PRN14 (Block IIR) time-varying amplitudes, 12-hour (black), 6-hour (blue), 4-hour (green), and 3-hour (red).

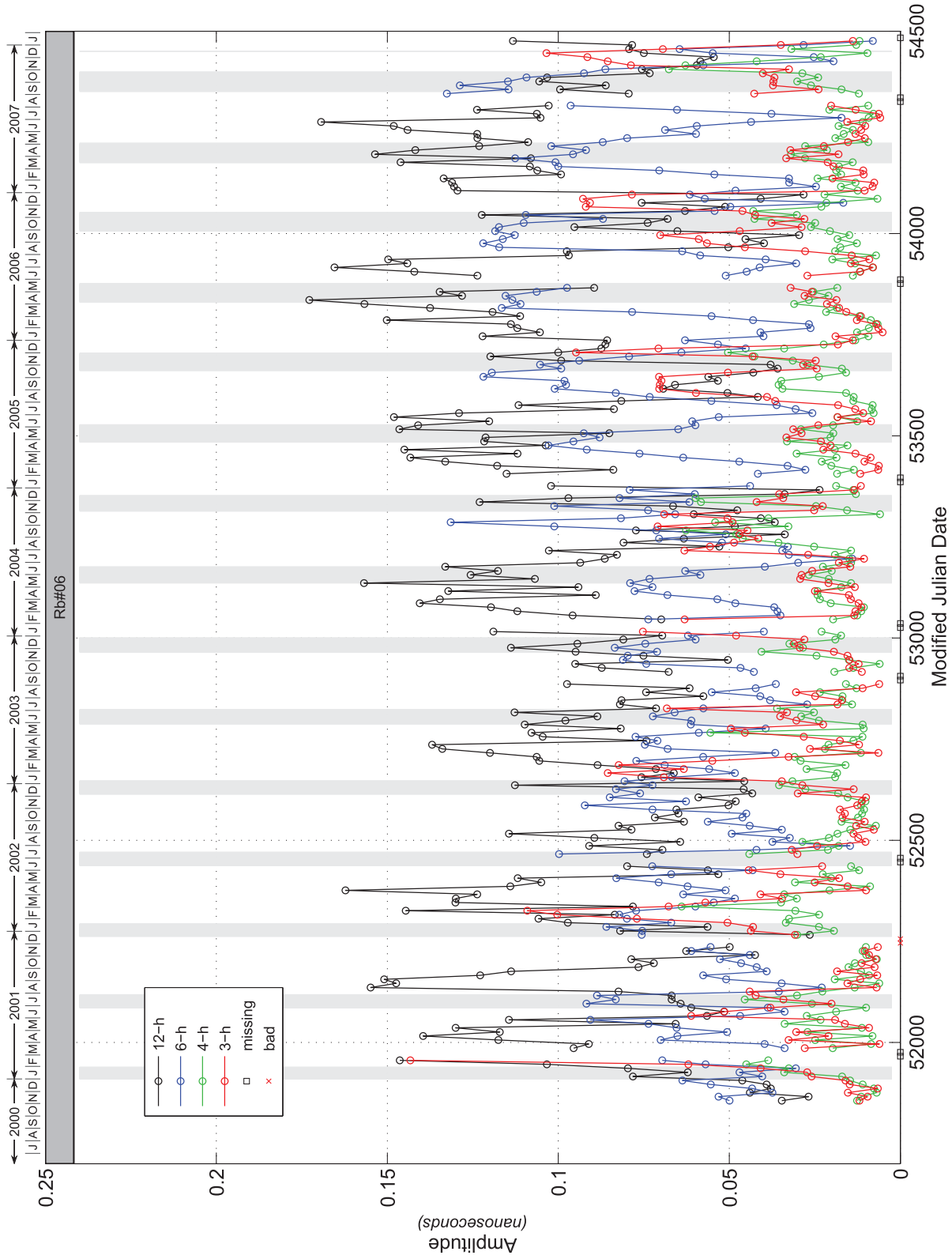


Fig. A25 — SVN43/PRN13 (Block IIR) time-varying amplitudes, 12-hour (black), 6-hour (blue), 4-hour (green), and 3-hour (red).

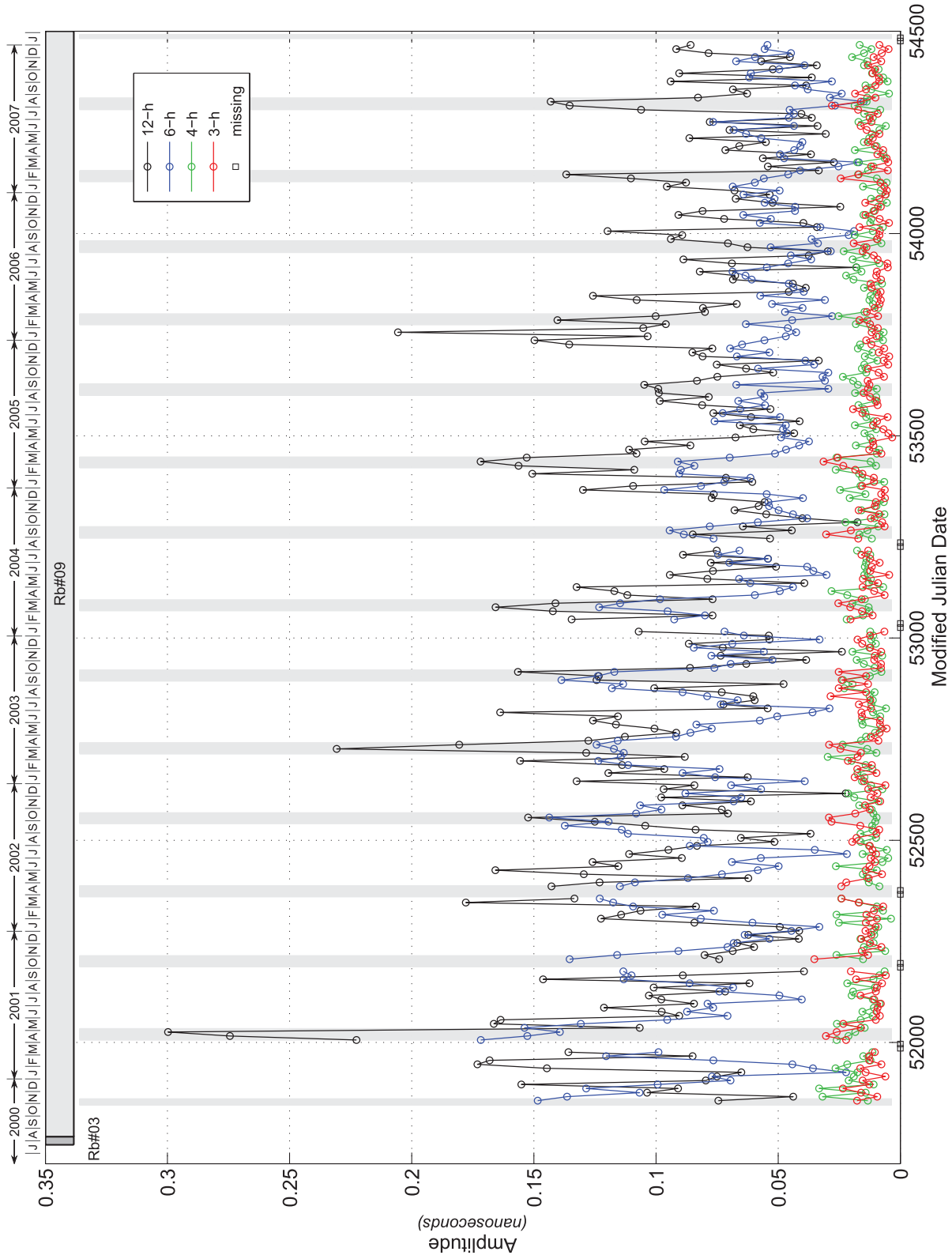


Fig. A26 — SVN44/PRN28 (Block IIR) time-varying amplitudes, 12-hour (black), 6-hour (blue), 4-hour (green), and 3-hour (red).

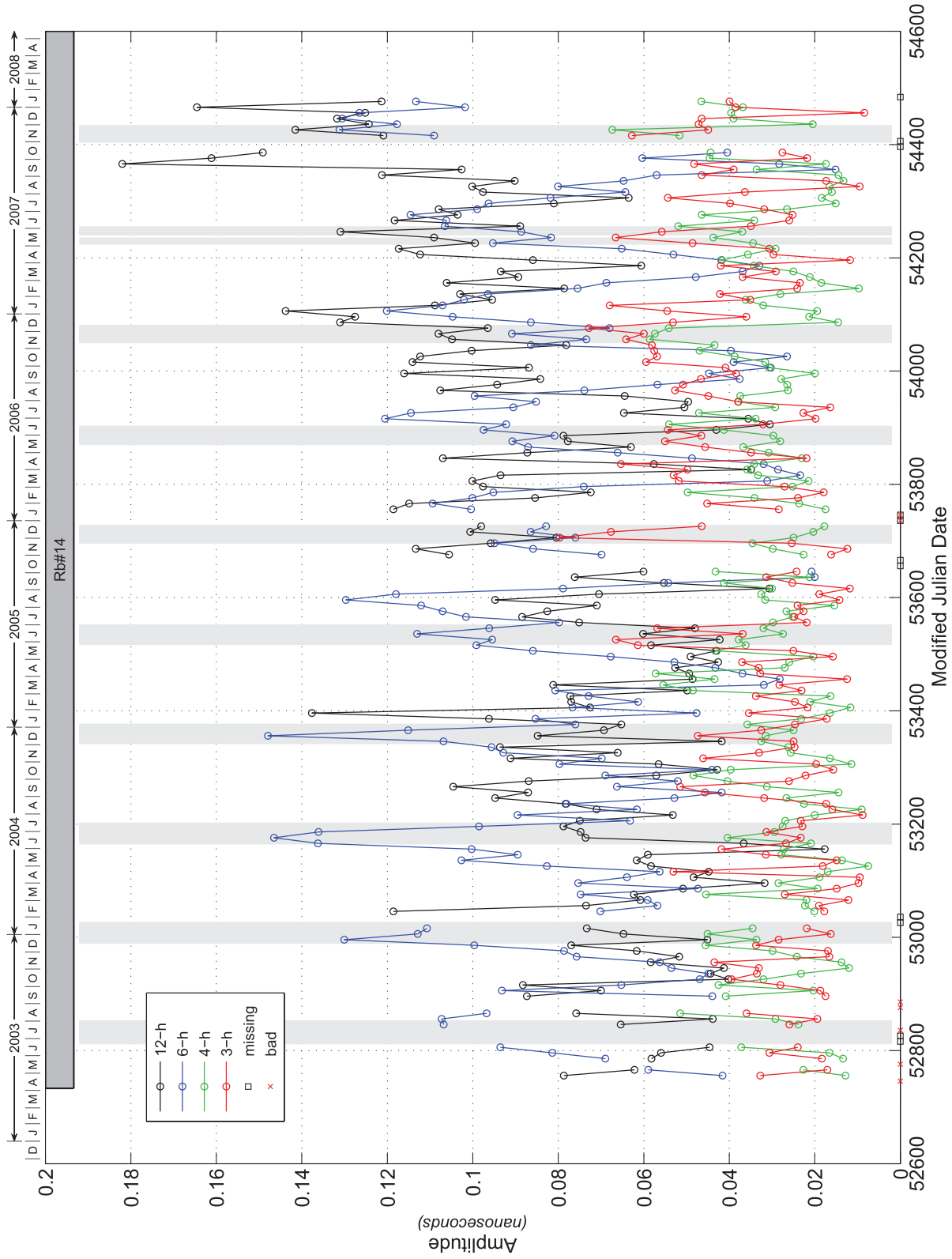


Fig. A27 — SVN45/PRN21 (Block IIR) time-varying amplitudes, 12-hour (black), 6-hour (blue), 4-hour (green), and 3-hour (red).

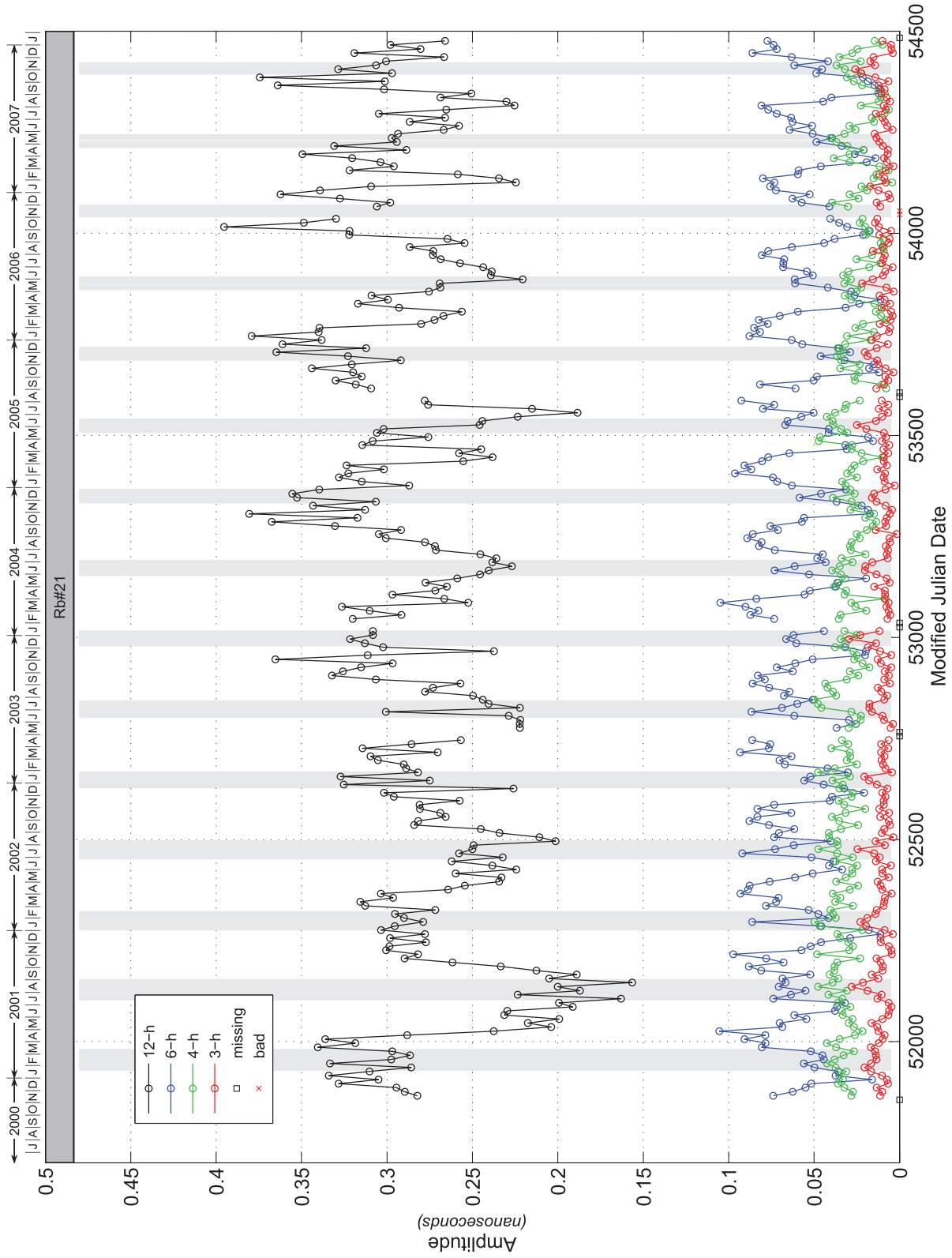


Fig. A28 — SVN46/PRN11 (Block IIR) time-varying amplitudes, 12-hour (black), 6-hour (blue), 4-hour (green), and 3-hour (red).

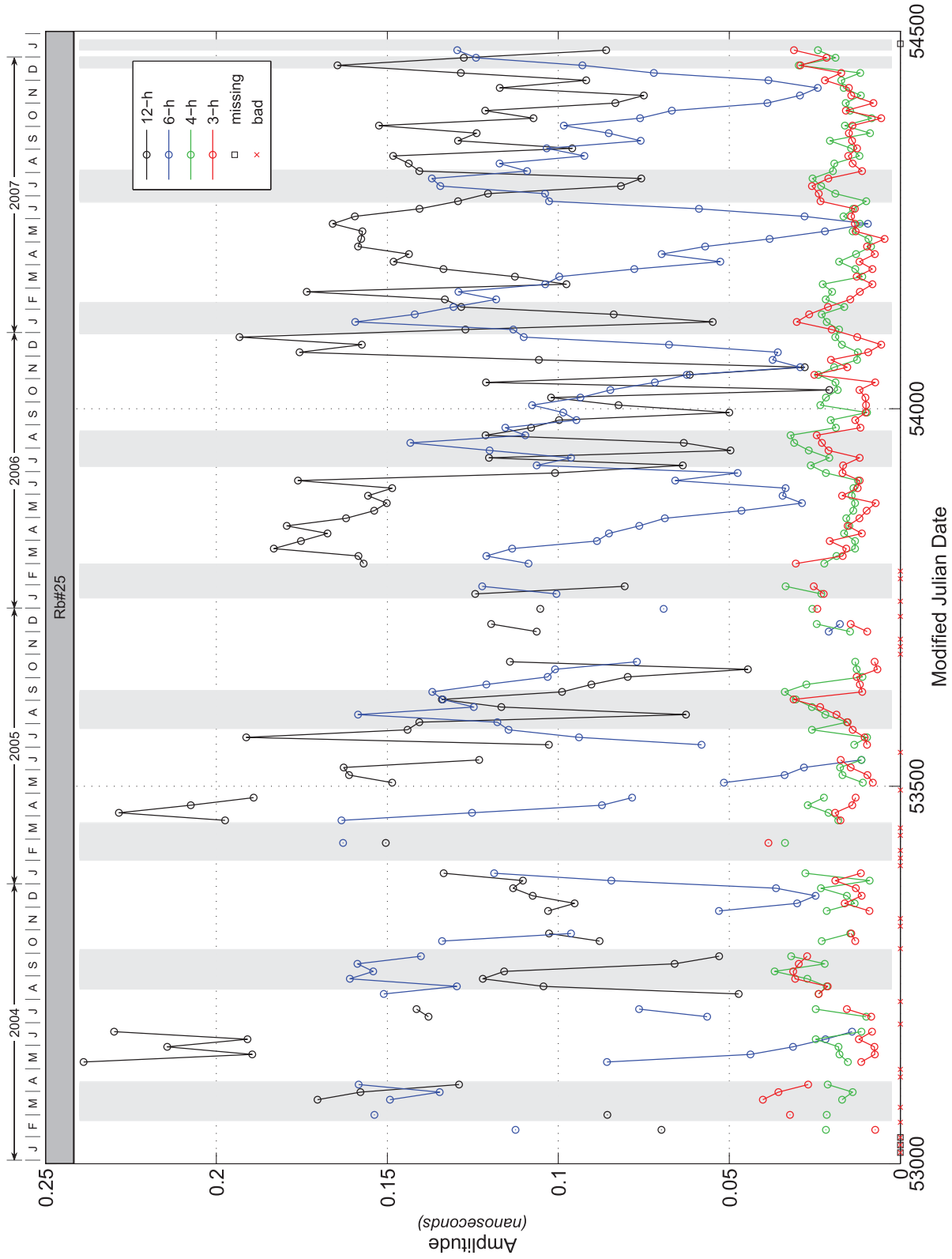


Fig. A29 — SVN47/PRN22 (Block IIR) time-varying amplitudes, 12-hour (black), 6-hour (blue), 4-hour (green), and 3-hour (red).

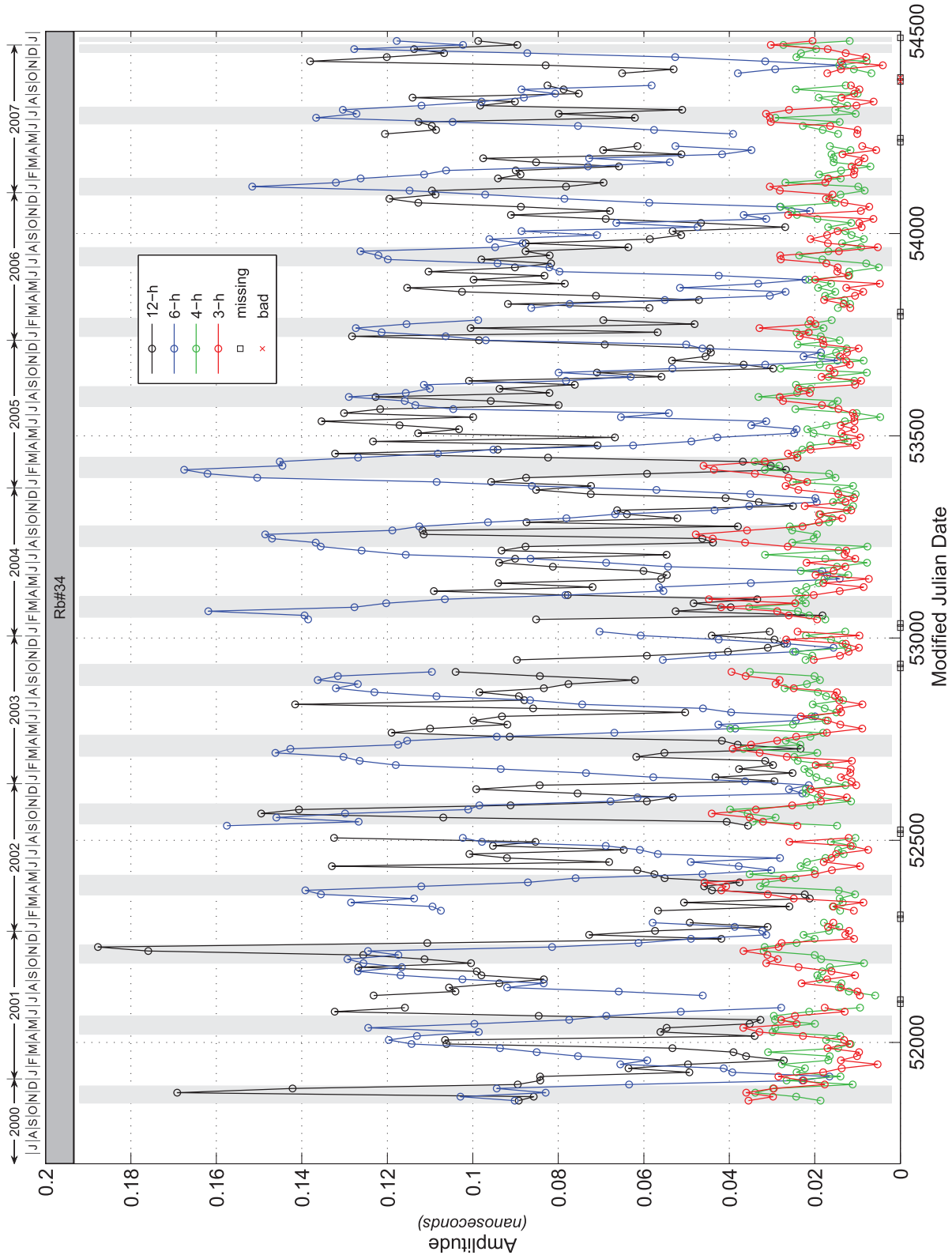


Fig. A30 — SVN51/PRN20 (Block IIR) time-varying amplitudes, 12-hour (black), 6-hour (blue), 4-hour (green), and 3-hour (red).

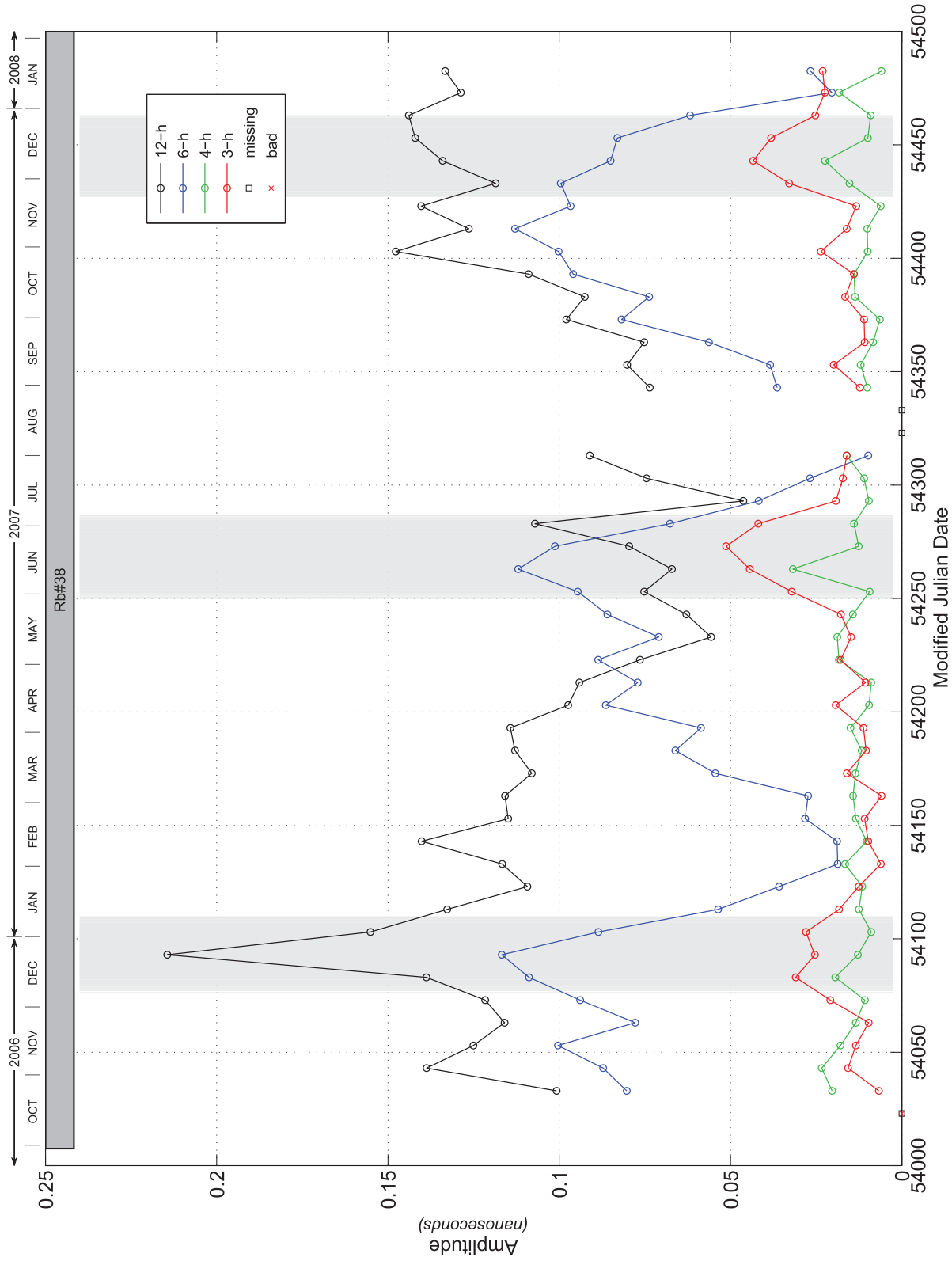


Fig. A31 — SVN52/PRN31 (Block IIR-M) time-varying amplitudes, 12-hour (black), 6-hour (blue), 4-hour (green), and 3-hour (red).

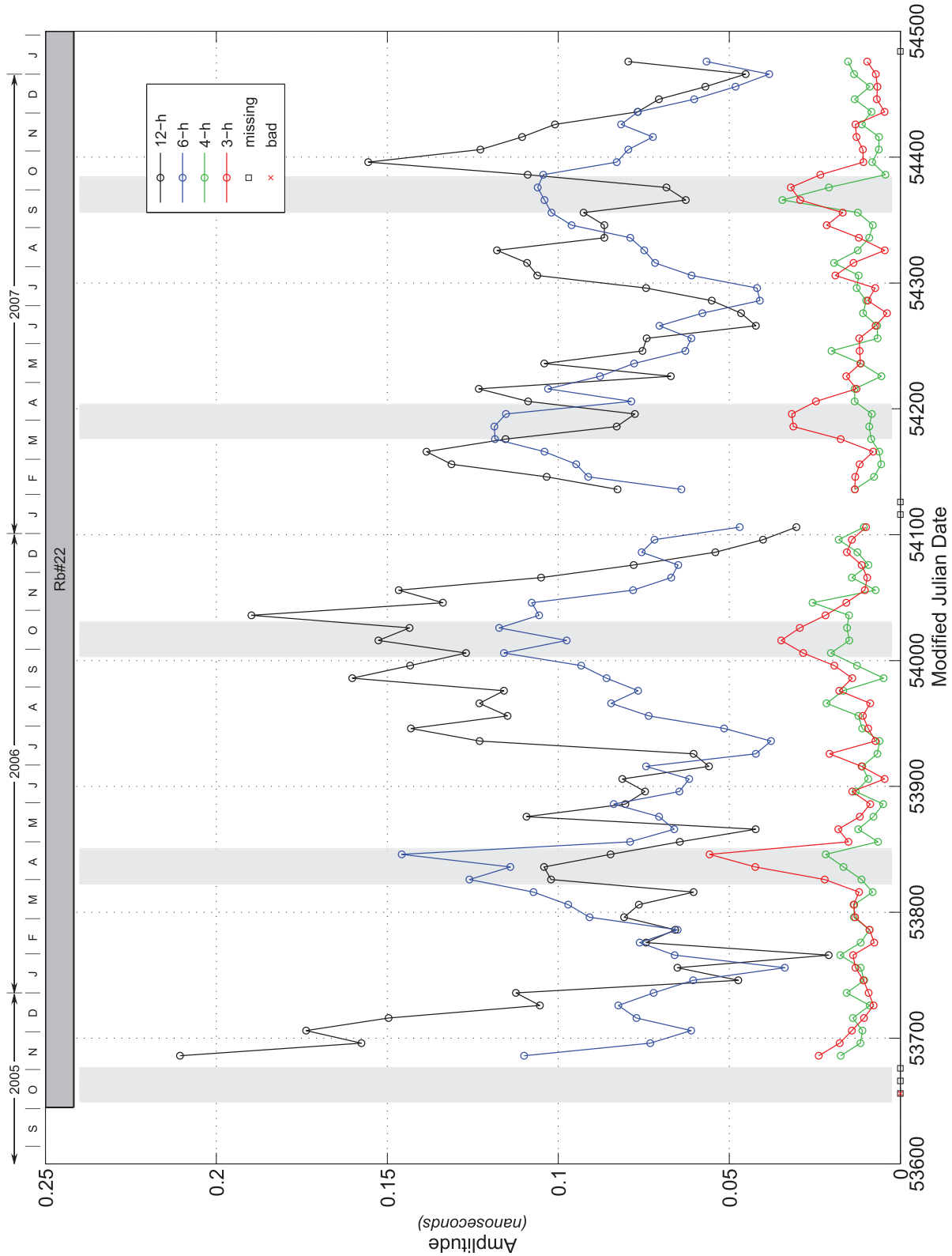


Fig. A32 — SVN53/PRN17 (Block IIR-M) time-varying amplitudes, 12-hour (black), 6-hour (blue), 4-hour (green), and 3-hour (red).

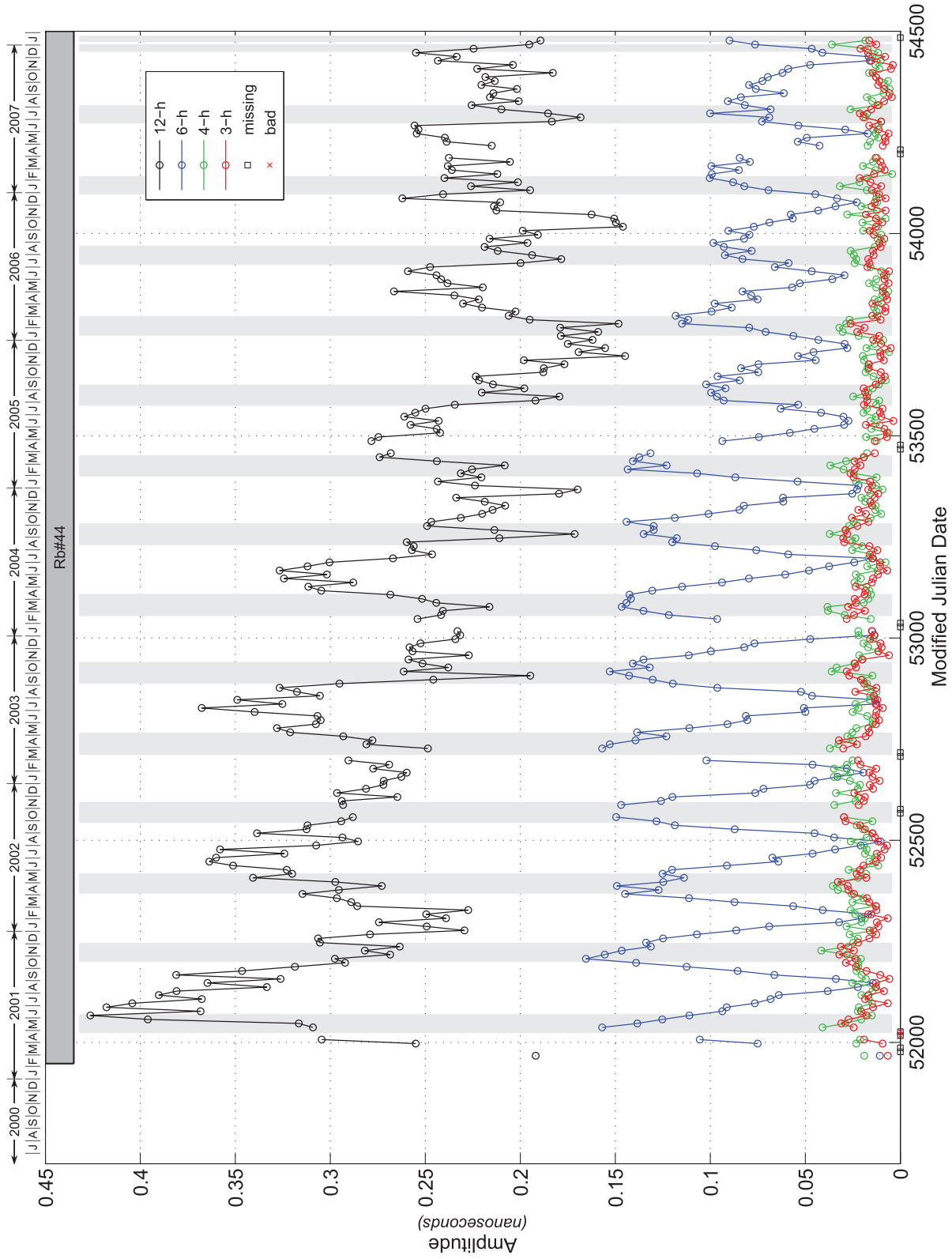


Fig. A33 — SVN54/PRN18 (Block IIR) time-varying amplitudes, 12-hour (black), 6-hour (blue), 4-hour (green), and 3-hour (red).

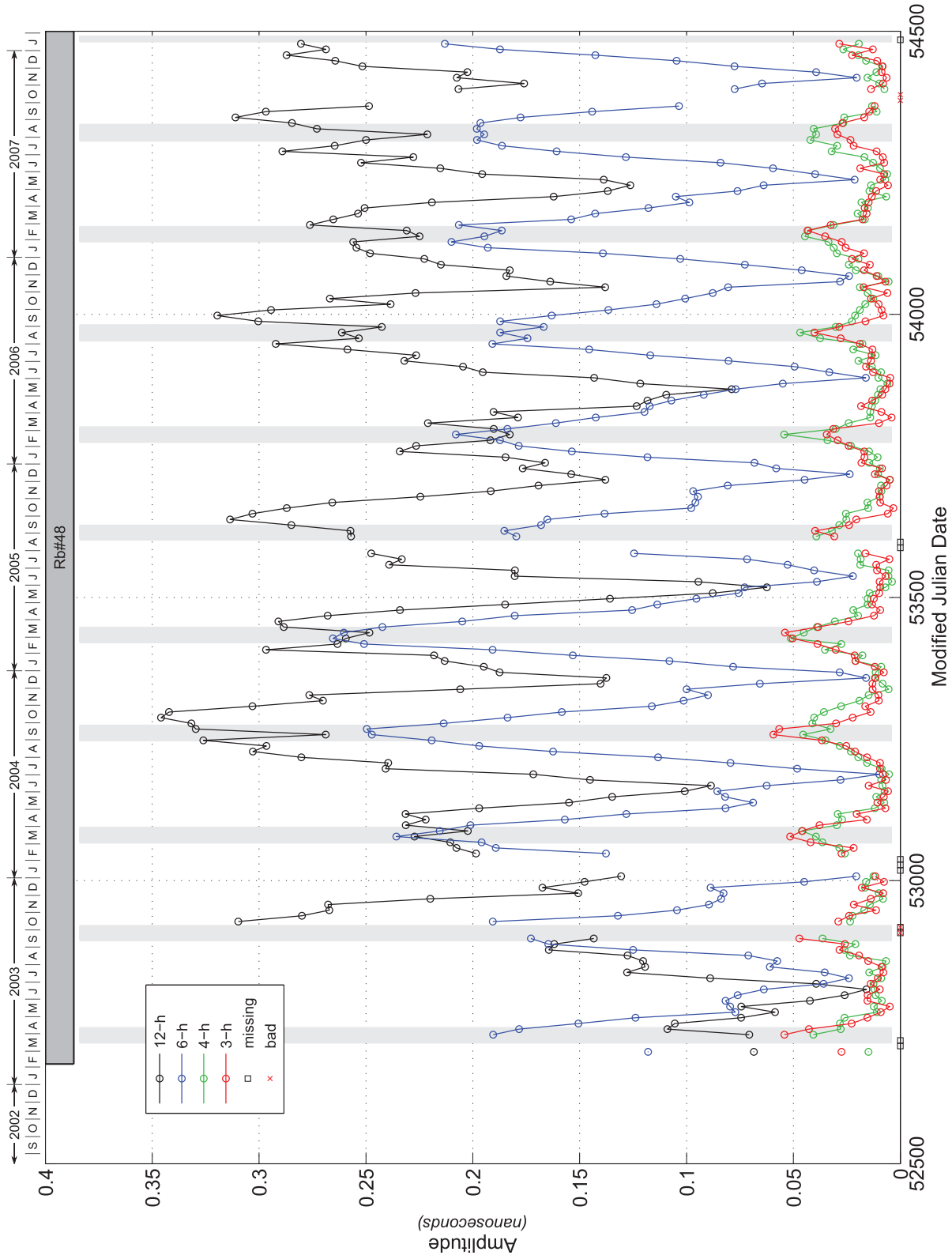


Fig. A34 — SVN56/PRN16 (Block IIR) time-varying amplitudes, 12-hour (black), 6-hour (blue), 4-hour (green), and 3-hour (red).

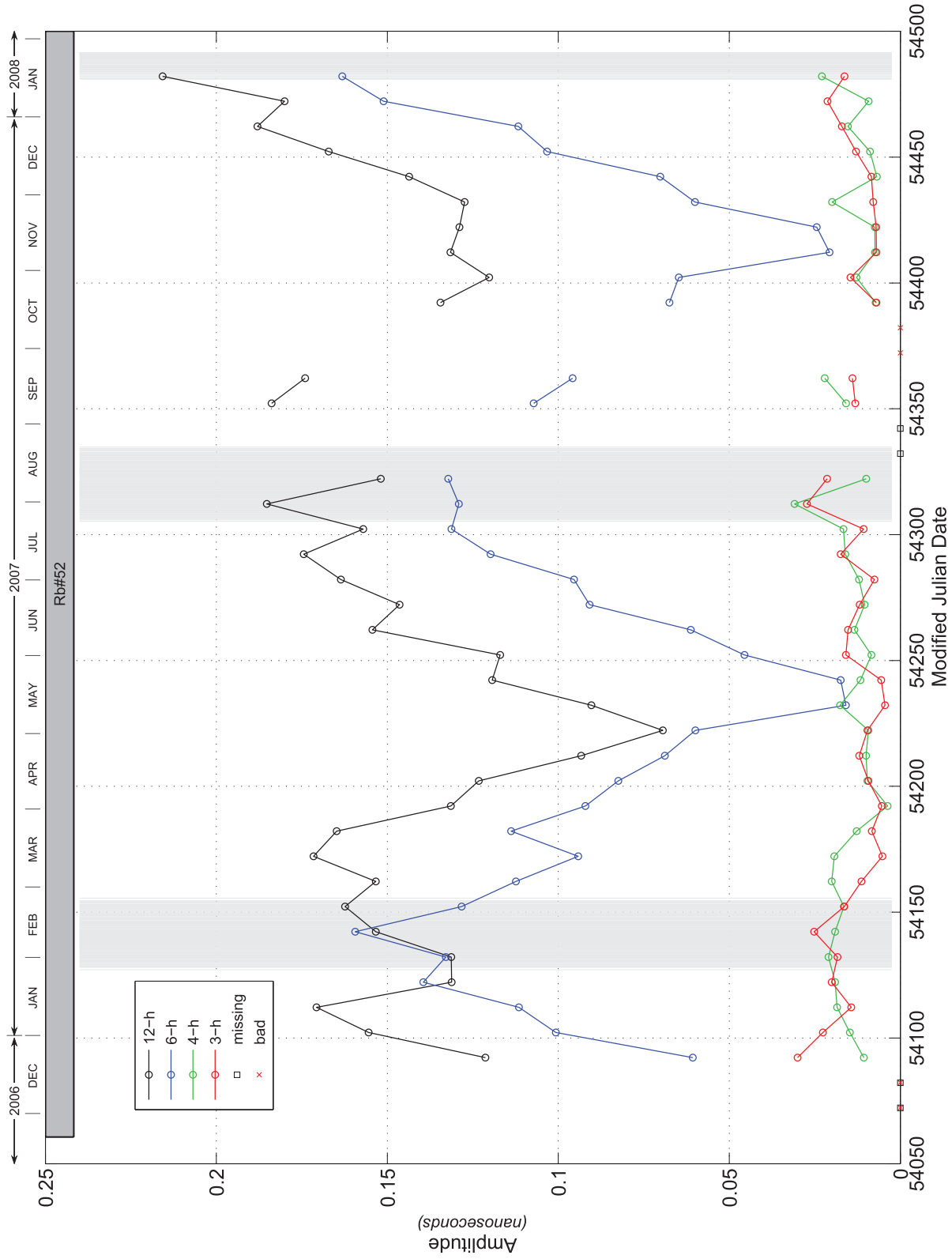


Fig. A35 — SVN58/PRN12 (Block IIR-M) time-varying amplitudes, 12-hour (black), 6-hour (blue), 4-hour (green), and 3-hour (red).

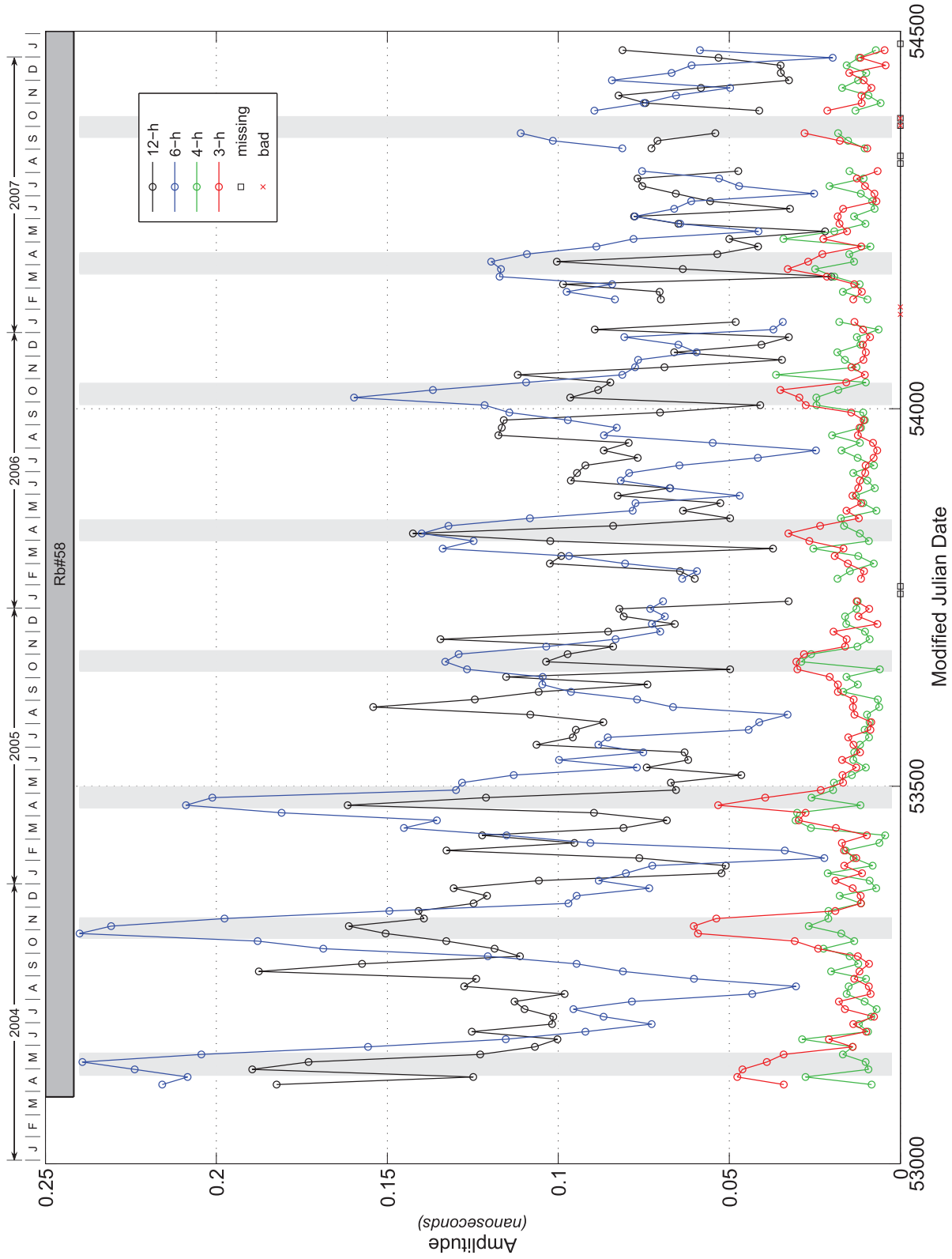


Fig. A36 — SVN59/PRN19 (Block IIR) time-varying amplitudes, 12-hour (black), 6-hour (blue), 4-hour (green), and 3-hour (red).

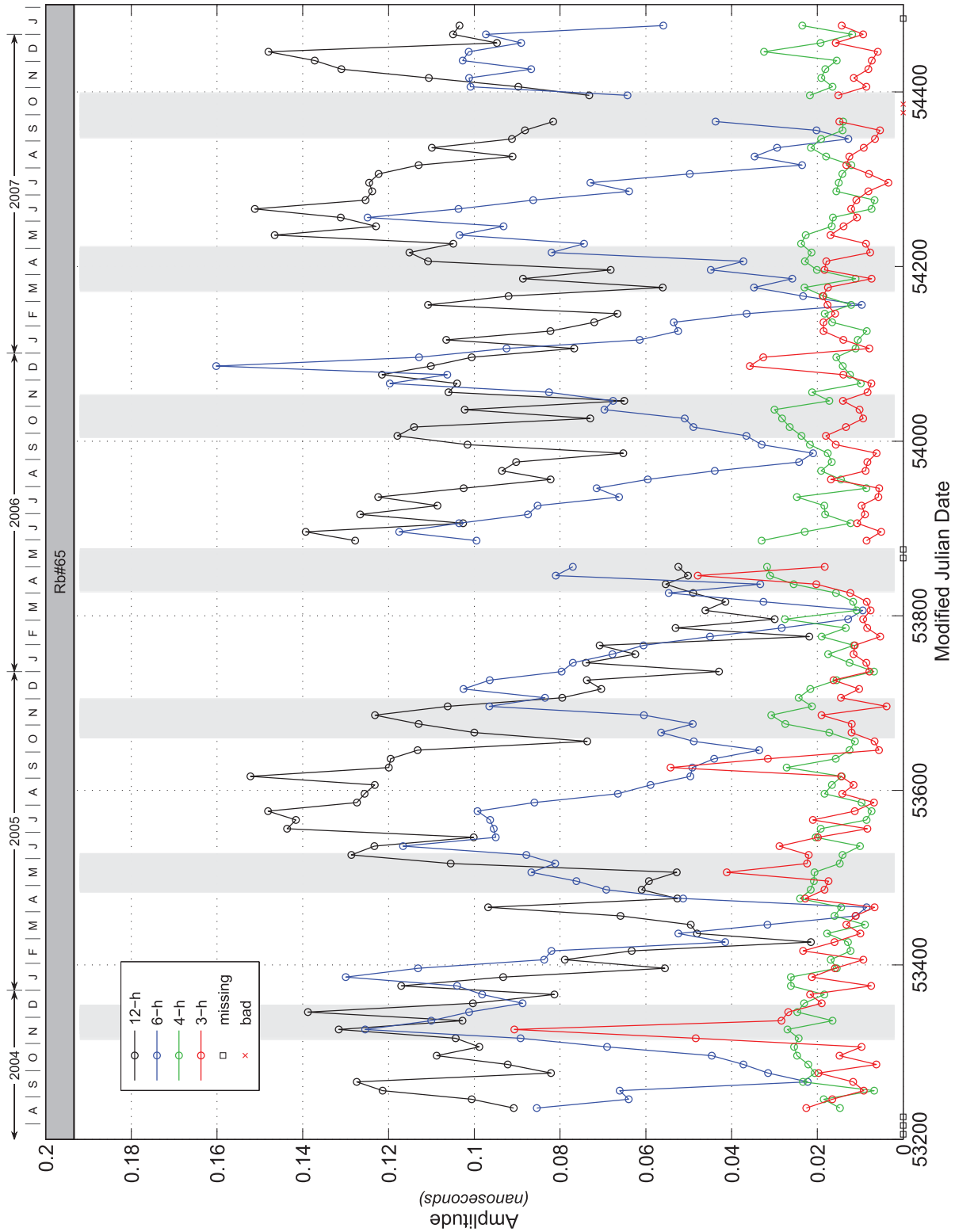


Fig. A37 — SVN60/PRN23 (Block IIR) time-varying amplitudes, 12-hour (black), 6-hour (blue), 4-hour (green), and 3-hour (red).

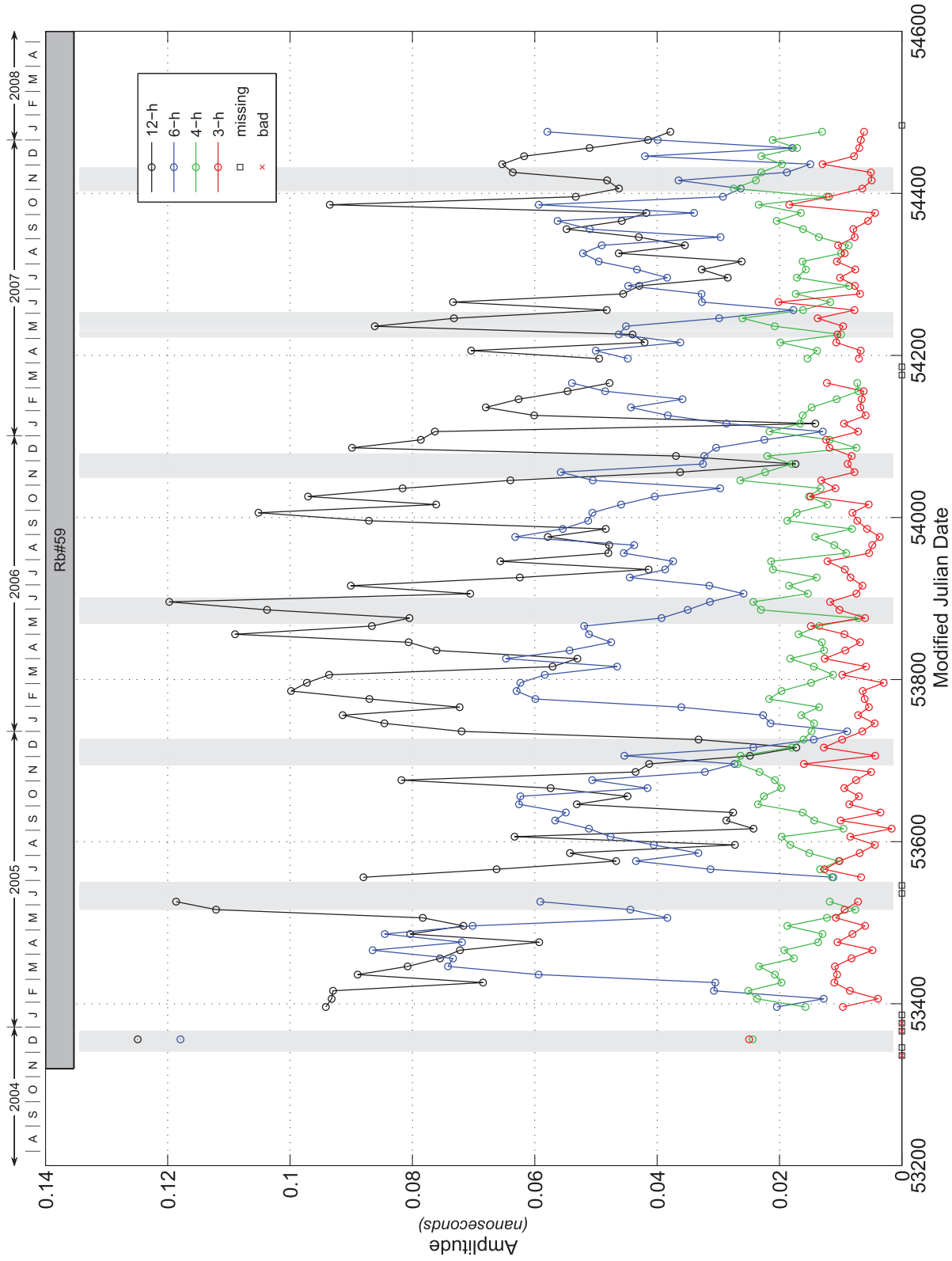


Fig. A38 — SVN61/PRN2 (Block IIR) time-varying amplitudes, 12-hour (black), 6-hour (blue), 4-hour (green), and 3-hour (red).